MODELING OF SPATIAL AND TEMPORAL HETEROGENEITY OF THE HUMAN LUNG

Del Michael Leary

Submitted in partial fulfillment of the requirements

for the degree of Doctor of Philosophy

at

Dalhousie University

Halifax, Nova Scotia

August 2013

To Brynn: may you continue to see beyond.

TABLE OF CONTENTS

LIST OF FIGURES

ABSTRACT

This thesis investigates variability in airway caliber and the distribution of ventilation within the human lung as thought to occur in asthma. Currently, the understanding of how an integrated network of airways can lead to temporal and spatial variation as found in the human lung is unclear. Throughout this thesis, a multibranch airway tree model was used in a forward modeling approach.

In a variability study, the mean airway resistance ($\overline{R_L}$) was observed to be proportional to the standard deviation in airway resistance (SDR_L) as reported in the literature under several conditions of airway diameter indicating the strong robustness of this behavior. The model predicted previously reported $\overline{R_L}$ distributions and the reported proportionality of SDR_L and $\overline{R_L}$, but only when we included coherency between airways.

In a second study, patient specific ventilation was investigated using an image functional approach by closing specific airways (creating defects) identified by hyperpolarized ^{3}He MRI from asthmatic subjects. Impedance predictions from the imposed heterogeneous ventilation were then calculated and correlated to ^{3}He MRI ventilation defect percent (VDP), plethysmography, and spirometry data. These predictions suggest the forced oscillation technique (FOT) to be a superior metric toward the evaluation of the VDP.

In a third study, we investigated how asymmetric branching could play a role in ventilation defect emergence and persistence. At high muscle activation levels simulating an asthmatic episode, airway trees with greater asymmetry reached steady state sooner, with defects that were more persistent in location, had lower R_L values (~50%), and greater E_L values (~25%) after bronchoconstriction. These results suggest the initial formation of ventilation defects was dependent on airway instability; however, the location and persistence of ventilation defects may be due to geometric airway structure.

By modeling the contribution of ventilation defects to lung impedance, we were able to show that defects can play a role in governing the relationship between *Rrs* and its variation, and the effect of defects through VDP could be better assessed using FOT. Moreover, lung structure contributed to the emergence and persistence of ventilation defects, meaning that defects could be potentially ameliorated through structural intervention.

LIST OF ABBREVIATIONS AND SYMBOLS USED

E	static elastance of the airway tree
E_L	lung elastance at 0.3 Hz
FEV_1	forced expired volume in 1 second (spirometry)
FRC	functional residual capacity
FOT	forced oscillation technique
FVC	forced vital capacity (spirometry)
H	entropy (Shannon entropy)
μ_d	mean of the diameter distribution
P_A	alveolar pressure
P_{lumen}	pressure within the lumen
P_{tm}	transmural pressure
φ	degree of coherency between mother and daughter airways
$r_f\ ratio$	ratio of sister airway radii at the end of the simulation
$r_i\ ratio$	ratio of sister airway radii at the start of the simulation
r_0	baseline radius
Raw	airway resistance
R_L	lung resistance
$\overline{R_L}$	mean value of the R_L over a number of instances
R_{L6}	lung resistance at 6 Hz
Rrs	respiratory system resistance
RV	residual volume
ρ_m	relative airway diameter
SDR_L	standard deviation of R_L
$SDRrs$	standard deviation of Rrs
$slope_d$	slope of σ_d over μ_d

$slope_R$	slope of SDR_L over R_L
σ_d	standard deviation of the diameter distribution
T_c	time constant $= R_{L6}/E$
TLC	total lung capacity
Tr	muscle activation
TV	tidal volume
τ	tethering stress
VDefs	ventilation defect
VDP	ventilation defect percent
VDV	ventilation defect volume
VC	vital capacity
X_{L6}	lung reactance at 6 Hz
Z_L	lung impedance
Zrs	respiratory impedance

ACKNOWLEDGEMENTS

I would like to thank the Canadian Thoracic Society for their studentship award and the Atlantic Canada Opportunities Agency for their Atlantic Innovation Fund award. I also want to thank the Natural Sciences and Engineering Research Council for their Canada Strategic Operating Grant. Together these awards have funded me during my course of study.

I would like to thank my supervisor, Dr. Geoffrey Maksym, who over the years has provided me with not only the supportive knowledge to help me though this work, but also with continued patience to explore new ideas and methodical thought to unravel problems, which have influenced me in many ways in my life outside academia. I would like to thank the entire lab group, including Swati Bhatawadekar, Ubong Peters, Hamed Hanafi, and Lucas Posada, for the interesting discussions at our weekly FOT lab meetings. I would like to thank my office mates both past and present, who have listened and helped me gather my thoughts. I would also like to thank M. Tawhai for the generous provision of the airway dimension data, which helped get me up and running at the early stages of this work.

I have been very fortunate to have had fantastic collaborators throughout this work. Dr, Grace Parraga at Robarts Imaging Research Laboratories at Western University in London, ON, has not only provided essential data and invaluable feedback on my work, but has also given me consistent inspiration to achieve. I am extremely grateful to Dr. Tilo Winkler at Harvard Medical School in Boston, MA, who has entertained countless discussions with me and provided focus that allowed me to think deeply about this work. I would also like to thank Anja Braune for her spirited conversations about our work. I have made many friends and truly enjoyed this research.

I have always had a loving family around me. From my extended family, the Coopers - most notably Susan, who helped me proofread the final throws of this thesis - to my parents Cam and Chris, as well as Helen and Ted and my brothers Trav and Keeth, they have all given me the courage to pursue and accomplish this work. Thank you to my little girl Brynn for her fail-safe laughter and smiles after a long day. Finally, I would like thank my wife Frances, who is truly the most supportive and understanding person I have ever known – without her this would have not been possible.

CHAPTER 1. INTRODUCTION

The lung is an essential organ for many air breathing life forms. It is an organ that has evolved into a dynamic network of fluidized tubes that are branched to optimize gas exchange. The branching is spatially optimized and is analogous to a branching structure of a tree where maximum gas exchange efficiency is desired from a limited volumetric footprint - in either the mass of the crowning canopy of the tree, or lung's physical boundary within the thoracic volume. Air is taken in through the mouth or nose then through the upper airway system consisting of the oropharynx, nasopharynx, larynx, and trachea then into approximately 26 generations of subdividing bronchi and bronchioles until finally reaching the alveoli where gas exchange takes place. Air is drawn into this network by creating a negative pressure relative to the atmosphere and then expelled by physical motions driven by musculoskeletal actions. In a healthy lung, the lung expands and contracts almost homogeneously during breathing cycles. However, in a lung challenged by obstructive disease, air flow and ventilation become spatially heterogeneous due to a complicated balancing act between pressure and volume. As the diseased lung struggles to continue to provide optimum gas exchange, the heterogeneous lung exhibits variability in both time and space.

Asthma has been shown to be a variable disease, with symptoms that are intermittent and variable in magnitude (Suki and Frey 2003; (Que, Kenyon et al. 2001; Lall, Cheng et al. 2007; Frey, Maksym et al. 2011). Changes in airway bronchoconstriction are cardinal features of asthma, varying over multiple time scales from months to minutes (Frey, Brodbeck et al. 2005). On the time scale of minutes,

variation in respiratory system resistance (variation in *Rrs*) can be monitored using the forced oscillation technique (FOT), and it is consistently reported that *Rrs* varies continuously (Que, Kenyon et al. 2001; Diba, Salome et al. 2007) likely caused by the activity of the airway smooth muscle that can be measured as the standard deviation in *Rrs* (*SDRrs*) increasing during bronchoconstriction (Que, Kenyon et al. 2001; Diba, Salome et al. 2007), and decreasing with bronchodilation (Lall, Cheng et al. 2007).

It is also now understood that airway obstruction leads to heterogeneous ventilation as observed via imaging of ventilation in asthma (Samee, Altes et al. 2003; Kaczka, Brown et al. 2009). Advances in functional lung imaging such as provided by hyperpolarized noble gas MRI can be used to identify regions of low ventilation or hypoventilation, often called ventilation defects (de Lange EE 1999; Altes TA 2001; Samee S 2003; de Lange, Altes et al. 2007; Parraga G 2007). Imaging has demonstrated the presence of ventilation heterogeneity to be a characteristic feature of obstructive lung diseases such as asthma (Samee S 2003; de Lange, Altes et al. 2007) and COPD (Mathew, Evans et al. 2008; Kirby M 2011). Furthermore, heterogeneity in ventilation observed from hyperpolarized ^{3}He imaging is more severe in asthma having larger and a greater number of ventilation defects (Tzeng, Lutchen et al. 2009) and has been associated with changes in lung mechanics in humans since Otis in 1959 (Otis 1957) and observed directly by forced oscillation in dogs (Kaczka, Brown et al. 2009) and in normal and asthmatic subjects (Tgavalekos, Musch et al. 2007;Campana, Kenyon et al. 2009).

Modeling studies predict that under asthmatic conditions, bronchoconstriction can lead to airway instability where a given airway can have multistate solutions in diameter where an airway can suddenly narrow (or dilate) while other airways paradoxically dilate

(or narrow) (Anafi and Wilson 2001). Heterogeneous ventilation was observed producing 'patchy' ventilation patterns using a symmetric airway tree in terms of geometry and airway properties suggesting that airway instability and airway interdependence could be principle mechanisms for the emergence of ventilation defects (VDefs) during bronchoconstriction (Venegas, Winkler et al. 2005).

My main objectives heading into this thesis were to expand the understanding of how temporal and spatial variability affect lung function. Specifically: 1) understand why *SDRrs* is highly correlated with *Rrs* across patient health, age, and location (Que, Kenyon et al. 2001; Diba, Salome et al. 2007), 2) to established how the heterogeneous ventilation recognized to occur in asthma in the formation of ventilation defects (VDefs) (Samee, Altes et al. 2003; de Lange, Altes et al. 2007) would affect lung resistance and reactance measured at the airway opening, and 3) how airway structure, by the degree of symmetry, can affect lung function, and the emergence and persistence of VDefs (de Lange, Altes et al. 2007; de Lange, Altes et al. 2009; Kirby M 2010).

To address these objectives, I have developed a multibranch airway model to characterize how variation in airway diameters could alter both the mean airway resistance as well as its standard deviation, exploring the effects of airway narrowing and variation amongst airway diameters. This model was first used to hypothesize that stochastic changes in airway diameter within a geometrically accurate airway tree may explain the statistical distribution of airway resistance, and the robust relationship between *Rrs* and *SDRrs* that exists in the literature for FOT measurements (Que, Kenyon et al. 2001; Diba, Salome et al. 2007).

The relationship between hyperpolarized ^{3}He MRI-derived ventilation defect percent (VDP) was compared to modeled predictions of lung impedance (Z_L) to examine the hypothesis that Z_L is sensitive to peripheral lung function and presence of ventilation defects, and that it may be better suited than spirometry currently used as the standard for assessing lung function. This study also allowed for patient-specific ventilation defects to be studied as an extension to the previously published work (Leary, Bhatawadekar et al. 2011).

I then examined the functional role of the asymmetric airway branching found in the human lung in its contribution to lung function during bronchoconstriction. Here I suggested the hypothesis that asymmetry could influence the emergence and persistence of ventilation defects when the lung is challenged through bronchoconstriction. To test this hypothesis, my model made predictions of lung resistance, reactance, and entropy on five different airway trees of varying degrees of airway asymmetry (from symmetric to anatomically human). The persistence of the location of VDefs was investigated by allowing a small amount of random variability in all airway diameters within the airway trees and rerunning the simulation multiple times.

1.1 OVERVIEW

Chapter 2 presents a brief introduction to modelling lung mechanics. A review of the literature is provided which examines the lung structure and mechanics relevant to this thesis. Some detail is provided relating to lung modeling mechanics specific to this thesis.

Chapter 3 presents the development of the asymmetric multibranch airway tree used for the stochastic approach used to predict the relationship between R_L and SDR_L found in patient data. This work also investigated how a single ventilation defect of different sizes would affect R_L and SDR_L.

Chapter 4 extends the models of Chapter 3 by introducing image guided modeling using ventilation distribution patterns from hyperpolarized 3He MRI. Patient specific images were used to alter airway sizes within the model to obtain ventilation defects that are spatially correlated. Lung function such as R_L and SDR_L are predicted as well as correlations between R_L and ventilation defect volume.

Chapter 5 uses a dynamic modeling approach to better understand how initial geometry can play a role in the emergence and persistence of defects. Varying levels of airway asymmetry were studied to investigate emerging defects as well as predicting the resultant lung function.

Chapter 6 discusses the scientific contributions made in this thesis, provides suggestions for further research, and a final summary.

CHAPTER 2. BACKGROUND

2.1 BASIC RESPIRATORY STRUCTURE AND FUNCTION

In the most basic of terms, the job of the respiratory system is to provide a way for oxygen to move from the external environment into the bloodstream and in contrast to help carbon dioxide to move out. The respiratory system can be divided into three major parts: the upper airway, the lung, and the chest wall (rib cage and diaphragm). The upper airway consisting of oropharynx, nasopharynx, and larynx that conduct air from the mouth and nose to the trachea is treated here as serial resistance of flow. The chest wall assists in breathing either actively during inspiration and forced expiration, or passively during normal exhalation. Upon inspiration, the lung inflates due to the negative pressure (with respect to atmosphere) applied at its surface by the respiratory muscles. Deflation normally occurs passively as a result of the static recoil of the lung and chest wall. Helping this process is the visceral parietal pleura which allows the ribcage, diaphragm and mediastinum lining to slide smoothly against one another. Although the lung itself does a number of life sustaining jobs engaged in secretion, clearance, and other maintenance functions, this thesis is focused on how changes in the variability of airway calibre and flow can alter lung function. Lung airway trees consist of an asymmetric tree-like structure branching through a series of bifurcations starting with the trachea that leads to tubules that continually bifurcate to various levels of bronchi exponentially populating the lung. These are successively smaller bronchi, lobar, segmental and sub-segmental bronchi, small bronchi, bronchioles, respiratory bronchioles that lead finally to terminal bronchioles (the smallest airways without alveoli) then the alveolar ducts and alveoli. The bronchi that make up the conducting airways of the lung are small in volume

(~150 ml[1]) compared to the volume of the alveolar gas (~3000 ml), which is refreshed during each breath in which the tidal volume (TV) provides approximately 500 ml of oxygen rich air. Some other important volumes used for assessing lung mechanics are shown in Figure 1. The total lung capacity (TLC) is the sum of the vital capacity (VC) which is the difference between TLC and the residual volume (RV) when all the air is exhaled in a living lung. When TV is at a minimum during normal breathing the remaining volume is the functional residual capacity (FRC).

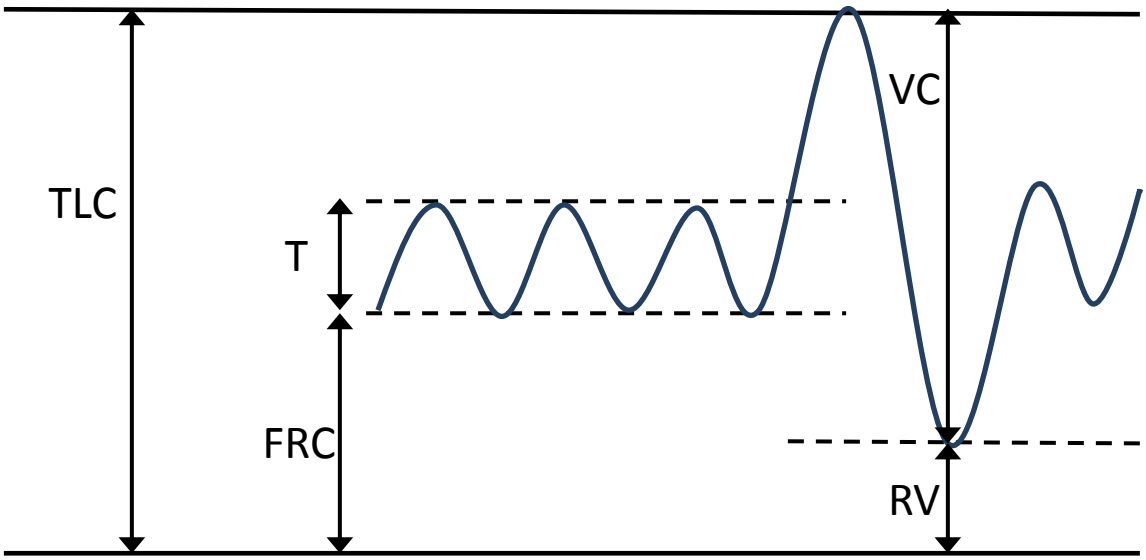

Figure 1. Important volumes of the lung used to assess lung function.

2.2. LUNG MEASUREMENTS

Spirometry involves the patient making a forced expiration following a deep inspiration, while air flow or volume at the mouth is measured. The diagnostic flow is measured as the air expired in the first second (FEV_1), and the diagnostic total volume is

[1] Values are approximate values for an adult male West, J. B. (1990). Respiratory Physiology. Baltimore, MD, Williams & Wilkins.

measured as the total volume of air expired (FVC). These are non-invasive and easily implemented in an outpatient setting and are the *de facto* standard in current lung assessment. However, due to the rather vigorous maneuvers required on the part of the patient, the measurement is not well suited for children under 5 years as well as patients with neuromuscular or cognitive defects.

The volume of gas in the lung after normal expiration (FRC) can be measured, for example, with a body plethysmograph, which is a large sealed upright box in which the subject sits. The subject undergoes maneuvers where after breathing normally for a period of time, a shutter will close in the ventilating tube located at the mouth. The subject then tries to inhale thereby expanding the gas (decreasing pressure) in their lungs and increasing the volume, and conversely the box pressure increases as the volume of the gas in the box decreases. Boyle's law can be applied in several steps to solve for FRC. The first step records low and high peaks of respiration within the box as $P_1$and P_2 for pressure and V_1 and V_2 for volume respectively. This can be written as

$$P_1V_1 = P_2(V_1 - \Delta V), \tag{1}$$

and thus ΔV can be obtained. Then Boyle's law is used a second time as

$$P_3V_{FRC} = P_4(V_{FRC} + \Delta V), \tag{2}$$

where P_3 and P_4 are the recorded pressure at the mouth before and after inspiratory effort, and V_{FRC} is the sought FRC volume. In practice, P_3 is approximated as the atmospheric pressure and the change in pressure at the airway opening (mouth) is $\Delta P_{ao} = P_3 - P_4$. The FRC volume can then be written as

$$V_{FRC} \approx \frac{(P_{atm} - \Delta P_{ao})\Delta V}{\Delta P_{ao}}. \quad (3)$$

Another major use of the body plethysmograph is the measure of the airway resistance (*Raw*). In this measurement, the patient breaths rapidly (~1Hz) into a pneumotachograph while pressures are once again recorded in the box and at the airway opening. Alveolar dry gas pressure (P_A) can be defined as the difference between ambient barometric pressure (P_{atm}) and saturated water vapor pressure at body temperature ($P_{H2O,sat}$) (Goldman, Smith et al. 2005).

$$P_A \approx P_{atm} - P_{H20,sat}. \quad (4)$$

Finally, the airway resistance is defined as the transairway pressure, defined as the difference between the pressure at the airway opening and alveolar pressure, divided by the flow,

$$R_{aw,pleth} = \frac{P_{ao} - P_A}{\dot{V}}. \quad (5)$$

The forced oscillation technique FOT was introduced in 1956 by Dubois et al. (Dubois, Brody et al. 1956) as a method of characterizing respiratory system mechanics using low-amplitude pressure oscillations applied at the patient's airway opening during normal breathing. By placing pressure transducers at the mouth, pressure and flow signals can be measured and the respiratory system impedance (*Zrs*) can be derived from the ratio of the Fourier transforms of pressure *P(f)* and flow *V(f)*. The American Thoracic Society (ATS) and the European Respiratory Society (ERS) published recommendations for the use of FOT as a clinical lung function measure(Oostveen, MacLeod et al. 2003; Miller, Crapo et al. 2005; Miller, Hankinson et al. 2005; Pellegrino, Viegi et al. 2005).

The FOT represents the current state-of-the art in lung function assessment and has reached a high level of sophistication (Bates, Irvin et al. 2011). FOT offers a non-invasive method of assessing lung mechanics, and in contrast to classic spirometry where the patient is required to actively participate, in FOT the active forced oscillation removes this requirement, and only passive subject cooperation is required allowing the technique to be used on young children(Srikasibhandha 1983; Desager, Buhr et al. 1991), debilitated (Peslin, da Felicio et al. 1993), and even mechanically ventilated patients(Van de Woestijne 1993). Additionally, where spirometry requires a deep inspiration, FOT does not, and therefore does not modify the airway smooth muscle tone(Oostveen, MacLeod et al. 2003). FOT is thus becoming increasingly recommended for obstruction testing (Oostveen, MacLeod et al. 2003; Bates, Irvin et al. 2011; Campana, Owens et al. 2011; Mochizuki, Hirai et al. 2012). The FOT device has also become more portable, potentially allowing measurements to be done outside of clinical settings such as at home allowing more frequent monitoring (Figure 2). This handheld device contains a simple electromagnetic actuator to drive the oscillating forced air along with sensors to measure the pressure and flow of air at the mouth.

Figure 2. The TremoFlo C-100 Airwave Oscillatory System, a handheld FOT device developed by Thorasys, Halifax, Canada

FOT has been shown to provide reproducible *Rrs* values as a function of gender, age, and height in both children and adults (Ducharme, Davis et al. ; Gimeno, van der Weele et al. 1993; Hayden, Petak et al. 1998). The *Rrs* value has also been found to provide reproducible data in healthy children, asthmatic children (Delacourt, Lorino et al. 2000) and children with cystic fibrosis (Hellinckx, De Boeck et al. 1998). In studies with adults, the FOT has shown that mean *Rrs* and *Xrs* can differentiate between asthma, COPD, cystic fibrosis, and sleep apnea (Van Noord, Clement et al. 1991; Farre, Peslin et al. 1999; Farre, Rigau et al. 2001; Campana, Owens et al. 2013). In addition, the variability in *Rrs* (*SDRrs*) has been reported to be sensitive to obstructive airway disease in both adults and children (Que, Kenyon et al. 2001; Trubel and Banikol 2005; Diba, Salome et al. 2007; Lall, Cheng et al. 2007).

2.3 AIRWAY TREE MODELS

There have been a number of different approaches to modeling the functionality of the human lung. The simplest form of a multibranch tree uses symmetric bifurcation where at each new generation; the branch will split into two airways of equal size. This type of model was used by Venegas and Winkler (Venegas, Winkler et al. 2005; Winkler and Venegas 2007) to demonstrate that even a symmetric lung with Anafi and Wilson airway mechanics (Anafi and Wilson 2001) can develop heterogeneous ventilation spatially within the lung. For realistic scale of the branching airway tree, Venegas and Winkler based their airway sizes on morphological data from Weibel (Weibel 1963) who obtained these values from measurements of a resin casted human lung, and were complete only to the 5^{th} generation and partially to the 10^{th} generation. Higher order transitory generations with diameters approximately 2 mm in diameter were made by microscopic measurements of airways within tissue samples from conventional histological techniques that were available in the early 1960s. Scaling laws were then applied for the very small airways within the respiratory zone having sub millimeter diameters assuming regular dichotomy. However, as a result, the asymmetrical bronchial anatomy was excluded. Later, Horsfield improved on this model (Horsfield and Cumming 1968) by introducing asymmetric dichotomy allowing variation in the diameters and lengths of the branches within a given generation. Airways that terminated before the last generation were scaled in radius to be equal to those terminated in the last generation as predicted by Weibel (Weibel 1963) . Parent airways were also adjusted until meeting a bifurcating point of a sister airway that had more distal generations.

A three dimensional model of the human airway tree was developed by Kitaoka et al.(Kitaoka and Suki 1997; Kitaoka, Takaki et al. 1999) using a deterministic algorithm based on the proportional fluid delivery to a region and the homogeneous arrangement of terminal branches.

With computational and imaging improvements came more advanced techniques to map the lung as exemplified by the techniques used by Tawhai and Hunter (Tawhai, Hunter et al. 2004), which were used in the airway tree used in this thesis. Briefly, the airway tree branching structure was initiated using multi-detector computer tomography (MDCT) to image large airways within a living subject ranging from five to eight generations typically, then a volume filling algorithm 'grew' airways to fill out the remaining space. With the use of the peripheral airways from the MDCT data, the volume filling (or mesh generating) algorithm proceeded as follows. A Monte Carlo approach was used to distribute a random scattering of points within the distal volume, from these points the center of mass was calculated. An airway would then be generated from the end of the parent branch toward the center of mass point. The length of the airway was set to be 40% of the length between these two points (Tawhai, Pullan et al. 2000). This process continued until the branches became terminal. A terminal branch was declared when the branch length was less than a minimum bronchiole length of 2 mm. The branch diameter for MDCT-measured airways is its average value between 25 and 75% of the branch length. For generated airways, the computed diameter D for any branch order x is found using the following equation.

$$\log D(x) = (x - N) log R_d + log D_N \qquad (6)$$

Here N is the highest order, D_N is the diameter of the trachea, and R_d is the branching ratio defined as the antilog of the slope of log(diameter) plotted against generation order.

2.4 LANDMARK MODELS OF LUNG MECHANICS

Human lungs have complex bifurcating airways that have been studied in a variety of models. Modeling allows insight into the underlying causes of observed behaviour that is often unobtainable through direct measurements on the lung. There are two main paradigms of modelling: forward modelling and inverse modelling. Forward modelling is essentially the construction of a model, controlling as many parameters as are necessary to test the set hypothesis, and then comparing the model behaviour to observations from measured data. Inverse modelling consists of first devising a model structure, and then parameters are chosen or 'fit' so the model matches observed behaviour within set criteria.

The following sections are a review of some of the models used in the past that are relevant to this thesis work. Many forward modelling approaches developed in the past attempt to reproduce the static behaviour of the lung determined from its elastic properties. For example, the elastic behaviour is the deformation response to an applied stress, and conversely the responsive stress can be predicted from an applied deformation. Lai Fook (Lai-Fook SJ, Wilson TA et al. 1976) found the bulk modulus to be an exponential function of the pressure while the shear modulus was linear. Inverse modelling has typically been used to model the lung's dynamic mechanical impedance. Measurements of pressure and flow can be taken at the mouth to record the respiratory

impedance and values for resistance, elastance, and inertance can be fit. The most basic are single airway-compartment lumped element models containing one resistance associated with the airway tube and one elastance associated with the compartment balloon. Increasing the number of elements in the model allows for more complex behavior to be investigated to attempt to improve the fit between numerical and experimental results. Later, resistances were described as a distribution thereby reducing the number of parameters resulting in a closed form analytical expression described by linear lumped element differential equations as in the constant phase model.

Even more recent models have utilized the improved computational power that is available, allowing the study of dynamic airway mechanics (such as Anafi/Wilson airway mechanics of a single airway described below) as an integrated approach to the entire lung describing each airway (>50,000), and even over breathing cycles allowing the lung to evolve in time to steady state after a provocation. The following sections describe the evolution of some of these lung models.

2.4.1 SINGLE AIRWAY

The simplest models that describe the lung use the single compartment model consisting of a tube to represent the conducting airways and a balloon to represent the elastic parenchymal tissue (Figure 3).

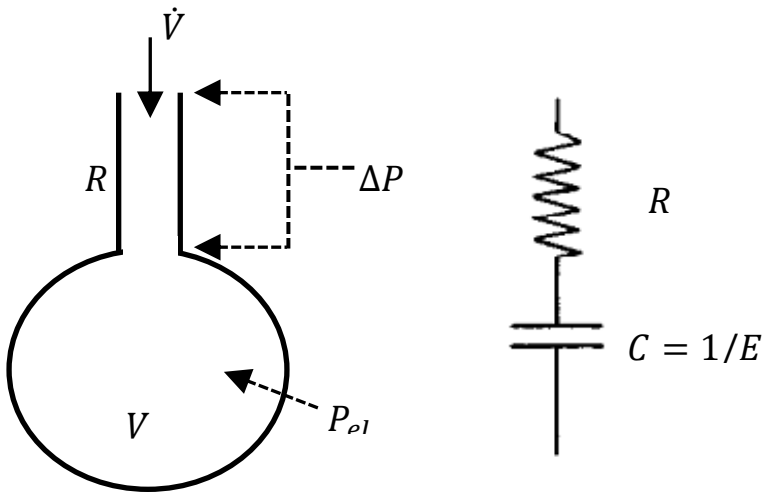

Figure 3. The single compartment model of the lung consists of two components. The first component, a tube, is used to represent the conducting airways with resistance R which governs the flow of gas ($\dot{V}$) across a pressure difference (ΔP). The second, a balloon, representing the elastic parenchymal tissue has elastic recoil pressure linearly related to its volume. This model has an electric circuit analogy with resistor and condenser connected in series. The capacitance (C) is equal to the inverse of the elastance (E).

This simplified construct provides key aspects of lung mechanics to construct an equation of motion. The total pressure of this model can be described as the sum of the pressure drop across the tube and the pressure within the balloon,

$$P = P_{el} + \Delta P = EV + R\dot{V}. \quad (7)$$

The values of resistance (R) and elastance (E) can be found by fitting the parameters to measured data using multiple linear regression. If the inertial component is also considered (particularly necessary at higher frequencies), the equation of motion includes the inertance (I) and becomes

$$P = P_{el} + \Delta P = EV + R\dot{V} + I\ddot{V} \quad (8)$$

2.4.2 MULTI COMPARTMENT MODELS

Although the simplicity of the single compartment model is attractive, the model cannot account for commonly found phenomenon such as the pendelluft effect, - where air can flow back and forth within the lung (Otis, McKerrow et al. 1956), double-exponential profile of expiration over time (Bates, Decramer et al. 1986), or low-frequency dependence of resistance and elastance (Hantos, Daroczy et al. 1987; Bates, Shardonofsky et al. 1989), which required inhomogeneity within the lung. These phenomena require models of at least two compartments to allow for time constants where gas travels down different paths at different rates. This advancement is particularly useful in the interpretation of pathological conditions, such as asthma and chronic obstructive pulmonary disease (COPD) where airway obstruction creates preferential flows throughout the airway tree.

To further improve the fit between model predictions and measured data, more elements were incorporated that fit the frequency response of the real (resistance) and imaginary (reactance) parts of the impedance. Andrew Jackson and Ken Lutchen used 3, 5, and 6 element models to fit impedance data in dogs (Jackson and Lutchen 1984). The constant phase model introduced by Hantos et al. (Hantos, B. et al. 1987) approached inverse modeling of the lung impedance as a power-low stress relaxation function rather than a lumped element approach. In the derivation of this model, there are a couple of key features. The tension (T) within a length of smooth muscle tissue can be described (after appropriate conditioning) as

$$T(t) = T_0 t^{-k} \tag{9}$$

where t is time, and k and T_0 are constants. Additionally, the ratio of the real and imaginary parts of the lung tissue is virtually constant over a wide range of oscillation frequencies. According to a basic result in linear systems theory (Bates 2009), the Fourier transform of this impulse response is the tissue impedance. Replacing T_0 with the pressure, P_0, gives the pressure response of the lung to an impulse input of flow, i.e.

$$Z_{ti} = F\{P_0 t^{-k}\} = \frac{G - iH}{\omega^{\alpha}}, \tag{10}$$

where G and H are the tissue damping and stiffness within the tissues, respectively. The exponent is defined as

$$\alpha = \frac{2}{\pi}\tan^{-1}\frac{H}{G} \tag{11}$$

which is fairly constant across frequency and gives rise to the model name of "constant phase." The ability and accuracy to describe impedance data with so few free parameters has made it the model of choice in all species below about 20 Hz (Bates, Irvin et al. 2011), and it has been found to be superior to describe viscoelastic properties of the lung and respiratory tissues (Suki, Barabasi et al. 1994).

2.4.3 NONLINEAR MODELS

Linear models of the lung and respiratory system are typically easier to use and to understand, and they give useful and fairly accurate predictive results under some conditions. Such conditions are usually encountered with the small amplitude oscillations around fairly stable lung volumes, such as functional residual capacity during measurements of respiratory impedance. However, one source of nonlinearity that can

arise is when the lung is forced to operate at high tidal volumes leading to high flows and/or volume dependent elastance; nonlinear dependences become important for accurate predictions. At high tidal volumes air flow may be high enough to be non-laminar and become turbulent, such as in the central airways during exercise or when air follows a tortuous pathway through the larynx. Then the mechanical properties of the airways begin to have a quadratic pressure-flow characteristic given by the *Rohrer's equation*

$$\Delta P = K_1\dot{V} + K_2\dot{V}\left|\dot{V}\right| \tag{12}$$

where K_1 and K_2 are parameters that collectively describe a quadratic dependence of resistance pressure on flow.

Another source of nonlinearity that can occur is when the lung operates at high lung volumes or is pathological, which can make the lung elasticity abnormally high and become volume dependent. In such situations, the pressure due to elastance is sometimes then modeled as a polynomial, such as

$$P_{el} = E_1V + E_2V^2 \tag{13}$$

where E_1 and E_2 are the respective linear and quadratic elastance parameters (Bates 2009), as well as other nonlinear functional forms, such as the exponential form in the Salazar and Knowles equation (Salazar and Knowles 1964).

There are many nonlinear models of the lung that can better describe the respiratory mechanics, not only to account for turbulent flows and volume dependent elastance, but also to describe the nonlinear rheological tissue behavior. For example, Wiener and Hammerstein systems have been used by Suki and others to model nonlinear

lung behavior (Suki 1993; Suki, Zhang et al. 1995). More specifically, Maksym and Bates (Maksym and Bates 1997) introduced a model for the nonlinear stress-strain curve based on the fundamentally different contributions of collagen and elastin fibers, which are based on the differential elastic properties of these two types of fibers, in which collagen fibers were progressively recruited with strain. Bates also predicted that any stress generated within the tissue will exponentially decay asymptotically to zero as the fibers reorient themselves randomly (Bates 1998).

In addition, recruitment and derecruitment of the alveoli can lead to large changes in the lung elastance and nonlinear behavior (Bates and Irvin 2002; Bates 2007). This has been shown to lead to an emergent phenomenon in which the sequential recruitment of collagen fibers with increasing strain causes them to progressively take over the load-bearing role from elastin (Suki and Bates 2011). These models described above comprise some of the examples that describe the interesting nonlinear behaviour of lung, but a comprehensive review is beyond the scope of this thesis, which largely uses linear models appropriate for small amplitude predictions of respiratory impedance, or specifically includes nonlinearities arising from the specific geometry of the airways as described in more detail in the subsequent sections.

2.4.4 THE ANAFI AND WILSON MODEL

The Anafi-Wilson model (Anafi and Wilson 2001) is a single airway model that describes feedback between flow and airway resistance mediated by parenchymal interdependence surrounding the airway and the mechanics of activated smooth muscle within the airway wall. In this model, the pressure-tidal volume relationship for a

constricted airway was shown to be sigmoidal, meaning that for a given airway entrance pressure, the airway radius has two stable states – one effectively open and one effectively closed. Assumptions of this model include (from experimental observations) that airway size is approximately constant during a breathing cycle, and that the peak values for airway smooth muscle force and length during cyclic stretching can be derived from the isometric force-length relationship (Figure 4). The balance of these forces depends on peak pressure differences at the airway wall, peak parenchyma forces, and smooth muscle activation.

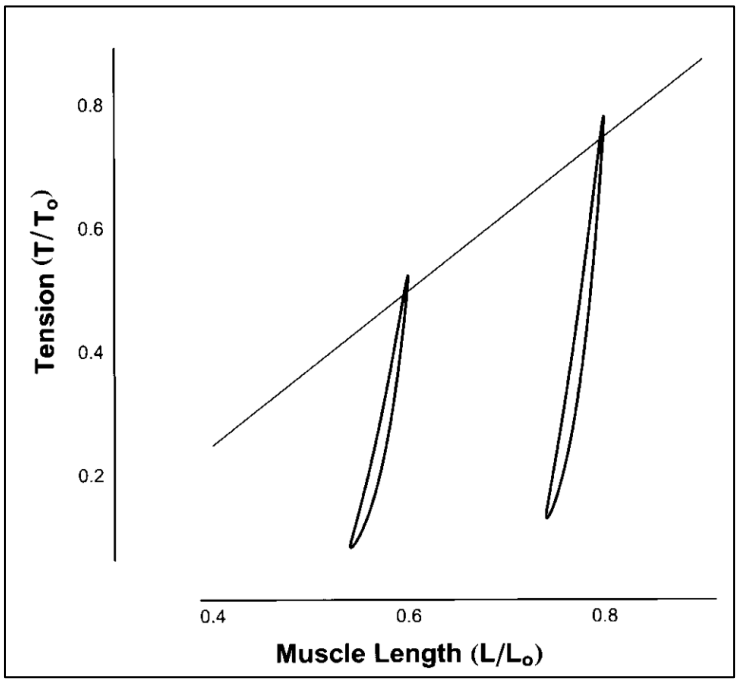

Figure 4. Representative curves of the tension-length behaviour of activated smooth muscle. The tension-length relationship for isometrically contracted muscle is shown by the thin line. Maximum isometric tension (T_0) occurs at muscle length L_0. Tension-length loops (thick loops), obtained from periodic stretch, are much steeper than the isometric line. Only small changes in muscle length result from large variations in applied tension. Peak tension during periodic stretch is approximately equal to isometric force at the same length. (from Anafi and Wilson)

The thin line in Figure 4 can be described by the linear equation

$$\frac{T}{T_0} = 1.25\frac{L}{L_0} - 0.25. \quad (14)$$

These observations suggest that the relation between T_{max} and L/L_0 during an oscillation is the same as the relation between T and L/L_0 during an isometric contraction. If oscillation length amplitude is increased, and mean length and force are free to vary, then the loop shifts rightward to longer lengths. This is described as fluctuation induced airway dilation(Gunst 1983; Fredberg, Inouye et al. 1997).

To develop a relationship for airway diameter embedded in lung parenchyma, Anafi and Wilson used the assumption that muscle length is L_0 when airway radius is r_0, and then proposed that $L/L_0 = \rho_m$ (the fractional change in the radius) and T_{max} is related to ρ_m by the equation

$$\frac{T_{max}}{T} = 1.25\rho_m - 0.25. \quad (15)$$

T_{max} can be substituted into the Laplace pressure equation to yield a value for the peak transmural pressure (P_{tm}) for a given airway size $r_0\rho_m$ as follows,

$$T_0\frac{(1.25\rho_m - 0.25)}{r_0\rho_m} = P_{tm}^{max}. \quad (16)$$

However, P_{tm} can also be defined as

$$P_{tm} = P_{lumen} - P_A + \tau, \quad (17)$$

where P_{luman} is the pressure within the airway, P_A is the pressure in the alveoli, and τ is the parenchymal tethering stress. These parameters are illustrated in Figure 5.

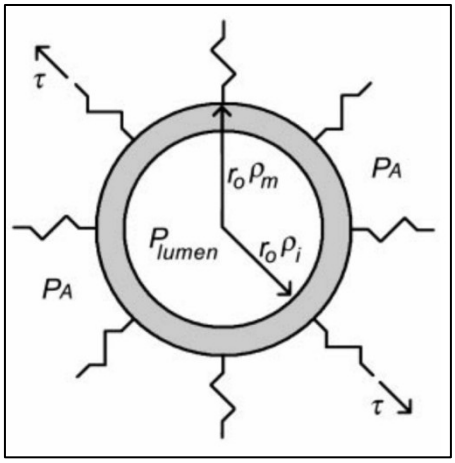

Figure 5. The non-dimensionalized radius of an unconstricted airway (r_o) at total lung capacity (TLC), is denoted by ρ_m. Lumen pressure (P_{lumen}) acts on the inner surface of the airway, $P_{A,}$ and parenchymal tethering stress (τ) contribute to the external (or peri-bronchial) pressure (Anafi and Wilson 2001).

P_{lumen} is taken as the average pressure in the airway between the pressure at the entrance of the airway P_{aw} and P_A . The magnitudes between these two pressures are related as

$$|P_A| = |P_{aw}| \frac{E}{\sqrt{E^2 + (wR_{aw})^2}}. \tag{18}$$

where E is the elastance of the alveoli, and the airway resistance is approximated using a modified Poiseuille flow equation with a viscosity η, length L, and radius r as

$$R_{aw} = \frac{8L\rho}{\pi r^4} \tag{19}$$

The pressure in the alveoli is approximately sinusoidal around the mean pressure ($\overline{P}$) with frequency ω as

$$P_A(t) = \bar{P} - |P_A| \sin(\omega t - \alpha). \tag{20}$$

where t is the time and α is a phase lag between the pressure in the alveoli and the pressure at the airway entrance. Finally, the parenchymal tethering from Eq. 4 describe by Lai-Fook is of the form

$$\tau = P_A + P_A(1.4x + 2.1x^2) \tag{21}$$

where

$$x = 1 - \left(\frac{\rho_m}{\nu^{\frac{1}{3}}}\right) \tag{22}$$

and

$$\nu = \frac{V_{RV} + (P_A/E)}{V_{TLC}}. \tag{23}$$

Here V_{RC} is the residual volume of the lung and V_{TLC} is the total lung capacity.

Peak transmural pressure (P_{tm}) described by either the Laplace pressure (Eq. 3) or by the force balance equation in Eq. 4. are plotted in Figure 6.

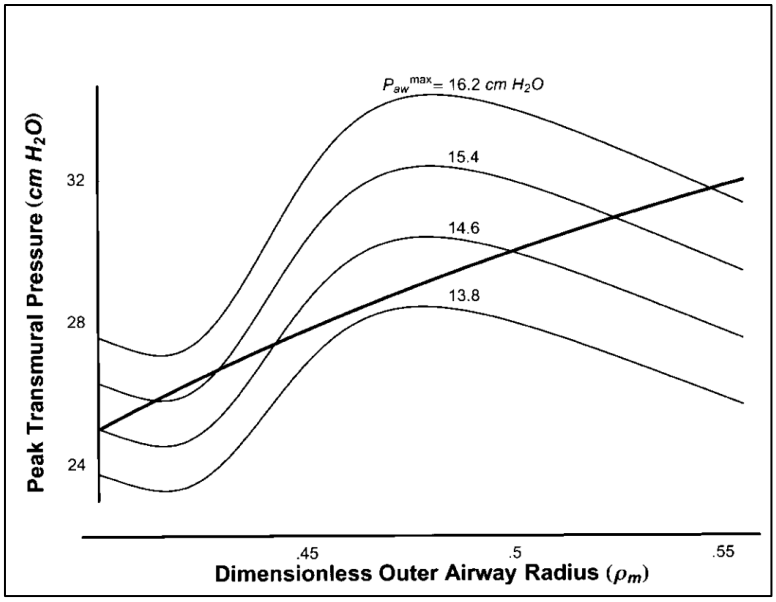

Figure 6. Peak transmural pressure (P_{tm}) vs.ρ_m. Each of the thin curves shows as a function of ρ_m for a fixed-peak pressure at the airway entrance. The single thick line shows the peak hoop stress produced by airway smooth muscle. (from Anafi and Wilson, (Anafi and Wilson 2001))

The intersecting points in Figure 6 are then found for various values of peak airway pressure ($P_{aw}^{\max}$) to determine the relationship between ρ_m and $P_{aw}^{\max}$ (Figure 7). This sigmoidal curve is responsible for the "bimodal" nature of airways that will cause sudden opening or closing of an airway. For example, if the state of an airway was on the lower part of the curve having the smallest possible airway radius, the radius would move along that curve with nearly a linear relationship. However, once the pressure passes ~15.7 cmH2O (in this scenario) the airway size would suddenly just up to the upper curve and dilate to a much larger radius. This airway would then remain in this large caliber state until the pressure drops below ~14 cmH2O. This is the key result from the Anafi and Wilson model used in this thesis.

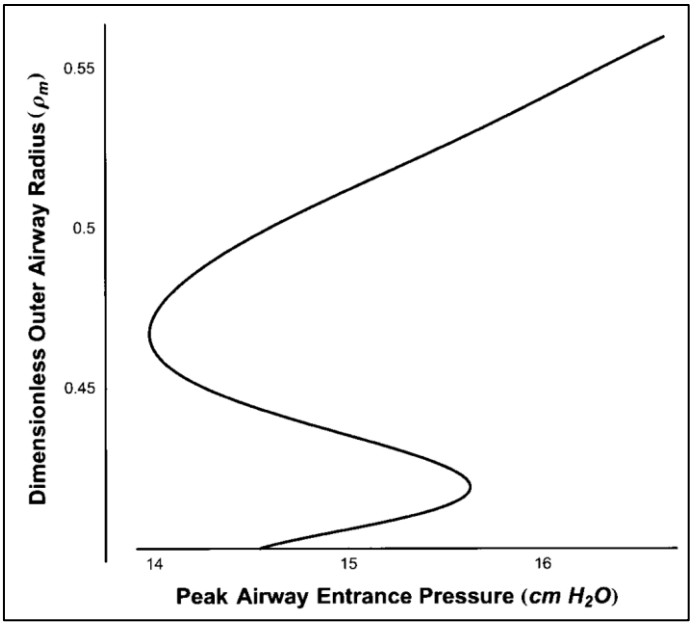

Figure 7. Fractional radius vs. peak airway entrance pressure. (from Anafi and Wilson,(Anafi and Wilson 2001))

2.4.5 INTEGRATED LUNG MODELS

Although the Anafi and Wilson model (Anafi and Wilson 2001) explains airway collapse and a separation between well and poorly ventilated modes, its local mechanisms are not sufficient to explain the spatial clustering of ventilation defects as observed in imaging studies that show large ventilation defects within a human subject after broncho-stimulation with methacholine. In order to properly describe the formation of ventilation defects, a model needs both the airway instability of Anafi and Wilson and a network of airways functioning as an integrated unit (Anafi and Wilson 2001; Venegas, Winkler et al. 2005).

The integrative model of bronchoconstriction describes the behavior of a network of airways, allowing the study of airway interactions beyond the local level. This can lead

to a feedback mechanism where small perturbations can have large effects (Winkler and Venegas 2007). The implementation of an integrative model is challenging but it is the only way to include the relevant connections within the hierarchical network of the multibranch bronchial airway tree and lung parenchyma. Interdependence in this model involves both serial and parallel interactions (Winkler 2007).

2.5 MAGNETIC RESONANCE IMAGING (MRI) WITH HYPERPOLARIZED GAS

MRI utilizes the magnetic dipole properties from nuclei that have an odd number of nucleons. Hydrogen, made up of a single proton is found in water which makes up approximately 60% of the body (Jackson 1985). The high concentration of hydrogen within the human body allows for small polarization levels ($\sim 10^{-5}$) to be suitable for MRI that can be achieved at thermal equilibrium. However, tissue voids, such as in the lungs, do not reveal much detail where water concentration is low.

Over the last few decades inhaled hyperpolarized gas has been used as a contrast agent to allow visualization of the gas distribution, and thus ventilation, within the lungs. Early work was described as a serendipitous finding in 1994 that showed inhaled hyperpolarized ^{129}Xe gas resident in murine lungs (Albert M.S. 1994). In order to make the imaging technique feasible, the inhaled gas was first magnetized or polarized using optical pumping methods that in effect 'hyperpolarized' the Xe gas. Hyperpolarization of the noble gas is done by beaming circularly polarized laser light into a glass vessel containing Rb vapor and the noble gas (Kauczor H. 1998). Typical configuration methods (Happer, Miron et al. 1984) for the polarization of ^{129}Xe gas, yield 8-10% polarization after a 6-8 hour period that produces an approximate improvement of 10^5 to 1 in the spin up to spin down configuration of the noble gas over its thermal equilibrium value (Albert

M.S. 1994). This large ratio allows the gas to have its own net magnetic moment and to be useful for MRI even at low concentrations. Improved signal to noise ratio (SNR) can be achieved using ^{3}He since the gyromagnetic ratio is 2.7 times greater than that of ^{129}Xe. Currently, HP MRI is moving back to ^{129}Xe rather than ^{3}He due to the lack of ^{3}He available for commercialization and translational research.

After the initial proof of concept using hyperpolarized MRI on mice lungs, humans were imaged within a few years (Ebert M. 1996; Kauczor H. 1998). Since then the technique has been widely applied in lung disease such as asthma (Altes TA 2001; Samee, Altes et al. 2003; Koumellis, van Beek et al. 2005; de Lange, Altes et al. 2006; de Lange, Altes et al. 2007; Tzeng, Hoffman et al. 2008; Wang C 2008), cystic fibrosis (Donnelly, MacFall et al. 1999; McMahon CJ 2006; Altes TA 2007; van Beek EJ 2007; Woodhouse N 2009), and lung transplant cases (McAdams HP 1999; Gast KK 2003; Zaporozhan J 2004). This technique continues to grow in popularity as is provides complementary and alternative information to x-ray, CT, and PET without ionizing radiation.

2.6 VENTILATION DEFECTS

Ventilation of inhaled gas within the lung is not always homogeneous. Unhealthy lungs have been observed to show heterogeneous gas distributions in different imaging modalities. Hyperpolarized gas MRI, as discussed in the previous section, has been used to assess gas distribution within the lung ranging from age-related changes in air space (Altes, Mata et al. 2006; Parraga G 2008), early detection and quantification of COPD

(Woods, Choong et al. 2006; Mathew, Kirby et al. 2011), evaluation of ventilation abnormalities in COPD (Mathew, Evans et al. 2008; Kirby M 2011) , asthma (Altes TA 2001; de Lange, Altes et al. 2006; de Lange, Altes et al. 2009; Tzeng, Lutchen et al. 2009; Costella M, Kirby M et al. 2012), and cystic fibrosis (Koumellis, van Beek et al. 2005; Mentore, Froh et al. 2005). Positron emission spectroscopy (PET) has also been used to assess ventilation heterogeneity (Tgavalekos, Venegas et al. 2003; Venegas, Schroeder et al. 2005; Venegas JG 2005; Tgavalekos, Musch et al. 2007). Although the spatial resolution is considerably lower in PET compared to MRI, PET imaging has often been also used to measure the corresponding perfusion (Musch 2005; Harris 2006; Harris, Fujii-Rios et al. 2012). However, with the move from ^{3}He to ^{129}Xe, perfusion studies in MRI are possible (Kauzor, Surkau et al. 1998; Fain, Schiebler et al. 2010). The exact quantification of ventilation defects can vary. For example, in the MRI studies used in this thesis, we have used a k-means algorithm to delineate various degrees of ventilation by associating each voxel with its closest cluster mean, with the lowest degree of ventilation being defined as a ventilation defect (Kirby M 2012). However, other imaging modalities using PET define VDefs as regions of the lung that are reduced to 15% of their baseline ventilation (Harris 2006). The ventilation defect percent (VDP) can then be calculated by dividing the volume of the defect by the total volume of the lung (Mathew, Kirby et al. 2011). This thesis will similarly use VDefs derived from MRI to quantify the relationship between lung impedance and VDP.

CHAPTER 3. MODELING STOCHASTIC AND SPATIAL HETEROGENEITY IN A HUMAN AIRWAY TREE TO DETERMINE VARIATION IN RESPIRATORY SYSTEM RESISTANCE

3.1 ABSTRACT

Asthma is a variable disease with changes in symptoms and airway function over many time scales. Airway resistance is variable and thought to reflect changes in airway smooth muscle activity, but just how variation throughout the airway tree and the influence of gas distribution abnormalities affect airway resistance is unclear. We used a multibranch airway lung model to evaluate variation in airway diameter size, the role of coherent regional variation, and the role of gas distribution abnormalities on mean airway resistance $\overline{R_L}$ and variation in airway resistance as described by the standard deviation (SDR_L). We modified an anatomically correct airway tree, provided by M. Tawhai (U. Auckland), consisting of nearly 4000 airways to produce temporal and spatial heterogeneity. As expected, we found that increasing the diameter variation by two-fold with no change in the mean diameter increased SDR_L more than four-fold. Perhaps surprisingly $\overline{R_L}$ was proportional to SDR_L under several conditions; when either mean diameter was fixed and its standard deviation varied or when mean diameter varied and standard deviation was fixed. Increasing the size of a regional absence in gas distribution (ventilation defect) also led to a proportionate increase in both $\overline{R_L}$ and in SDR_L. However, introducing regional dependence of connected airways strongly increased

SDR_L by as much as 6-fold with little change in $\overline{R_L}$. The model was able to predict previously reported $\overline{R_L}$ distributions and correlation of SDR_L on $\overline{R_L}$. In healthy and asthmatic subjects, the ratio of SDR_L to $\overline{R_L}$ depended most strongly on inter-airway coherent variation, and only had a slight dependence on ventilation defect size. These findings may explain the linear correlation between variation and mean values of airway resistance, but also suggest that regional alterations in gas distribution and local coordination in ventilation amplifies any underlying variation in airway diameters throughout the airway tree.

3.2 INTRODUCTION

Asthma is a variable disease, with symptoms that are intermittent and variable in magnitude (Suki and Frey 2003). Changes in airway bronchoconstriction are cardinal features of asthma, varying over multiple time scales from months to minutes (Frey, Brodbeck et al. 2005). Most commonly, variation in airway function has been evaluated using changes in peak expired flow or variation in airway resistance, both of which have been associated with airway diameter alterations (Jensen, Atileh et al. 2001; Black, Dellaca et al. 2003).

On the time scale of minutes, variation in respiratory system resistance (variation in *Rrs*) can be monitored using the forced oscillation technique (FOT), and it is consistently reported that *Rrs* varies continuously (Que, Kenyon et al. 2001; Diba, Salome et al. 2007). The magnitude of the variation is related to changes that affect airway diameter and are thought to be affected by the activity of the airway smooth muscle. Indeed, bronchoconstriction via methacholine increases the standard deviation in *Rrs (SDRrs)* (Que, Kenyon et al. 2001; Diba, Salome et al. 2007), and bronchodilation via albuterol decreases *SDRrs* (Lall, Cheng et al. 2007). In a similar fashion, unloading and narrowing of the airways in the supine position increases *SDRrs* (Que, Kenyon et al. 2001). The fluctuations in airway resistance are also higher in asthma in both children and adults (Delacourt, Lorino et al. 2000; Que, Kenyon et al. 2001; Diba, Salome et al. 2007; Lall, Cheng et al. 2007). However, *SDRrs* is also highly correlated with *Rrs* indicating that like *Rrs*, *SDRrs* depends on airway diameter, but why these may be so tightly coupled is not well understood (Diba, Salome et al. 2007). Moreover, it not established how heterogeneity of ventilation recognized to occur in asthma would affect

airway resistance measured at the airway opening (Samee, Altes et al. 2003; de Lange, Altes et al. 2007).

Animal studies suggest that airway obstruction is heterogeneous (Brown, Kaczka et al. 2008), modeling studies predict heterogeneous airway narrowing (Venegas, Winkler et al. 2005), and imaging of ventilation in asthma has also identified marked spatial heterogeneity in regional lung ventilation(Samee, Altes et al. 2003; Kaczka, Brown et al. 2009). Furthermore, heterogeneity in ventilation from hyperpolarized ^{3}He-3 imaging is quantitatively higher in asthma (Tzeng, Lutchen et al. 2009) and has been associated with changes in lung mechanics by forced oscillation in dogs (Kaczka, Brown et al. 2009) and in normal and asthmatic subjects (Tgavalekos, Musch et al. 2007; Campana, Kenyon et al. 2009). These studies imply dramatic differences in regional airway narrowing that occur within the lung. It has been argued that in airway obstruction, many airways may be changing diameter together continuously, both randomly and by changes in activation and airway loading, which leads to the reported continuous variation in airway resistance measured by forced oscillation (Que, Kenyon et al. 2001). However, it is yet unclear how alterations in airway diameter in a multibranch lung can lead to the observed variation of airway resistance.

Here we examined how stochastic changes in airway diameter within a geometrically accurate airway tree may explain the statistical distribution of airway resistance, described via *Rrs* and *SDRrs*. We developed a multibranch airway model to characterize how statistical variation in airway diameters could alter both the mean airway resistance as well as its standard deviation, exploring the effects of airway narrowing or mean airway diameter and altered variation amongst airway diameters via

the standard deviation of airway diameters. We also explored the effect of interaction of amongst airway diameters via correlated and uncorrelated airway diameter variation, and the effects of large scale heterogeneity via the introduction of large ventilation abnormalities, or defects. Predictions of airway resistance and its standard deviation were then compared to previously reported FOT data obtained from healthy and asthmatic subjects.

3.3 METHODS

3.3.1 MULTIBRANCH AIRWAY TREE

The lung model developed here was based on an anatomically correct 3D human airway geometry as previously described and provided by M. Tawhai (U. of Auckland) up to the twelfth generation governing 3915 airways (Tawhai, Hunter et al. 2004). The airway tree model was generated by using a subject-specific host volume derived from x-ray multi-detector computed tomography (MDCT) imaging (Tawhai, Nash et al. 2009). Beyond the eighth generation, a volume-filling algorithm (Tawhai, Nash et al. 2009) was used to generate the remaining airway tree maintaining daughter diameter ratios consistent with established morphometry (Horsfield and Cumming 1968). The airway tree was terminated at the 12^{th} generation similar to Venegas et al (Venegas, Winkler et al. 2005) which represented airway diameters approximately 1 mm in size. This end point was chosen as a compromise between computational feasibility and realistic impedance predictions. Since the Tawhai model is at TLC, we reduced the airway diameters to 0.7 of the Tawhai values, which assumed a homogenous volume change with a ratio of FRC to

TLC of 0.3. This serves as a reference point only as airway diameters were altered over a wide range as described below.

The impedance of the airway tree for a given realization of airway diameter distribution was calculated using a lumped element approach where the impedance of the airways was summed following the branching patterns using well known series and parallel network impedance relations. Airway resistance for each branch was approximated using Pouseille's flow given by

$$R = \frac{128\eta L}{\pi d^4} \tag{24}$$

Where η is the dynamic viscosity of humid air at 37 C, L is the length, and d is the diameter of the airway.

Each terminal airway was prescribed an elastance E to act functionally as the peripheral airway wall compliance distal to the 12th generation in our model, and the alveoli calculated from the product of the number of terminal airways and normal elastance of the lung (Tgavalekos, Venegas et al. 2003). This neglects any contribution to the impedance from gas compression or central or intermediate airway wall compliance, but these are both much smaller than the contribution from the peripheral airways and alveoli. The impedance for a terminal airway was defined as

$$Z = R + iI\omega - \frac{iE}{\omega} \tag{25}$$

and airway impedance for a non-terminal airway was calculated as

$$Z = R + iI\omega \tag{26}$$

where I is the inertance calculated as $\rho_{air}L/(\pi r^4)$ with ρ_{air} the air density, L the length of a branch, and r its radius, E is the elastance, and ω is the angular FOT frequency. This

resulted in a resonant frequency near 6 Hz which is normal in humans. The airway impedance of the entire airway tree could then be calculated numerically and further separated into real (resistance) and imaginary (reactance) parts. Because parallel pathways in a heterogeneous lung can lead to the product of reactances, the real part of the total impedance will have some dependence on the elastance and inertance, as was originally demonstrated in the two compartment parallel Otis lung model (Otis, McKerrow et al. 1956).

3.3.2 SIMULATIONS

In a multibranch airway tree, the magnitude of variation of airway resistance at the airway opening is affected by the magnitude of variation at the level of the airway diameter, and as will be demonstrated, the degree to which airways behave similarly, and the presence of ventilation defects. Each simulation consisted of at least 2000 repeated realizations of the model with each airway diameter varied according to a prescribed distribution with a set mean and standard deviation relative to the initial airway diameter from the Tawhai model, as described in more detail below. From each realization we computed a lung resistance value, R_L, and from all the realizations for a given simulation, we obtained a probability distribution for airway resistance. To explore the effect of the magnitude of variation in diameters, we first considered how increasing the amount of diameter variation throughout the lung would affect the total respiratory resistance. This would occur if airway smooth muscle activity contributed to increasing variability of airway diameters as had been previously postulated for example (Que, Kenyon et al. 2001). While we did not include periodic contributions to variations in airway diameter

such as during lung volume changes associated with breathing, we also examined all simulations at different mean airway diameters, representing changes in average airway constriction or changes in lung volume that would occur with breathing. Further, we investigated how interactions between airways affected the distribution of airway resistance which we describe as incoherent or coherent variation depending if parent and daughter connected airways vary independently or vary together. Finally, we investigated how different sizes of ventilation defects affected the distribution of airway resistance. Each of these simulations is described following.

3.3.3 VARIATION OF THE AIRWAY DIAMETERS

Variation in airway diameters throughout the airway tree model leads to total variation in resistance of the lung. The variation in airway diameters was controlled by setting a prescribed mean and standard deviation relative to the initial diameters set by the initial airway geometry given in the Tawhai model.

$$d_i = d_{base,i} \cdot N_i(\mu_d, \sigma_d) \qquad (27)$$

where d_i is the diameter of a particular airway for a given realization of the model, $d_{base,i}$ is the diameter of a particular airway from the Tawhai model, and $N_i(\mu_d,\sigma_d)$, is a random number from a modified Gaussian distribution with relative airway diameter μ_d, and relative airway diameter standard deviation σ_d. For the different simulations, σ_d was either held constant while airway diameter was changed (fixed variation model), altered at different fixed mean diameters (fixed mean model), or adjusted in proportion to the mean airway diameter (fixed slope, $slope_d$ model). Airway diameters were changed below their FRC baseline by altering the mean of the relative airway diameter distributions as

$$\mu_d = \left(1 - \frac{\xi}{100}\right) \tag{28}$$

with ξ = 2.5, 5, 7.5, 12.5, 17.5, 22.5, and 27.5%. Variation was changed by altering the standard deviation of airway diameters, σ_d as

$$\sigma_d = \lambda \mu_d \tag{29}$$

with λ = 0.08, 0.12, 0.16 and 0.2.

The constant $slope_d$ model (Figure 8a) was evaluated as the results could be compared with the analytical solution in a single airway model by Lall et al (Lall, Cheng et al. 2007). An illustration of how the diameter distribution was altered for the fixed mean model and the fixed $slope_d$ model is shown in Figure 8b. As mentioned previously, this process was repeated for the entire airway tree for a minimum of 2000 R_L calculations of different airway diameters randomly chosen within the specified distribution to compute the statistical mean ($\overline{R_L}$) and standard deviation (SDR_L) of the entire model (Figure 8d).

The diameters of all airways were randomly chosen from a modified Gaussian distribution to prevent extremely low values of airway diameter as follows: We limited the maximum narrowing for generations 0 to 4 to be no less than 50% of their baseline diameter representing the effect of cartilage limiting airway narrowing and any airway from generation 5 to 12 was limited to narrowing by 90% to 10% of its baseline diameter value. These limits were invoked infrequently; typically occurring less than 1.2% of the time at 27.5% mean constriction with standard deviation equal to 10% of the mean diameter. Also, diameters were restricted from exceeding twice the constricted mean.

3.3.4 AIRWAY DIAMETER VARIATION AND REGIONAL COHERENCY

To investigate the possibility that airways in a localized region may vary similarly, as might be due from physical attachment or local similarity in activation or mechanical properties, we introduced a variable, φ, which could control the degree of spatial coherent variation in connected airways in a gradual and regional manner, thus generating regional heterogeneity. The diameter of the daughter airway, for example, $d_{i+1,}$ was then determined either independently or in relation to the parent airway d_i according to

$$d_{i+1} = \varphi d_i \left(\frac{d_{base,i+1}}{d_{base,i}}\right) + (1-\varphi) d_{base,i+1} \cdot N_{i+1}(\mu_d, \sigma_d) \qquad (30)$$

The coherence parameter, φ, is bound between 0 and 1. For φ = 0, d_{i+1} is independent from its parent airway, and would vary with no coherent change in diameter relative to its parent airway. For φ=1, d_{i+1} is fully coherently varying with its parent airway and thus all other airways throughout the lung. At φ = 0.6, the parent is 60% coherent with its daughter, 36% with its granddaughter, with decreasing coherence for further generations distant to the parent. Thus, larger values of φ increase the degree of regional spatial coherency (Figure 8b).

3.3.5 SIMULATING GAS DISTRIBUTION ABNORMALITIES

Studies using hyperpolarized ^{3}He magnetic resonance imaging (MRI) have identified spatial and temporal heterogeneity in airway function. These are specific to obstructive lung diseases like asthma or can be produced in healthy subjects with induced bronchoconstriction. Focal ventilation defects where there is a ^{3}He signal void in anatomical regions related to airways narrowing can be visualized and quantified (de Lange, Mugler et al. 1999; Salerno, Altes et al. 2001). Such ventilation defects can be

significantly large in comparison to the volume of the lung and spatially and temporally persistent (de Lange, Altes et al. 2007). To explore the effect of such apparent ventilation defects, and more specifically, the airway narrowing that we hypothesize is the determinant of such functional abnormalities, we modeled single ventilation defect, at different airway generations to explore the effect of defect size on $\overline{R_L}$ and SDR_L. In our model, we assumed that ventilation defects were generated by constricting a single airway at a given generation to 10% of its initial baseline value. While the etiology of ^{3}He MRI ventilation defects is yet unclear, we made the assumption that in asthma, defects are related to airway narrowing.

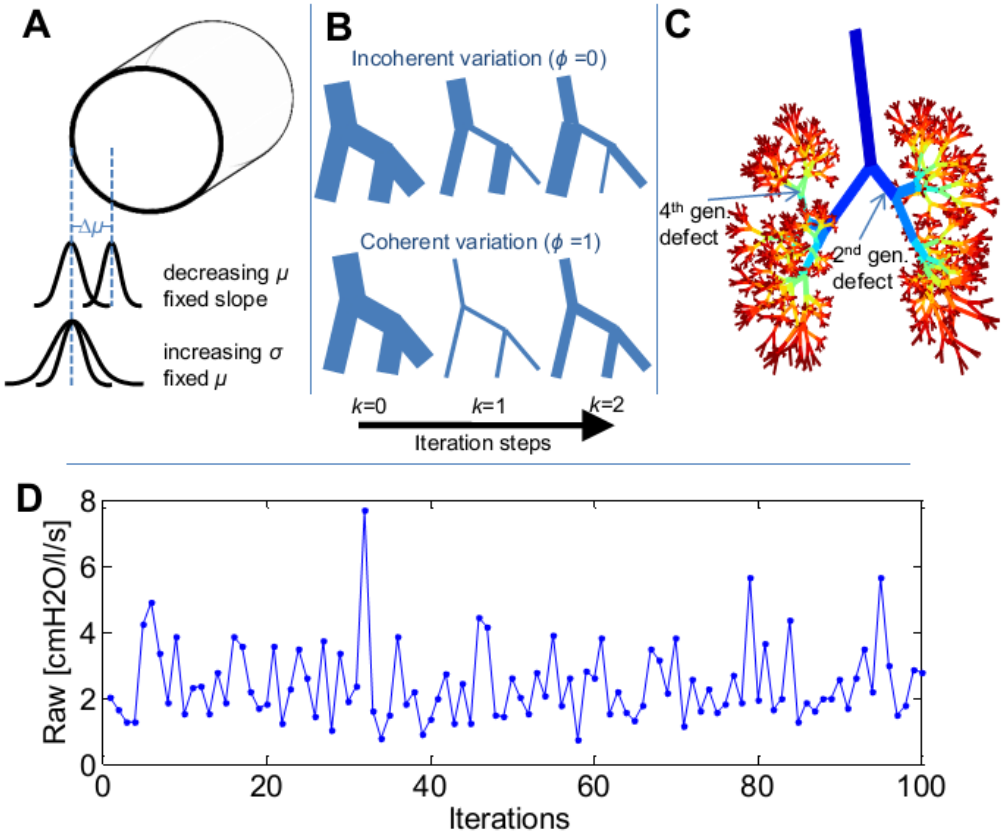

Figure 8. a) The diameters of airways are varied at each iterative step by adjusting the diameter to a prescribed distribution maintaining either a fixed mean, fixed standard deviation (not shown), or fixed $slope_d$. b) Diameters of adjacent airways could vary at various levels of coherent variation shown here are examples of either fully incoherent or fully coherent variation between mother and daughter airways. c) The multibranch airway tree consists of twelve generations for airway resistance predictions with the colors here representing the airway generation number. The resistance d) for the entire airway tree is calculated at each iterative step.

3.3.6 SINGLE AIRWAY MODEL

In order to help validate the multibranch model and to investigate the role of the transformation of the nonlinear transformation between airway diameter and airway resistance, we compared our predicted $\overline{R_L}$ from the multibranch airway model with

totally coherent variation to a single airway model with varying airway diameter distributions. The single airway radius was derived from the arithmetic mean of all the airways in the multibranch lung model, and the length was then altered to achieve the same baseline resistance as the multibranch model.

3.3.7 COMPARISON WITH RECORDED DISTRIBUTION OF AIRWAY IMPEDANCE

We compared model predicted distributions of $\overline{R_L}$ to *Rrs* obtained from asthmatic and normal subjects as reported previously (Que, Kenyon et al. 2001). The six healthy subjects (5 men and 1 woman) had no history of pulmonary disease, were not hyperreponsive by methacholine challenge, and asthmatic subjects were identified by the respirologist in charge of the clinic and had FEV_1 measurements that varied between 64 and 92 percent predicted as taken prior to being tested. The FOT data from this study are from 6 Hz pressure oscillations digitized at 256 Hz over 15 minutes of normal breathing providing up to 5400 values excepting artifacts from coughs, swallows or glottal closures that were removed as described (Que, Kenyon et al. 2001). The average of the mean resistances from the normal patients was 1.86 (SD 2.60) $cmH_2O/l/s$, and from the asthmatic patients was 5.20 (SD 3.35) $cmH_2O/l/s$.

3.4 RESULTS

3.4.1 INCREASING AIRWAY DIAMETER

When the relative average airway diameter was changed, but the standard deviations of airway diameters kept constant, $\overline{R_L}$ increased as expected. However, the

SDR_L also increased as seen by the increase in the width of the distribution of $\overline{R_L}$ despite no change in airway diameter variation (Figure 9a).

3.4.2 INCREASING AIRWAY DIAMETER VARIATION

Similarly, when the standard deviation of airway diameters σ_d was increased while keeping the mean diameters μ_d fixed, SDR_L increased as expected, however $\overline{R_L}$ also increased despite no change in the μ_d (Figure 9b). In both cases, $\overline{R_L}$ and SDR_L increased proportionately, but when σ_d was increased at fixed average diameter, the slope of SDR_L vs. $\overline{R_L}$ was greatest (Figure 9c).

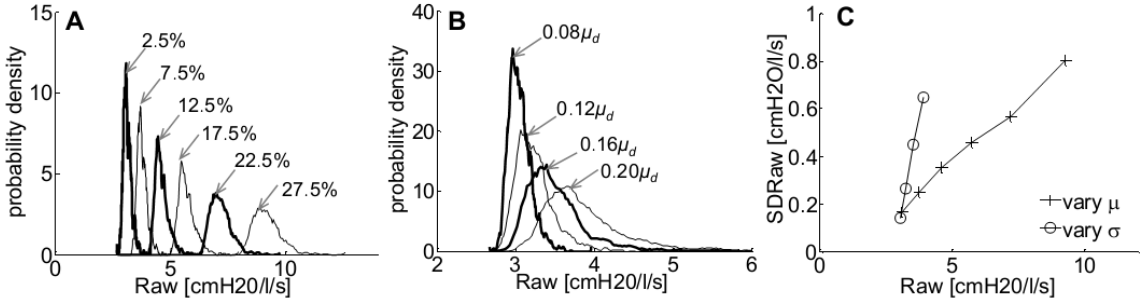

Figure 9. Probability distributions of R_L for increasing a) mean diameter while fixing the variability in diameter constant, and b) increasing the variability in diameter at a fixed mean. c) Comparison of the respective SDR_L versus $\overline{R_L}$ for these simulations.

3.4.3 IMPOSING GAS DISTRIBUTION ABNORMALITIES OR VENTILATION DEFECTS

By closing different airways within each chosen generation, simulating regional gas distribution differences or ventilation defects we created multiple simulations for single defects of different sizes within a generation (i.e. occluding 4 different airways at the 3rd generation) and across generations (generation 4 to 2). We observed that $\overline{R_L}$

increased as expected and was dependent on defect size, with larger defects causing a larger change in $\overline{R_L}$ (Figure 10). The addition of ventilation defects resulted in an increase in SDR_L, however this effect was modest compared with the effect of increasing $\overline{R_L}$ as shown by the small slope in Figure 10 (circles) particularly when compared with the model with increasing diameter variation alone (Figure 10, crosses).

3.4.4 COHERENT VARIATION IN AIRWAY DIAMETER

When the amount of coherency in airway variation between connected airways was increased from 0 to 100% with 10% intervals, the standard deviation of airway resistance increased substantially and mean airway resistance remained largely unchanged, as shown in Figure 10 (open squares). Up until φ began to exceed 0.6 there was little effect on SDR_L, but the effect on SDR_L increased greatly for larger φ. The common crossing point in Figure 9c and Figure 10 is the baseline condition common to all simulations, with incoherent diameter fluctuations, σ_d at 10% of the diameter mean, and without defects.

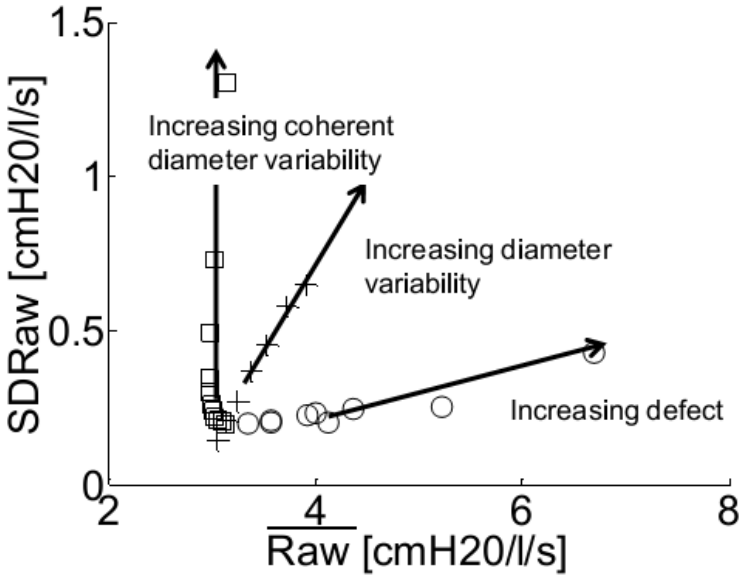

Figure 10. This figure shows the dependence of SDR_L on $\overline{R_L}$ for increasing coherent variation, increasing diameter variability and increasing defect size. Increasing airway diameter standard deviation from 8% to 20% in 2% steps (+), and increasing airway variation coherency from 0% (incoherent) to 100% in 10% steps (□) and increasing the ventilation defect size from 4th generation airway to the 2nd generation (○).

3.4.5 COMBINING WITH AIRWAY DIAMETER NARROWING

The above effects on the airway model were also tested at different airway diameters decreasing from FRC (Figure 11a). Over the same range in average airway diameters, a larger σ_d led to a shift to both higher $\overline{R_L}$, and SDR_L, but SDR_L was more strongly affected as indicated by the higher $slope_R$ which increased approximately two-fold (Figure 11b).

We also tested how the coherency of variation of the airway diameter at different constrictions would affect the probability distribution of $\overline{R_L}$ by comparing two extremes: the fully incoherent, where airways vary with no relationships to each other, and the coherent extreme where all the airways vary in unison. Comparing the results of these

two extremes of incoherent and coherent variation we found that the $slope_R$ was greater for a coherently varying airway tree by a factor of 6 as can be seen when comparing Figure 11a and Figure 11c respectively. While airways that vary totally in unison is inconceivable if driven actively by the smooth muscle, it is a reasonable approximation to breathing. Furthermore, the $\varphi = 1$ case is the simplification of the multibranch lung to a single airway, and the case matching our single airway model provides further validation of the model (Figure 11e).

The effects of adding a large defect can be seen in Figure 11d via obstruction in a 2^{nd} generation airway. The defect causes both the mean and standard deviation of airway resistance to increase, and maintains a nearly constant $slope_R$.

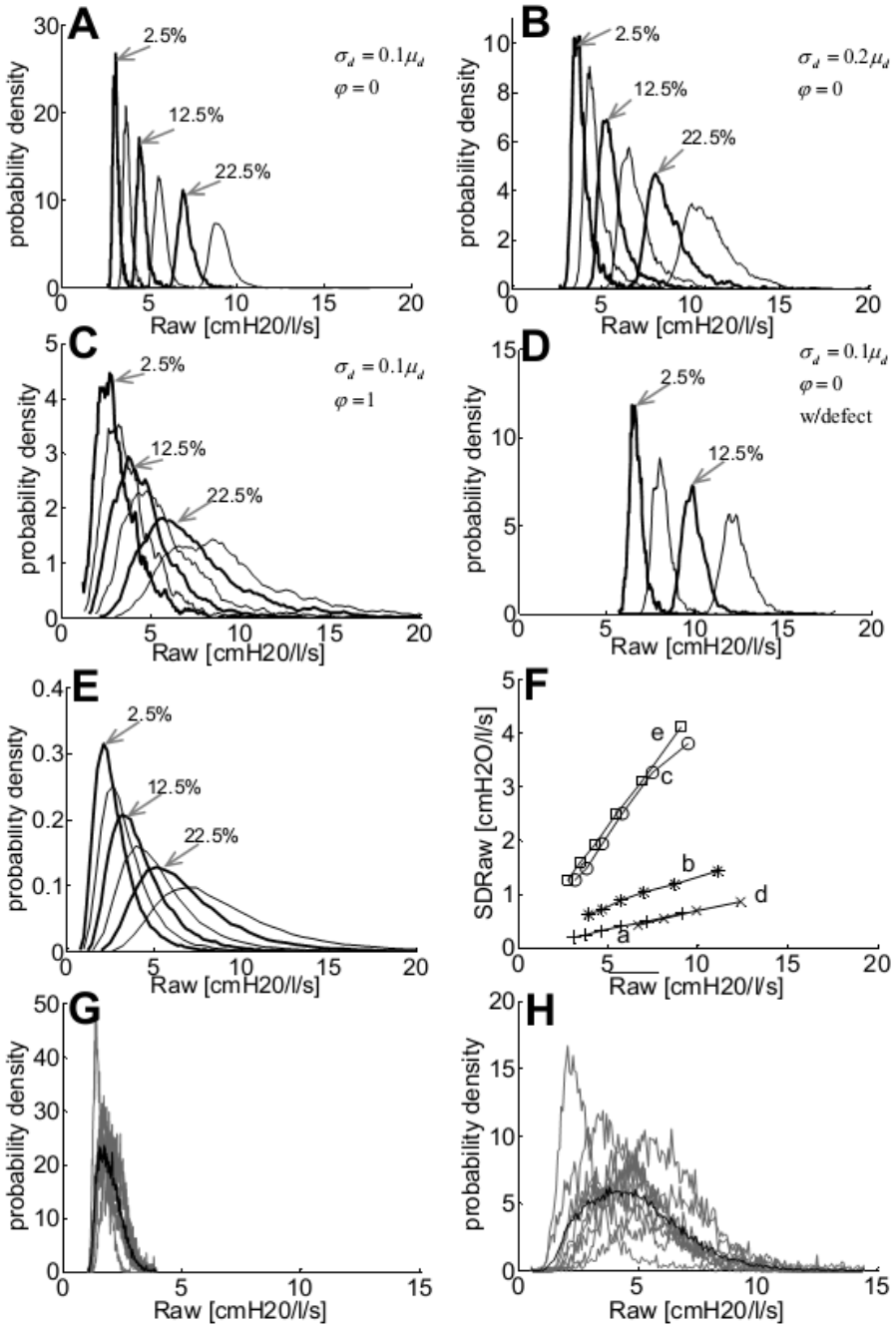

Figure 11. Resistance histograms at various levels of mean airway constriction and different model effects in panels b-e. a) Histograms are generated with the initial conditions of $\sigma_d = 0.1\mu$, $\varphi = 0$, with no defects. In b) σ_d is doubled, in c) the coherency is set at its maximum of $\varphi = 1$, and in d) a large defect is added at the second generation airway. The total coherent scenario c) is very similar to the single airway model (e). In f) are shown the dependence of SDR_L on $\overline{R_L}$ for the different simulations. These simulated distributions can be compared to FOT *Rrs* distributions from Que et al. (Que, Kenyon et al. 2001) comparing normal subjects g) to asthma subjects h). Each gray line is the distribution from an individual, and the bold line indicates the mean for the group.

3.4.6 FOT DATA FROM PATIENTS

Data collected from asthmatic and normal patients by Que et al.(Que, Kenyon et al. 2001) were analyzed by comparing the average histograms from each group, which were significantly different as previously reported. *Rrs* from the asthmatic patients (solid line Figure 12) were right-shifted, with a more broad distribution and increases in *SDRrs* compared to normal patients (Figure 11g and Figure 11h).

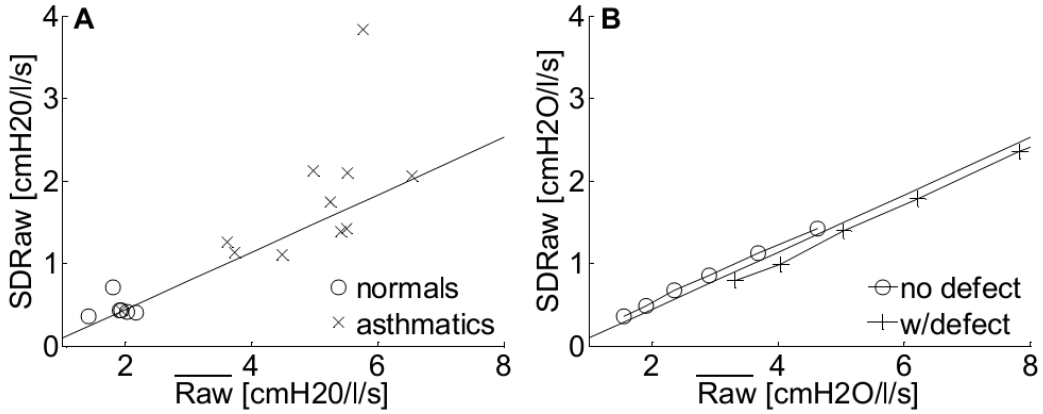

Figure 12. a) Comparing the slope of SDR_L to R_L from the model predictions to the estimated average $slope_R$ value in patients measured from Diba et al. (Diba, Salome et al. 2007) and from Que et al. (Que, Kenyon et al. 2001) . b) Introducing a large defect into lungs with different levels of constriction (ξ increasing from 2.5% as described in Methods) increased both $\overline{R_L}$ and SDR_L as seen in the rightward and upward shift, but along the same slope.

3.5 DISCUSSION

Here we used a statistical distribution approach to explore the sensitivity of $\overline{R_L}$ to several factors that can influence airway resistance levels and its variation that may be presented in a multibranch airway tree including dependence on diameter mean and

variation, regional coherency of variation, and the presence of ventilation defects. We demonstrated that Gaussian variation in airway diameter could produce distributions in R_L similar to that reported for *Rrs* in vivo. The presence of large ventilation defects and any decrease in average airway diameter increased both mean airway resistance as well as its variation, and predicted a robust relationship between SDR_L and R_L that mimicked the relationship between *SDRrs* and *Rrs* in vivo. The most potent influence on SDR_L was coherency in diameter variation between parent and daughter airways, but this was required to match FOT *Rrs* distributions.

Variation in lung function is a well-established feature of asthma over both long and short time scales. At long time scales, variation in peak expired flow is higher in asthma and is thought to arise from complex interactions between fluctuations in environmental stimuli and inflammatory status, amongst other factors (Suki and Frey 2003). Interestingly the variation in peak expired flow has been shown to exhibit temporal correlations that can be used to predict the likelihood of future declines in lung function as measured by FEV_1 (Frey, Brodbeck et al. 2005). Variation at shorter time scale is observed as fluctuations in airway impedance or resistance that are increased in asthma, and the fluctuations are thought to arise from changes in the activity of the airway smooth muscle. While variation at long and short time scales both involve changes in airway function and thus diameter, it is not clear if they share underlying mechanisms, although both are increased in asthma. In our model, the distributions of airway diameter and thus the $\overline{R_L}$ distributions are independent of any time-scale, and could be used to examine either behavior. Here we used the model to investigate variation over short time scales in *Zrs* for which there is ample available data.

We showed that increasing the variation of airway diameters throughout the airway tree not only increased SDR_L, but also $\overline{R_L}$. We have showed that the importance of variation in narrowing and coherency in variation at an anatomical level can alter the dependence between SDR_L and $\overline{R_L}$ while effect of ventilation defects plays a negligible role. While we demonstrated several factors arising from the multibranching airway tree that influence this dependence, the single airway model showed that this can arise solely from the transformation of the random diameter distribution via the inverse fourth power law dependence of resistance on diameter $\overline{R_L} \propto 1/d^4$. The strongly nonlinear geometric dependence of $\overline{R_L}$ on airway diameter strongly skews the original diameter distribution, producing long tails to high $\overline{R_L}$ values. When the diameter distribution of a single airway is widened through increasing σ_d, average airway resistance must increase as the effects on $\overline{R_L}$ with decreasing diameter are much greater than with increasing diameter. Similarly, in a multibranch lung, airways that narrowed had a stronger effect on total lung resistance than those that dilate, and would similarly skew the distribution increasing both $\overline{R_L}$ and SDR_L. This was true even while the standard deviation of airway diameter σ_d was increased and mean diameter μ_d was constant, increasing SDR_L and modestly increasing $\overline{R_L}$ (Figure 9c). We found importantly that SDR_L was consistently dependent on $\overline{R_L}$. This occurred whether σ_d was increased with no change in μ_d, or when μ_d was decreased with no change in σ_d, although when σ_d was unchanged the slope was lower as expected (Figure 9c). Similarly, when σ_d was increased in proportion to μ_d, such that they were increased together keeping the $slope_d$ of airway diameters constant, SDR_L and $\overline{R_L}$ also increased linearly (Figure 10, crosses). There exists an analytical solution for this particular case in the single airway model, helping to validate the model presented (Lall,

Cheng et al. 2007). The fact that a linear relationship is predicted in each case arises from the choice of variable that was independently varied in each case, and does not mean that a linear relationship between SDR_L and $\overline{R_L}$ is inevitable, as changing both μ_d,and σ_d arbitrarily can produce any point bound by the upper and lower curves in Figure 2. However, the linear relationship well matches baseline *Rrs* and *SDRrs* data across subjects in asthma and health, and for some subjects pre and post-bronchodilator changes in *Rrs* and *SDRr* within individual children with asthma (Lall, Cheng et al. 2007). Thus it is possible that the conditions for linear dependence that we have demonstrated may explain the reported linear dependence of *SDRrs* on *Rrs* in normal and asthmatic subjects as we discuss further below. Further, we explored several factors that may influence this dependence that arise within a multibranch lung.

3.5.1 REGIONAL COHERENT VARIATION

In obstructive disease the lungs tend to have regions that are poorly ventilated, often described as ventilation defects observed using hyperpolarized ^{3}He MRI, PET or CT, while other regions can be hyperventilated, thought to arise as the lung compensates to maintain an equal tidal volume. One mechanism thought to explain the development of regions of poor ventilation or 'patchy' ventilation in asthma is the mechanism of bi-stability of airway diameters in the lung. This bi-stability intrinsically arises from the softening and dilating behavior of airway smooth muscle exposed to oscillations in loading such as breathing in combination with parenchymal tethering and bifurcating airways as developed by Anafi and Wilson (Anafi and Wilson 2001) in their model of a single terminal unit embedded in parenchyma, and developed further in a multibranch

lung model by Winkler et al. (Venegas, Winkler et al. 2005; Winkler and Venegas 2007). Winkler and colleagues demonstrated the formation of regions of poor and well ventilated regions in the lung grew as airway narrowing migrated serially up and down connected airways. This occurred as fluctuations afforded airways by parenchymal tethering were decreased by a local loss of ventilation. With less ventilation to a particular region of the lung, oscillations that act to relax airway smooth muscle decrease, allowing local spreading of airway narrowing – providing one explanation for why airway diameter variation could behave dependently and coherently. Of course more directly, parent and daughter airways are mechanically connected and share local fluctuations in parenchymal tethering and thus would be expected to change diameter somewhat coherently. Here we simulated the effects of this interdependence of airway diameter up and down the airway tree by using a coherency parameter φ that controlled the similarity in dilation or contraction between parent airways and their daughters. We found that increasing coherency, while the distribution of variation amongst airway diameters was unchanged led to patchiness in airway narrowing, but also led to an increase in SDR_L with almost no change in $\overline{R_L}$. This was readily apparent with large φ (greater than 0.6, Figure 10). The patchiness in airway narrowing we observed is reminiscent of the patchy ventilation reported by Winkler et al. in their models and subjects (see video in online supplement). That coherency of airway diameter variation had perhaps the most potent effect on SDR_L relative to $\overline{R_L}$ implies that any mechanisms that leads to interdependence and regional airway narrowing tends to increase the slope of the SDR_L vs. $\overline{R_L}$relationship, compared with simply random fluctuations in airway diameter within the airway tree.

As described above, *SDRrs* is proportional to *Rrs* across subjects with asthma and healthy controls, and in fact all subjects appear to fall on a single relationship. Diba et al. (Diba, Salome et al. 2007) reported *SDRrs* was highly correlated with *Rrs* with regression coefficient of $r = 0.81$ from 102 nonasthmatics and $r = 0.91$ from 38 asthmatics with apparently the same dependence with slope estimated from their data of 0.35. Que et al. (Que, Kenyon et al. 2001) also reported *SDRrs* and *Rrs* data from asthma and control subjects, and when we compute the slope here, it well matches the data of Diba et al. (Diba, Salome et al. 2007) with a slope of 0.31, similar y-intercept, and $r = 0.67$ (Figure 6a). Indeed, the fact that two studies that report *SDRrs* and *Rrs* from two different countries can have nearly the same $slope_R$ is noteworthy, given the range in *Rrs* amongst subjects was from 1 to 7 $cmH_20/l/s$. and that asthmatic subjects in Que et al. (Que, Kenyon et al. 2001) had a much higher resistance of 4.90 (SD 1.06) $cmH_2O/l/s$ compared to the controls with *Rrs* of 1.80 SD 1.06) $cmH_2O/l/s$. In both studies, subjects with asthma had higher *Rrs*, but also higher *SDRrs* in proportion such that the presence of asthma is represented by a shift up the line, rather than any change above or below the line. This is surprising as it likely limits the number of mechanisms for how fluctuations in airway diameter may lead to fluctuations in *Rrs*. For example, explaining the increased *SDRrs* in asthma via increased coherency of ventilation alone is not likely, since this should lead to greater changes in *SDRrs* than *Rrs*.

As an exercise to compare our model to these measured data, we generated results with similar slope, at $\varphi = 0.88$, and σ_d a constant fraction of the mean diameter at $0.11\mu_d$ (Figure 12a). While other parameter choices in models could nearly match the data, this model was perhaps the most reasonable compared with constant μ_d or σ_d models which

are unlikely. While Figure 12a shows the *SDRrs* vs. *Rrs* relationship from Diba et al. together with this multibranch model prediction, we do not imply these parameters correspond precisely to the actual variation of airway diameters within the lung. One reason is that we limited the contribution to variation in $\overline{R_L}$ to arise solely from airway diameter fluctuations, while other factors will contribute to the total airway variation in airway resistance in a recording such as breathing and transducer noise. However the fact that tuning a simple coherency parameter and using a fixed $slope_d$ model predicts the same observed relationship as in FOT measurements between SDR_L and $\overline{R_L}$ is remarkable.

3.5.2 DEFECTS

As mentioned, ventilation defects have been identified using hyperpolarized MRI and other techniques. They are commonly defined in MRI as a focal signal void within a region of the lung. Ventilation abnormalities are hallmark findings in obstructive airway-related lung diseases such as asthma (Kaczka, Ingenito et al. 1997; de Lange, Altes et al. 2007) and COPD (Parraga, Ouriadov et al. 2007; Parraga, Mathew et al. 2008) and can vary in volume and number, and importantly these are absent in healthy young never-smokers. We found that adding a large defect increased both $\overline{R_L}$ and SDR_L, but maintained a similar $slope_R$ (Figure 12b). The increase in $\overline{R_L}$ from a defect was expected due to the loss in parallel airway resistance pathways, but the reason for the slight increase in SDR_L is less clear. A plausible mechanism is that because a defect removes some airways from contributing to R_L, it thus also removes the ability of those airways to compensate for other airways in the unaffected portion of the lung. That is, the number of

available configurations or states for the set of airway diameters within the lung were reduced leading to an increased sensitivity of SDR_L to airway diameter variation. Indeed with no defects, we would expect the overall variation in SDR_L to be its lowest as there are a maximum number of airways varying able to compensate for changes in each other. This predicts that stable defects, consistent with persistent defects observed in asthma (Samee, Altes et al. 2003) may contribute to increased variation in airway resistance, with larger or more numerous defects having a greater effect. However, the increase in SDR_L we predict could be reversed if either hyperventilation in non-defective regions or an increase in FRC were sufficient to increase mean airway diameter, but this is inconsistent with *SDRrs* changes in *Rrs* observed with asthma (Que, Kenyon et al. 2001; Diba, Salome et al. 2007; Lall, Cheng et al. 2007).

3.5.3 LIMITATIONS

This model examined the effects of varying airway diameters on $\overline{R_L}$ and SDR_L including some multibranch factors such as coherency and ventilation defects. We did not seek to predict the temporal behavior of $\overline{R_L}$ here concentrating only on parameters of the amplitude distribution, specifically mean airway resistance and is variation computed by SDR_L. Thus this model explicitly excluded temporal features of airway narrowing, and does not track changes in $\overline{R_L}$ from excitation-contraction and load-dependent airway narrowing as well as viscoelastic behavior or redistribution of ventilation via the pendelluft effect (Otis, McKerrow et al. 1956). The model was instead an examination of the potential effects on the statistical distribution of $\overline{R_L}$ of heterogeneity in airway narrowing, including changes in diameter fluctuation distributions and the presence of

large scale ventilation defects. This resulted in a computationally feasible examination of $\overline{R_L}$ and its distribution properties. However, it is possible that temporal dynamics may have an effect on the shapes of the distribution function for $\overline{R_L}$ and could thus alter the particular slopes we determined between SDR_L and $\overline{R_L}$ for example. However it is unlikely temporal dynamics would greatly affect the roles of the mean airway diameter, standard deviation of airway diameter, coherency, or presence of defects. Furthermore, temporal dynamics were apparently not needed to predict the established distribution profile for *Rrs* or reported correlation of *SDRrs* on *Rrs*.

As we did not have temporal dynamics, we also did not have breathing explicitly included in our model. However, if breathing is considered to be a homogenous effect increasing and decreasing airway diameters, this condition is like that of the 100% coherently varying lung, with airways varying in concert, for which we also explored altering mean airway diameter and its standard deviation . Other contributions to SDR_L obtained *in vivo* could include artifactual glottis closures, intermittent leaks or events such as coughs or swallows. While obvious artifacts were removed by Diba et al. (Diba, Salome et al. 2007) and Que et al. (Que, Kenyon et al. 2001) it is possible that some artifacts were undetected contributing to increased SDR_L that would be predicted for a given parameter set in our model.

Similar to other models, we neglected any contribution to lung impedance from gas compression or airway elastance, as lung elastance is dominated by the highly compliant lung tissue (Kaczka, Ingenito et al. 1997; Kaczka, Ingenito et al. 1999). Elastance was then assigned to the terminal airspaces, but was essential since these can contribute to determining airway resistance in a lung with time-constant heterogeneity as

first demonstrated by Otis (Otis, McKerrow et al. 1956). However heterogeneity in airway compliances would likely somewhat broaden the distribution of R_L.

3.5.4 PHYSIOLOGICAL INTERPRETATION OF CONSTANT SLOPE$_R$

Why *SDRrs* is proportional to *Rrs* giving nearly a constant $slope_R$ of approximately 0.35 across all subjects, with or without asthma, is an interesting question. This implies that factors with a strong influence on the slope of *SDRrs* to *Rrs* are unlikely to vary substantially across individuals. Since coherency of ventilation had a potent effect in our model, whatever coherency in diameter motions that may be present in vivo between daughter and parent airways is unlikely to change much amongst individuals. Yet why the ratio of *SDRrs* to *Rrs* should be so apparently consistent amongst individuals and be approximately 0.35 is unclear. We have shown in our model that changes in mean airway diameter such as would occur with lung growth, airway constriction or dilation, or with body size does not affect the $slope_R$, and the effect can arise from a lung modeled as a single airway which suggests as dominant mechanism is from the inverse 4^{th} power law dependence of airway resistance on diameter and thus is geometrical in origin as suggested by Lall et al.(Lall, Cheng et al. 2007).

The single airway or branching tree model did not include other sources of resistance such as turbulent or transitional flow that would occur in the glottis and upper airways. This could be better described using Womersley flow rather than Poiseuille flow, but this is complicated, especially if interactions with breathing are considered. Louis and Isabey (Louis and Isabey 1993) indicated that this begins to affect *Rrs* estimated by FOT in humans at 7 Hz for breathing > 0.5 l/s which indicates this may be a

small factor and we may underestimate lung resistance, and could affect the $slope_R$ in our model. Either transitional or turbulent flow does not have any appreciable effect as the model could produce similar linear SDR_L vs $\overline{R_L}$ to that in vivo, or other factors may contribute to the fixed $slope_R$ in vivo. However, deviations from this relationship in vivo have been reported with bronchodilator administration. Lall et al found that changes in *SDRrs* with bronchodilator exceeded decreases in *Rrs* in a subset of children with asthma, and *SDRrs* and *Rrs* were not proportional in this group (Lall, Cheng et al. 2007). This means that in some children, the additional variation in *Rrs* at baseline might have been attributable to additional abnormal fluctuations in airway diameter, possibly reflective of asthma control (Frey, Maksym et al. 2011). If a consistent $slope_R$ arises largely from geometrical factors, then it is possible that at extreme lung volumes $slope_R$ may be altered, but this has not been examined, and there was little change in the proportionality of *SDRrs* to *Rrs* with upright and supine positions (Diba, Salome et al. 2007).

We observed that a large defect could substantially increase $\overline{R_L}$ and SDR_L, shifting the values rightwards and upwards but with no change in the slope of SDR_L to $\overline{R_L}$ (Figure 11B). The fact that adding a defect led to an increase in $\overline{R_L}$ is intuitive, but that it has a similar effect on its variation is not. This prediction is potentially useful because as defects are known to increase in both volume and number in asthmatic (de Lange, Mugler et al. 1999; de Lange, Altes et al. 2009) as well as COPD (Parraga, Ouriadov et al. 2007; Parraga, Mathew et al. 2008) patients, and are thought to be largely persistent over timescales of hours to weeks (Suki and Frey 2003).

In summary, we observed several conditions that predicted a linear relationship between $\overline{R_L}$ and SDR_L similar to established data. Likely SDR_L and $\overline{R_L}$ together depend on

airway diameter as described above, and both scale with homogeneous changes in airway dimensions on average as might occur with bronchoconstrictors and bronchodilators. The model predicted that airways must exhibit some localized coherency in airway diameter changes in order to exhibit regional ventilation heterogeneity and to approximate the reported slope of *SDRrs* to *Rrs*. These findings establish possible mechanisms for the relationship between *SDRrs* on *Rrs*. An increase in the SDR_L with an increase in defect size was also predicted, possibly representing an emergent phenomenon of the model, arising from a reduced number of available configurations within the airway tree, and thus increasing sensitivity of $\overline{R_L}$ to fluctuations amongst airway diameters. Thus SDR_L can be altered by several possible mechanisms independent of $\overline{R_L}$, yet the many mechanisms that act to constrain SDR_L and $\overline{R_L}$ support that this is likely a robust relationship that cannot be easily altered.

3.6 CHAPTER 3 REFERENCES

1. **Anafi RC, and Wilson TA**. Airway stability and heterogeneity in the constricted lung. *JApplPhysiol* 91: 1185-1192, 2001.

2. **Black LD, Dellaca R, Jung K, Atileh H, Israel E, Ingenito EP, and Lutchen KR**. Tracking variations in airway caliber by using total respiratory vs. airway resistance in healthy and asthmatic subjects. *J Appl Physiol* 95: 511-518, 2003.

3. **Brown RH, Kaczka DW, Fallano K, Chen S, and Mitzner W**. Temporal variability in the responses of individual canine airways to methacholine. *J Appl Physiol* 104: 1381-1386, 2008.

4. **Campana L, Kenyon J, Zhalehdoust-Sani S, Tzeng YS, Sun Y, Albert M, and Lutchen KR**. Probing airway conditions governing ventilation defects in asthma via hyperpolarized MRI image functional modeling. *JApplPhysiol* 106: 1293-1300, 2009.

5. **de Lange EE, Altes TA, Patrie JT, Battiston JJ, Juersivich AP, Mugler JP, III, and Platts-Mills TA**. Changes in regional airflow obstruction over time in the lungs of patients with asthma: evaluation with 3He MR imaging. *Radiology* 250: 567-575, 2009.

6. **de Lange EE, Altes TA, Patrie JT, Parmar J, Brookeman JR, Mugler JP, 3rd, and Platts-Mills TA**. The variability of regional airflow obstruction within the lungs of patients with asthma: assessment with hyperpolarized helium-3 magnetic resonance imaging. *J Allergy Clin Immunol* 119: 1072-1078, 2007.

7. **de Lange EE, Mugler JP, 3rd, Brookeman JR, Knight-Scott J, Truwit JD, Teates CD, Daniel TM, Bogorad PL, and Cates GD**. Lung air spaces: MR imaging evaluation with hyperpolarized 3He gas. *Radiology* 210: 851-857, 1999.

8. **Delacourt C, Lorino H, Herve-Guillot M, Reinert P, Harf A, and Housset B**. Use of the forced oscillation technique to assess airway obstruction and reversibility in children. *AmJRespirCrit Care Med* 161: 730-736, 2000.

9. **Diba C, Salome CM, Reddel HK, Thorpe CW, Toelle B, and King GG**. Short term variability of airway calibre - a marker of asthma? *JApplPhysiol* 2007.

10. **Frey U, Brodbeck T, Majumdar A, Taylor DR, Town GI, Silverman M, and Suki B**. Risk of severe asthma episodes predicted from fluctuation analysis of airway function. *Nature* 438: 667-670, 2005.

11. **Frey U, Maksym GN, and Suki B**. Temporal Complexity in Clinical Manifestations of Lung Disease. *J Appl Physiol* 2011.

12. **Horsfield K, and Cumming G**. Morphology of the bronchial tree in man. *J Appl Physiol* 24: 373-383, 1968.

13. **Jensen A, Atileh H, Suki B, Ingenito EP, and Lutchen KR**. Selected contribution: airway caliber in healthy and asthmatic subjects: effects of bronchial challenge and deep inspirations. *JApplPhysiol* 91: 506-515, 2001.

14. **Kaczka DW, Brown RH, and Mitzner W**. Assessment of heterogeneous airway constriction in dogs: a structure-function analysis. *J Appl Physiol* 106: 520-530, 2009.

15. **Kaczka DW, Ingenito EP, Israel E, and Lutchen KR**. Airway and lung tissue mechanics in asthma. Effects of albuterol. *Am J Respir Crit Care Med* 159: 169-178, 1999.

16. **Kaczka DW, Ingenito EP, Suki B, and Lutchen KR**. Partitioning airway and lung tissue resistances in humans: effects of bronchoconstriction. *J Appl Physiol* 82: 1531-1541, 1997.

17. **Lall CA, Cheng N, Hernandez P, Pianosi PT, Dali Z, Abouzied A, and Maksym GN**. Airway resistance variability and response to bronchodilator in children with asthma. *EurRespirJ* 2007.

18. **Louis B, and Isabey D**. Interaction of oscillatory and steady turbulent flows in airway tubes during impedance measurement. *Journal of Applied Physiology* 74: 116-125, 1993.

19. **Otis A, McKerrow C, Bartlett R, and et al.** Mechanical factors in distribution of pulmonary ventilation. *J Appl Physiol* 8: 427-443, 1956.

20. **Parraga G, Mathew L, Etemad-Rezai R, McCormack DG, and Santyr GE**. Hyperpolarized 3He magnetic resonance imaging of ventilation defects in healthy elderly volunteers: initial findings at 3.0 Tesla. *Acad Radiol* 15: 776-785, 2008.

21. **Parraga G, Ouriadov A, Evans A, McKay S, Lam WW, Fenster A, Etemad-Rezai R, McCormack D, and Santyr G**. Hyperpolarized 3He ventilation defects and apparent diffusion coefficients in chronic obstructive pulmonary disease: preliminary results at 3.0 Tesla. *Invest Radiol* 42: 384-391, 2007.

22. **Que CL, Kenyon CM, Olivenstein R, Macklem PT, and Maksym GN**. Homeokinesis and short-term variability of human airway caliber. *JApplPhysiol* 91: 1131-1141, 2001.

23. **Salerno M, Altes TA, Mugler JP, 3rd, Nakatsu M, Hatabu H, and de Lange EE**. Hyperpolarized noble gas MR imaging of the lung: potential clinical applications. *Eur J Radiol* 40: 33-44, 2001.

24. **Samee S, Altes T, Powers P, de Lange EE, Knight-Scott J, Rakes G, Mugler JP, III, Ciambotti JM, Alford BA, Brookeman JR, and Platts-Mills TA**. Imaging the lungs in asthmatic patients by using hyperpolarized helium-3 magnetic resonance: assessment of response to methacholine and exercise challenge. *JAllergy ClinImmunol* 111: 1205-1211, 2003.

25. **Suki B, and Frey U**. Temporal dynamics of recurrent airway symptoms and cellular random walk. *J Appl Physiol* 95: 2122-2127, 2003.

26. **Tawhai MH, Hunter P, Tschirren J, Reinhardt J, McLennan G, and Hoffman EA**. CT-based geometry analysis and finite element models of the human and ovine bronchial tree. *J Appl Physiol* 97: 2310-2321, 2004.

27. **Tawhai MH, Nash MP, Lin CL, and Hoffman EA**. Supine and prone differences in regional lung density and pleural pressure gradients in the human lung with constant shape. *J Appl Physiol* 107: 912-920, 2009.

28. **Tgavalekos NT, Musch G, Harris RS, Vidal Melo MF, Winkler T, Schroeder T, Callahan R, Lutchen KR, and Venegas JG**. Relationship between airway narrowing, patchy ventilation and lung mechanics in asthmatics. *EurRespirJ* 29: 1174-1181, 2007.

29. **Tgavalekos NT, Venegas JG, Suki B, and Lutchen KR**. Relation between structure, function, and imaging in a three-dimensional model of the lung. *AnnBiomedEng* 31: 363-373, 2003.

30. **Tzeng YS, Lutchen K, and Albert M**. The difference in ventilation heterogeneity between asthmatic and healthy subjects quantified using hyperpolarized 3He MRI. *JApplPhysiol* 106: 813-822, 2009.

31. **Venegas JG, Winkler T, Musch G, Vidal Melo MF, Layfield D, Tgavalekos N, Fischman AJ, Callahan RJ, Bellani G, and Harris RS**. Self-organized patchiness in asthma as a prelude to catastrophic shifts. *Nature* 434: 777-782, 2005.

32. **Winkler T, and Venegas JG**. Complex airway behavior and paradoxical responses to bronchoprovocation. *JApplPhysiol* 2007.

CHAPTER 4. HYPERPOLARIZED ^{3}HE MAGNETIC RESONANCE IMAGING VENTILATION DEFECTS IN ASTHMA: RELATIONSHIP TO AIRWAY MECHANICS

4.1 ABSTRACT

Ventilation heterogeneity is a hallmark finding in obstructive lung diseases such as asthma and chronic obstructive pulmonary disease (COPD). Although functional pulmonary magnetic resonance imaging (MRI) has been previously used to identify focal ventilation defects that are in fact regions of diminished or abnormal gas distribution, it is not clear how the presence and magnitude of ventilation defects relate to clinically relevant measurements of airway function. Here, we extend modeling approaches to explore the relationship of hyperpolarized ^{3}He MRI ventilation defects (VDefs) with lung resistance (R_L) and lung reactance (X_L). To accomplish this, we modified an anatomically correct airway tree (by constricting specific airways) to incorporate the regional heterogeneity of pulmonary ventilation estimated using hyperpolarized ^{3}He MRI. MRI ventilation maps acquired for 25 asthma subjects were used to generate masks that were co-registered to the model airway tree; airways determined to be within ventilation defect regions were constricted to 10% of their baseline value and variation in lung resistance was achieved by altering the baseline airway diameters to 11% of the mean according to specific random distribution functions. Impedance was calculated for the entire lung using a lumped element approach. We observed that the slope relating the standard deviation of R_L (SDR_L) and R_L was significantly smaller than what was previously observed for models of homogeneous bronchoconstriction; these findings suggest that

ventilation heterogeneity and homogeneous bronchoconstriction have different effects on the relationship between SDR_L and R_L. Plethysmography measurements of airway resistance were a stronger predictor of ventilation defects compared to FEV_1. Furthermore, lung impedance (Z_L) generated in the model based on MRI-derived ventilation heterogeneity was strongly related to VDefs, and significantly stronger than plethysmography estimates of airway resistance and FEV_1, when restricting the relationship based on terminal airway generations.

4.2 INTRODUCTION

Functional lung imaging methods such as provided by hyperpolarized noble gas magnetic resonance imaging (MRI) have previously shown the presence of regionally persistent gas distribution or ventilation abnormalities, more commonly referred to as ventilation defects (VDefs) (de Lange, Mugler et al. 1999; Altes TA 2001; Samee, Altes et al. 2003; de Lange, Altes et al. 2007; Parraga G 2007) in obstructive lung diseases such as chronic obstructive lung disease (COPD) and asthma. At the same time, and in accordance with these findings, ventilation heterogeneity has also been observed using multiple breath nitrogen washout studies (Suki 1993; Downie, Salome et al. 2007) and positron emission tomography (PET) (Venegas, Schroeder et al. 2005; Venegas JG 2005) in a number of chronic respiratory conditions.

The size and extent of MRI-derived VDefs has been evaluated in relation to well-established measurements of pulmonary function such as the forced expiratory volume within 1 s (FEV_1) and showed rather modest but significant correlations in asthma (de Lange, Altes et al. 2006) and COPD (Kirby M 2011). Previous work (Costella M, Kirby M et al. 2012) also suggested the contrary, in that no significant relationships were reported in 25 well-controlled asthma subjects for ^{3}He MRI ventilation defect percent (*VDP*) and $FEV_{1\%pred}$. It is clear that the relationship between FEV_1 and hyperpolarized ^{3}He *VDP* is not fully understood, nor are the exact structural/morphological/anatomical determinants of VDefs in pulmonary disease (Kirby M 2010).

The forced oscillation technique (FOT) is another lung function measurement tool that provides an estimate of respiratory impedance over time. Similar to breath-hold imaging methods, the FOT measurement is acquired at a particular breathing volume,

such as FRC. Importantly, the variability of respiratory impedance has been shown to be a predictor of future asthmatic episodes (Frey, Brodbeck et al. 2005) and therefore measurements of respiratory impedance may be clinically important. Que et al. previously observed that the variability in respiratory system impedance (*Zrs*) approximated a log-normal distribution and that the degree of variability of *Zrs* was significantly lower in healthy subjects compared to those with asthma (Que, Kenyon et al. 2001). Diba et al., Lall et al., and Muskulus et al. each later showed that although there was greater variability of *Zrs* in asthma subjects than in healthy subjects, the variability was increased in proportion to the mean respiratory system impedance, implying that the mechanism governing airway impedance similarly governed the variability of *Zrs* (Diba, Salome et al. 2007; Lall, Cheng et al. 2007; Muskulus, Stats et al. 2010).

To better understand the relationship between heterogeneous ventilation patterns visualized using MRI and respiratory system impedance, we investigated a model whereby predictions of lung impedance *(Z_L)* were driven by MRI ventilation defect maps acquired in asthmatic subjects. Predictions of lung impedance were generated using a multibranch airway lung model where airways that were spatially related to MRI-derived hypo-ventilated regions were reduced to 10% of their baseline value. The same lung airway model was previously developed to evaluate how fluctuations in airway diameters could explain airway resistance (R_L) and the standard deviation of R_L (SDR_L) (Leary, Bhatawadekar et al. 2011). We want to better understand the underlying physiological and airway mechanical constraints that drive the generation or resolution of VDefs. To begin to accomplish this, we used the airway model system to explore how the presence of experimentally derived ^{3}He MRI VDefs in asthmatics is related to computationally

derived $R_{L,}$ SDR_L and lung reactance (X_L) and how this compared with experimental measurements of FEV_1 and plethysmography *Raw*.

4.3 METHODS

We adapted a computational model of a three-dimensional (3D) anatomically guided airway tree consisting of 64,895 airways (provided by M. Tawhai, U. Auckland). This airway tree model was used to predict impedance as previously described (Leary, Bhatawadekar et al. 2011), but with adaptive airway closure 25 asthmatic patients and regionally specific VDefs estimated using hyperpolarized ^{3}He MRI.

4.3.1 STUDY SUBJECTS AND DESIGN

As previously described (Costella M, Kirby M et al. 2012), 25 subjects with asthma between 18 and 60 years of age with a diagnosis of asthma and $FEV_1 \geq 60\%$ provided written informed consent to a Health Insurance Portability Accountability Act (HIPAA)-compliant protocol approved by Health Canada and the local research ethics board at Western University. During a single two hour visit, medical history and vital signs were recorded and baseline pulmonary function tests completed. MRI was performed at baseline, post-MCh (at the provocative concentration causing a 20% decrease in FEV_1 (PC_{20}) or the final dose) and on a third occasion, 25 minutes after administration of 200mg salbutamol through a pressurized metered dose inhaler (pMDI) and *Aero Chamber Plus* valved holding chamber (Trudell Medical International, London, Canada).

4.3.2 IMAGE ACQUISITION

MRI was performed as previously described (Parraga G 2007; Costella M, Kirby M et al. 2012) on a whole body 3.0 T Discovery 750 scanner (General Electric Health Care (GEHC), Milwaukee, WI) in the coronal plane using a fast gradient-recalled echo method (14 s breath hold; repetition time (TR) = 4.3 ms; echo time (TE) = 1.4 ms; flip angle = 7 degrees; field of view = 40cm x 40cm; matrix, 128 x 128; 14 - 17 slices; slice thickness = 1.5 cm)). ^{3}He gas was polarized by a turn-key, spin-exchange polarizer system and doses of the gas (5 ml/kg body weight) were administered in one liter Tedlar® bags diluted with ultrahigh purity, medical grade nitrogen (Spectra Gases, Alpha, NJ). Hyperpolarized 3He MRI was acquired in breath-hold after inspiration of a 1L gas mixture from FRC as previously described (Parraga G 2007). All scans were performed in the supine position and were completed within five minutes of patient positioning in the scanner.

4.3.3 IMAGE ANALYSIS AND GUIDANCE

^{3}He MRI semi-automated segmentation was performed using custom software generated using MATLAB R2007b (The Mathworks Inc., Natick, MA, USA), as previously described (Kirby M 2012). Briefly, ^{3}He MRI static ventilation images were segmented using a K-means approach that classified voxel intensity values into five clusters ranging from signal void (cluster 1, C1 or ventilation defect volume (VDV)) and hypo-intense (or partial volume) to hyper-intense signal (C5). For delineation of the ventilation defect boundaries, a seeded region growing algorithm (American Thoracic Society 2000) was used to segment the ^{1}H MRI thoracic cavity for registration to the

cluster-map, and ^{3}He VDP was generated using VDV normalized to the thoracic cavity volume (Figure 13).

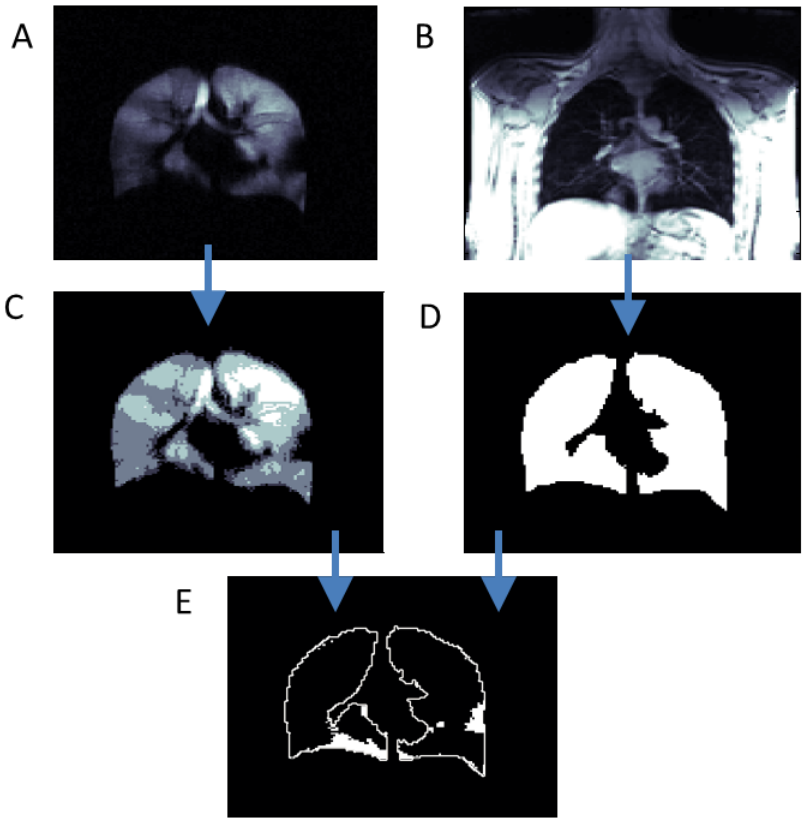

Figure 13. Identification of VDefs from MRI data. Starting from raw data of A) HP 3He MRI and B) conventional proton MRI, levels of ventilation from A) are identified in C) using the k-means algorithm described. These data are the registered onto the D) the proton mask to yield the final data in E). Here the regions with the lowest level of ventilation that are within the proton mask are considered VDefs.

Deformable registration was used to normalize all the patients to have the same sized lung as the mesh airway tree model. Briefly, each MRI ventilation map was co-registered to the mesh lung by resizing the 3D scan in the volumetric space of the mesh model lung (Figure 14). The physical boundaries of the mesh lung were found as follows. First the posterior/anterior boundaries of the mesh lung were divided into an equivalent

number of coronal MRI slices. The superior/inferior boundaries of each MRI slice were then scaled to the mesh lung. Next, eight evenly spaced fiducial markers were then located along the lateral left and right boundaries for each MRI slice and scaled to the mesh lung. This process allowed each image set to be scaled to the corresponding lung mesh (*in silico* airway tree) and allowed normalized impedance predictions that were not altered by patient specific lung volumes.

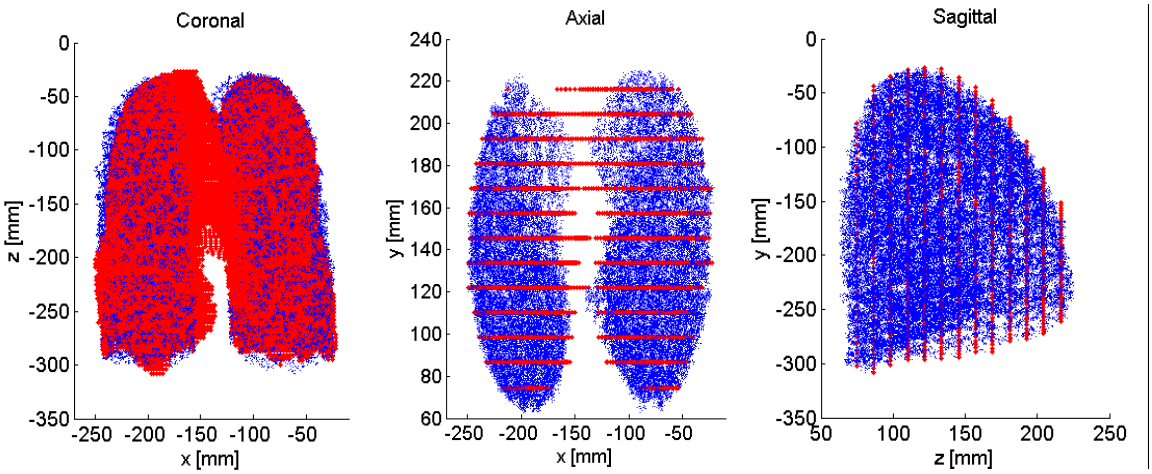

Figure 14. The registration fitting between the MRI proton mask and the mesh lung airway tree. The mesh lung is represented as tiny dots and can be distinguished from the MRI data which has the obvious slice acquisition method.

Once the corresponding slices of the MRI scanned image and the 3D lung mesh model were co-registered, any airway within the 3D mesh slice that intersected a ventilation defect was closed to 10% of their initial diameter. This effectively greatly increased the ventilation time constant for this region. This was performed under three different airway diameter criteria: closing airways in distal generations up to 4, 9 or 14th generations having maximum diameters of 4.4, 0.8, and 0.5 mm respectively. A visual example of the spatial airway closing is shown in Figure 15 with airways, shown in

black, proximal to VDefs (pixels in red) are closed to 10%. In Figure 15, only airways that have been reduced in diameter are plotted.

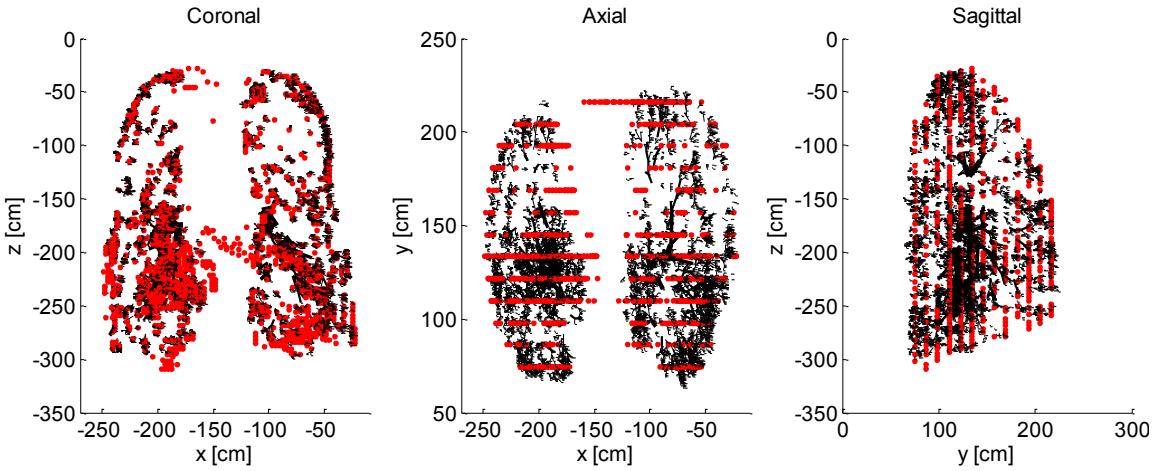

Figure 15. Visual comparison of closing airways in the mesh airway tree that correspond to the location of VDefs. The three planes are shown. Red dots indicate where a pixel of a defect has been located from the MRI scans and the black segments are airways that were identified as airways from the mesh model to have crossed into a ventilation defect region.

4.3.4 IMPEDANCE PREDICTIONS

The lung impedance was calculated for the entire lung using a lumped element approach as previously described (Leary, Bhatawadekar et al. 2011). The model was used to predict airway impedance over the time scale of several breaths. Although pressure and volume changes due to breathing were not included, the random variation in R_L observed in impedance measurements was replicated as follows. The remaining airways were allowed to fluctuate where the airway diameters would vary at 11% of the mean according to defined random distribution functions. As previously described, we also allowed for similarity between connecting airways by invoking correlation in stretch or contraction between parent and daughter airways of 88%. This model replicated both the

size and shape of recorded distributions of R_L from healthy subjects and asthmatic subjects (Que, Kenyon et al. 2001).

4.3.5 PULMONARY FUNCTION TESTS

Spirometry was performed before, during and after methacholine challenge using an *nddEasyOne* spirometer (ndd Medizintechnik AG, Zurich, Switzerland). Plethysmography including calculation of *Raw* was performed just prior to methacholine challenge using a *MedGraphics Elite Series* plethysmograph (MedGraphics, St. Paul, MN). Methacholine challenge was performed in the seated position according to ATS guidelines (American Thoracic Society 2000) using an *AeroEclipse II Breath Actuated Nebulizer* (Trudell Medical International) until PC_{20} was achieved or a maximum dose of 16.0 mg/ml was administered.

4.3.6 STATISTICAL ANALYSIS

Relationships were evaluated using Pearson correlations generated using GraphPad Prism version 4.00 (GraphPad Software, Inc., San Diego, CA, USA). Results were considered statistically significant when the probability of a null hypothesis was less than 5% ($p<0.05$). The Fisher z transformation was used to determine the significant differences between Pearson R values.

4.4 RESULTS

4.4.1 PATIENT SPIROMETRY

Experimentally acquired FEV_1%pred and hyperpolarized ^3He ventilation defect percent (*VDP*) showed a moderate linear correlation ($R = -0.54$, $p<0.001$) (Figure 16). Subject baseline data are shown using circles (○), post-bronchoconstriction (x), and post-salbutamol data with squares (□). Recall these are normalized values (using FEV_1% and VDP) that do not depend on the absolute size of the subject.

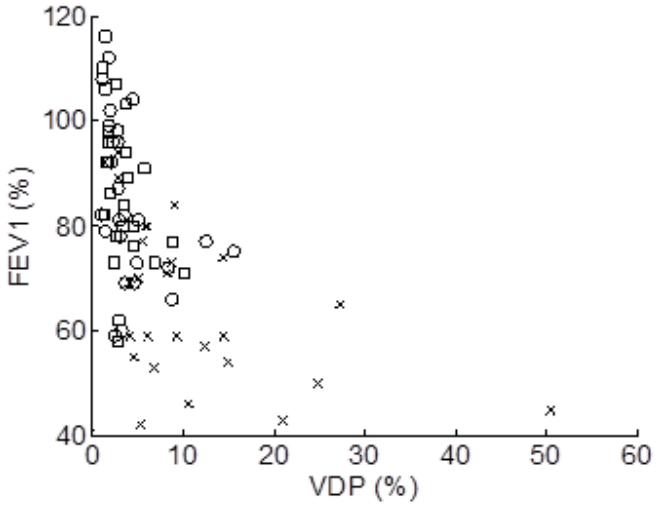

Figure 16. FEV1 % measurements plotted as a function of VDP (%) for each of the 25 patients under various lung stress conditions, at baseline (○), post bronchoconstriction (x), and post salbutamol (□).

VDP and FEV_1were also compared to the airway resistance (*Raw*) data that was acquired using whole body plethysmography of the patients at baseline. In Figure 17

moderate but significant correlations are shown for plethysmograph *Raw* and FEV_1 %pred (R=-0.500, p<0.001), and for plethysmograph *Raw* and *VDP* (R=0.711, p<0.001) (Figure 17b). Plethysmograph *Raw* values were found to be correlated to the predicted R_L values from our model when closing airways distal to and including the 9th generation (R=0.575, p<0.001) (Fig. 5c), and then closing airways distal to and including the 14th generation (Figure 17d).

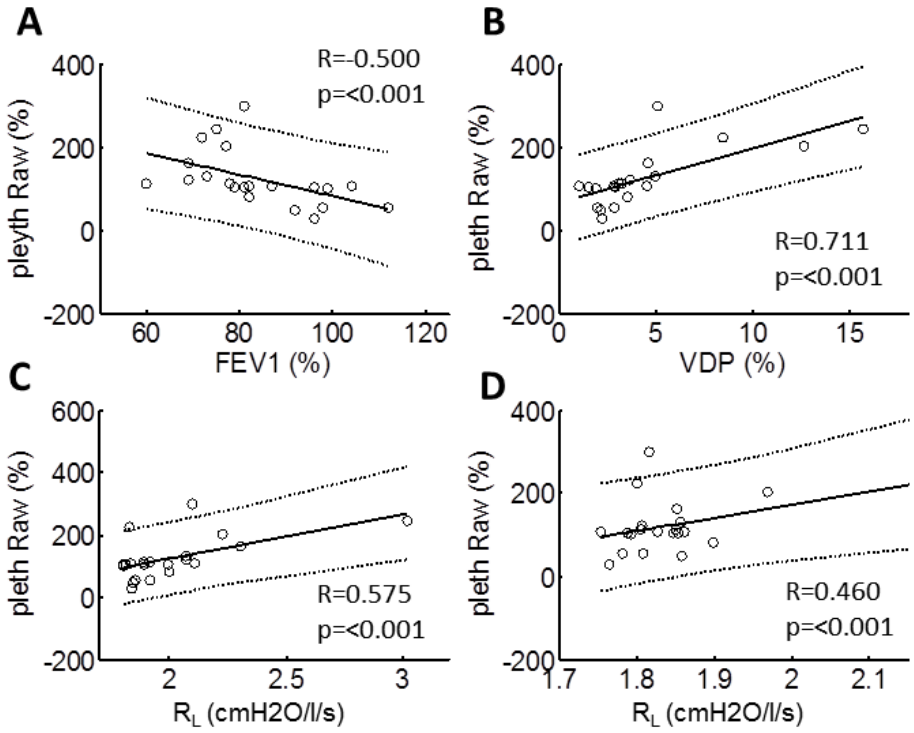

Figure 17. Raw % predicted values measured using the plethysmograph for patients at baseline compared to A) FEV1 predicted, B) ventilation defect percentage (VDP) , C) model predictions based on defects having a maximum generation closure at generation nine and distal, and D), same data but airway closure restricted to the fourteenth and distal generations.

The *VDP* for each of the 25 subjects at baseline, post-methacholine, and post-salbutamol were compared to model predictions for R_L and showed there were strong and significant correlations. In Figure 18a, shows the case whereby airways from the 9th generation and distal were closed (R=0.865, p<0.001) and Figure 18b (R=-0.931, p<0.001) shows the case where airways from the 14th generation and distal were closed (R=0.903, p<0.001). Lung reactance (X_L) for airway trees with the same closed respective airways is shown in Figure 18c (R=-0.799, p<0.001) and Figure 18d (R=-0.931, p<0.001). As shown in Figures 17 to 18, correlations were stronger for predicted R_L as compared to plethysmography *Raw* and this was confirmed statistically using Fisher z transforms, that showed that the predicted $R_{L>14}$ - *VDP* correlation was stronger than either plethysmography *Raw* - *VDP* correlation (z=2.22, p=0.026) or FEV_1 – *VDP* correlation (z=5.21, p<0.001). However when more central airways were allowed to close in the model, the model predictions of $R_{L>9}$ had a significantly stronger correlation with *VDP* than did FEV_1 (z=4.37, p<0.001), but this was not significantly different than the plethysmography *Raw* correlation with *VDP* (z=1.69, p=0.09). In addition, plethysmography *Raw* was significantly more strongly correlated with *VDP* than was FEV_1 (z=1.07, p=0.28). The strongest correlations with *VDP* from the model were observed when airways within the 14th and distal generations were closed. The significance of a stronger or weaker statistical relationship was also evaluated (Figure 18) by comparing closing airways within the 9th and distal generations (>9) with closing airways distal and including the 14th generation (>14) by calculating the Fisher z' transformation for both R_L and X_L. The correlation between $X_{L>14}$ and *VDP* was significantly stronger than the correlation between $X_{L>9}$ and *VDP* (z=4.81, p<.0001) and

the correlation coefficients between $R_{L>14}$ and $R_{L>9}$ were not significantly different (z=1.51, p=0.13).

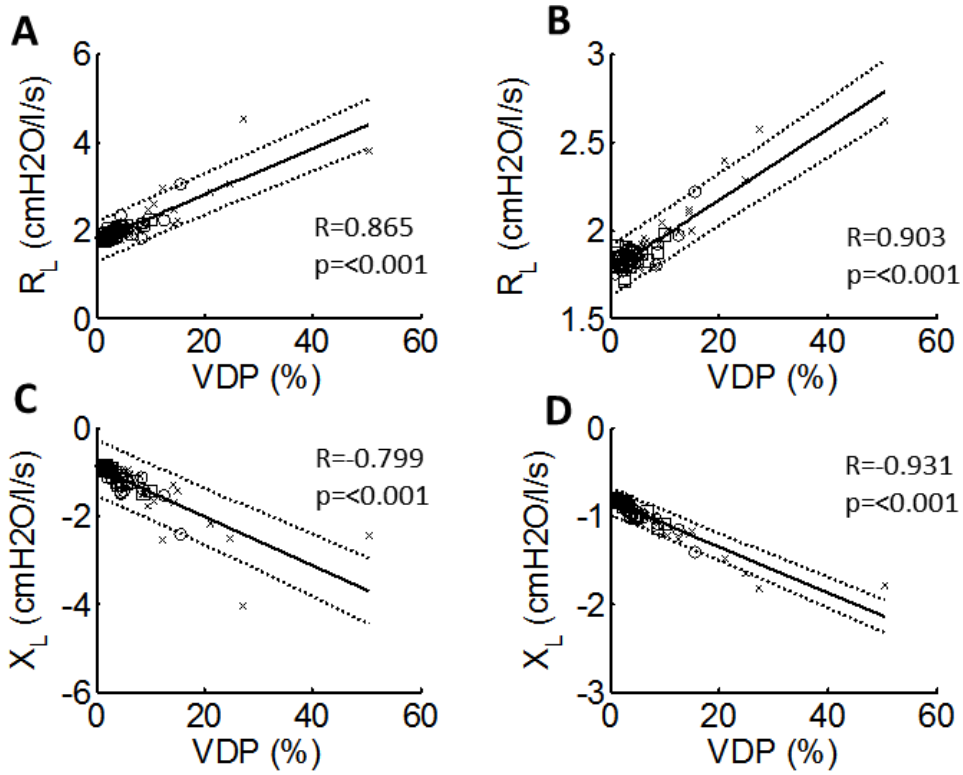

Figure 18. The correlation between VDP and RL at the 9th (A) and 14th (B) minimum allowed generation for airway closure, and the correlations between VDP with XL at the 9th (C) and 14th (D) generation. . Symbols as defined in Figure 16.

Previously, we observed that the robust relationship between SDR_L and $\overline{R_L}$ found in patient measurements using FOT can be explained by homogeneous bronchoconstriction with a given degree of airway diameter variability and coherency between mother and daughter airways (Leary, Bhatawadekar et al. 2011). From that work, we used the same parameters for variability and coherency to reproduce the slope found in patient data between SDR_L and $\overline{R_L}$ (Que, Kenyon et al. 2001; Diba, Salome et al. 2007), but here we included the addition of the 25 asthma subject specific VDef data to revisit the influence of VDefs on resistance variability. The relationship between SDR_L

and R_L yielded a smaller slope when distributions of defects were present as compared to predictions using only homogeneous airway constriction as indicated by a the straight line in Figure 19.

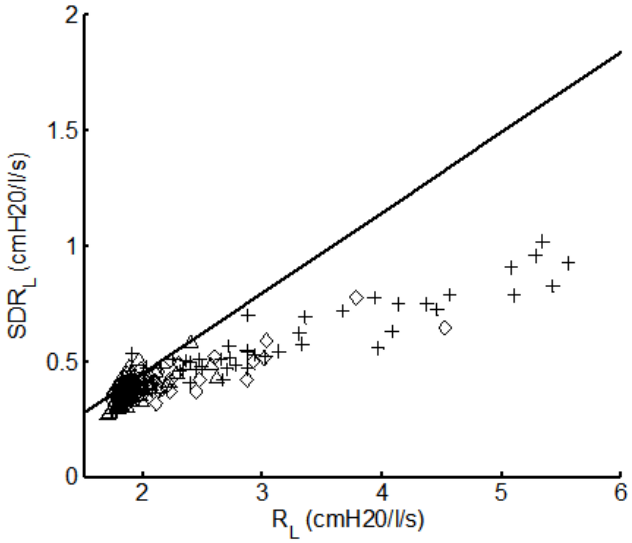

Figure 19. The relationship between SDR_L and R_L for airway closure models spanning different generations: airways in generations 14th and more distal are shown in triangles (Δ), airways in the 9th generation and distal are shown in diamonds (◊), and airways from the 4th generation and distal are shown as crosses (+) . As more airways are allowed to close from a greater number of generations, the resistance increases as expected. However, the SDR_L increase is disproportionally smaller than was previously observed with homogeneous constriction (shown as a solid black line).

4.5 DISCUSSION

Recent advances in pulmonary functional imaging have increased our understanding of regional nature of heterogeneous ventilation in asthma. How the presence of these defects contributes or can account for changes in lung mechanics in asthma has only recently been investigated. In other words, while pulmonary functional imaging provides information about the regional distribution of inhaled gases, we still do

not understand the etiology of ventilation abnormalities in asthma, or how gas distribution specifically relates to spirometry and measurements of lung mechanics. On the other hand, FOT measurements of the variability in respiratory impedance is also well documented but poorly understood, although it has been proposed to originate from fluctuations in airway dimensions associated with asthma airway pathologies. (Que, Kenyon et al. 2001). Understanding how abnormal airways impair inhaled gas ventilation and how they are related to the measures of the mechanical impedance of airflow is an important step towards understanding the meaning of these mechanical measurements in heterogeneous lung disease, and potentially in guiding therapy. To that end, this modelling study resulted in a number of important observations: 1) in 25 asthmatics, *VDP* was moderately but significantly correlated with FEV_1, 2) plethysmography *Raw* measurements had a stronger relationship with *VDP* than did FEV_1, and, 3) using a multibranch airway tree model, impedance predictions of R_L and X_L were strong and significant predictors of VDP and stronger than either FEV_1 and plethysmography *Raw*..

Studies that have compared FEV_1 to respiratory resistance measurements (*Rrs*) from FOT have found reasonably good correlations for the relative changes during bronchodilation using salbutamol (Zerah, Lorino et al. 1995). Because both FEV_1 and *Rrs* are indices of obstruction this would suggest that either FEV_1 or *Rrs* would be useful for evaluating ventilation heterogeneity and ^{3}He MRI *VDP*. However, here we show that FEV_1 is poorly related to ventilation defects, but measurements of airway resistance as we report here with plethysmography are better related to the lung dysfunction indicated by the presences of VDefs. We further show that our model predictions of impedance are also better correlated to VDefs. This appears to mean that measurements of airway

resistance are more sensitive to the functional impairment caused by the creation of VDefs. This may be important since FEV_1 has only shown weak or no correlations with *VDP* in asthma (de Lange, Altes et al. 2006), and moderate relationships in COPD (Kirby M 2010). This may be due to the fact that FEV_1 is a polyvalent measure that integrates airflow limitation over the full range of lung volumes, and while being sensitive to lung disease, it lacks specificity and is difficult to link to structure (Mead 1979). However, impedance measurements may be more sensitive to the presences of VDefs where the elastance is greatly increased due to derecruitment of the alveoli (Dellaca, Olerud et al. 2009). Furthermore, impedance measurements assess the lung function during tidal breathing which is at FRC, which is quite similar to the lung volume at which VDefs are determined during hyperpolarized ^{3}He MRI, despite the change in position from upright for plethysmography and normal impedance measurement to supine for MRI.

The work of Tgavalekos et al. also used an image functional modeling approach and showed very good agreement between VDefs and lung impedance, and also found that small and distal, airway closure was necessary for good agreement (Tgavalekos, Tawhai et al. 2005). In our study, we also found X_L was more strongly correlated with *VDP* when considering more distal airways located in generations (14^{th} generation and beyond) as compared to airways in generations 9 and beyond. This suggests that the VDefs were better described using more distal airways, and X_L may be more sensitive to the specific airways that were closed leading to VDefs. Conversely, we did not observe a significant difference between the R_L and *VDP* correlations when closing airways in generations 9 and beyond as compared to generations 14 and beyond. This suggests that although R_L is sensitive to defects, R_L may be less sensitive to specific airway closure

compared to X_L. This is consistent with data from pigs where R_L was sensitive to airway narrowing and X_L more sensitive to defects caused by occluded airways (Dellaca, Olerud et al. 2009).

Ventilation defects are common in both asthma and COPD, but the mechanisms responsible for these VDefs are likely not the same. For example, airway narrowing in asthma is due to increased muscle activation acting against a normal parenchymal tethering load and due to mucous plugging (Downie, Salome et al. 2007), and airway narrowing in COPD is thought to be due to loss of radial traction from the surrounding parenchyma, without necessarily a change in airway smooth muscle force. Regardless, the result is a restriction of airflow leading to regions of poor ventilation.

The relationship between the plethysmograph *Raw* and the modeled R_L was significant, but not strong. This may be due to differences in how the measurements were obtained as the patient pants during plethysmography leading to differences in contributions from the upper airway and possibly the chest wall. In addition, the breath-hold and increased diffusion rate of ^{3}He gas used during imaging may actually bias the ventilation map to show better ventilation in regions with long time constants that would not be ventilated during rapid or normal breathing cycles with room air as required for plethysmography or FOT measurements. However, regardless of the origin of the differences between the relationship of plethysmography *Raw* and modeled R_L, the fact that $R_{L>14}$ had a significantly stronger correlation with *VDP* as compared to plethysmography *Raw* is worth noting and generates hypotheses to test in future.

The predictions from the model do not account for small degrees of constriction or dilation in airway caliber throughout the remaining airways and this is important

because lung airways outside of ventilation defects may be partially inflated or hyperinflated that would alter R_L. This leads to a possible future improvement in the existing modeling approach whereby more sophisticated airway lumen sizing technique could be used to scale airway diameters according to relative change in ventilation from baseline. This could potentially further result in new information and understandings about the relationship between impedance predictions and ventilation heterogeneity or *VDP*.

Our investigations of the variation of R_L demonstrated that VDefs not only increase R_L but can also increase the variation of R_L (measured as SDR_L) which is in agreement with previous work (Leary, Bhatawadekar et al. 2011). Here we observed that adding different spatial distributions of VDefs based on patient data also generated a SDR_L and R_L relationship, although the slope that described this relationship was smaller than the slope that resulted when modeling homogeneous bronchoconstriction Fig. 7. This may suggest that ventilation heterogeneity in a parallel branching airway tree results in SDR_L to R_L relationships that are different as compared to homogeneous airway narrowing and lead to a useful way to diagnose an atypical increase in number of ventilation defects with a lower amount of bronchoconstriction typically observed in subjects.

Here we used a previously developed airway tree model and showed using data from 25 asthmatics that there were strong and significant correlations between MRI-derived *VDP* and model predictions of airway impedance. We showed that FEV_1 was weakly correlated with *VDP*, whereas *Raw* measured using plethysmography provided significantly stronger *VDP* correlations. Importantly, lung impedance predictions derived

from the model (and modified based on MRI VDefs) provided the strongest correlations with *VDP*. These findings contribute to the necessary first steps towards understanding ventilation heterogeneity in asthmatics and their relationship with airway mechanics such as measured using impedance. Taken together, our results suggest that measurements of airway impedance and not FEV_1 may provide a more appropriate estimate of asthmatic airway behavior that result in VDefs.

.

4.6 CHAPTER 4 REFERENCES:

1. **Altes TA PP, Knight-Scott J et al.** . Hyperpolarized 3He MR lung ventilation imaging in asthmatics: preliminary findings. *J Magn Reson Imaging* 13: 378-384, 2001.
2. **Anafi RC aWT**. Airway stability and heterogeneity in the constricted lung. *J Appl Physiol* 91: 1185-1192, 2001.
3. **Costella S, Kirby M, Maksym GN, McCormack DG, Paterson NAM, and G. P**. Regional pulmonary response to a methacholine challenge using hyperpolarized ^{3}He magnetic resonance imaging. *Respirology* 17: 1238-1246, 2012.
4. **de Lange EE, Altes TA, Patrie JT, Gaare JD, Knake JJ, Mugler JP, and Platts-Mills TA**. Evaluation of Asthma With Hyperpolarized Helium-3 MRI: Correlation With Clinical Severity and Spirometry. *Chest* 130: 1055-1062, 2006.
5. **de Lange EE, Altes TA, Patrie JT, Parmar J, Brookeman JR, Mugler JP, and Platts-Mills TAE**. The variability of regional airflow obstruction within the lungs of patients with asthma: Assessment with hyperpolarized helium-3 magnetic resonance imaging. *Journal of Allergy and Clinical Immunology* 119: 1072-1078, 2007.
6. **de Lange EE MJ, Brookeman JR, Knight-Scott J, Truwit JD, Teates CD, Daniel TM, Bogorad PL, and Cates GD**. Lung Air Spaces: MR Imaging Evaluation with Hyperpolarized ^{3}He Gas. *Radiology* 210: 851-857, 1999.
7. **Diba C, Salome CM, Reddel HK, Thorpe CW, Toelle B, and King GG**. Short-term variability of airway caliber--a marker of asthma? *Journal of Applied Physiology* 103: 296-304, 2007.
8. **Downie SR, Salome CM, Verbanck S, Thompson B, Berend N, and King GG**. Ventilation heterogeneity is a major determinant of airway hyperresponsiveness in asthma, independent of airway inflammation. *Thorax* 62: 684-689, 2007.
9. **Kirby M HM, Svenningsen S, Wheately A, McCormack DG, Etemad-Rezai R, and Parraga G.** Hyperpolarized ^{3}He Magnetic Resonance Functional Imaging Semiautomated Segmentation. *Academic Radiology* 19: 141-152, 2012.
10. **Kirby M ML, Heydarian M, Etemad-Rezai R, McCormack DG, and Parraga G.** Chronic Obstructive Pulmonary Disease: Quantification of Bronchodilator Effects by Using Hyperpolarized ^{3}He MR Imaging. *Radiology* 261: 283-292, 2011.

11. **Kirby M ML, Wheatley A, Santyr GE, McCormack DG, and Parraga G.** Chronic Obstructive Pulmonary Disease: Longitudinal Hyperpolarized ^{3}He MR Imaging *Radiology* 256: 280-289, 2010.
12. **Leary D, Bhatawadekar SA, Parraga G, and Maksym G**. Modeling stochastic and spatial heterogeneity in a human airway tree to determine variation in variation system resistance. *J Appl Physiol* (in press): 2011.
13. **Muskulus M SA, Sterk PJ, and Verduyn-Lunel S**. Fluctuations and determinism of respiratory impedance in asthma and chronic

obstructive pulmonary disease. *J Appl Physiol* 109: 1582-1591, 2010.
14. **Parraga G OA, Evans A, McKay S, Lam WW, Fenster A, Etemad-Rezai R, McCormack D, and Santyr G.** Hyperpolarized 3He ventilation defects and apparent diffusion coefficients in chronic obstructive pulmonary disease: preliminary results at 3.0 Tesla. *Invest Radiol* 42: 384-391, 2007.
15. **Que CL, Kenyon CM, Olivenstein R, Macklem PT, and Maksym GN**. Homeokinesis and short-term variability of human airway caliber. *JApplPhysiol* 91: 1131-1141, 2001.
16. **Samee S AT, Powers P et al.** Imaging the lungs in asthmatic patients by using hyperpolarized helium-3 magnetic resonance: assessment of respose to methacholine and exercise challenge. *J Alllergy Clin Immunol* 111: 1205-1211, 2003.
17. **Society AT**. Guidelines for Methacholine and Exercise Challenge Testing-1999. Am J Respir Crit Care Med, 2000, p. 309-329.
18. **Venegas J, Schroeder T, Harris S, Winkler R, and Melo M**. The distribution of ventilation during bronchoconstriction is patchy and bimodal: A PET imaging study. *Respiratory Physiology & Neurobiology* 148: 57-64, 2005.
19. **Venegas JG WT, Musch G, Vidal Melo MF, Layfield D, Tgavalekos N, Fischman AJ, Callahan RJ, Bellani G, and Harris RS**. Self-organized patchiness in asthma as a prelude to catastrophic shifts. *Nature* 434: 777-782, 2005.
20. **Verbanck S, Schuermans D, Paiva M, and Vincken W**. Nonreversible conductive airway ventilation heterogeneity in mild asthma. *J Appl Physiol* 94: 1380-1386, 2003.
21. **Wesseling GJ, Wanderhoven-Augustin IML, and Wouters EFM**. Forced oscillation technique and spirometry in cold air provocation tests. *Thorax* 48: 254-259, 1993.
22. **Winkler T, and Venegas JG**. Complex airway behavior and paradoxical response to bronchoprovocation. *J Appl Physiol* 103: 655 - 663, 2007.
23. **Zerah F, Lorino AM, Lorino H, Harf A, and Macquin-Mavier I**. Forced oscillation technique vs spirometry to assess bronchodilatation in patients with asthma and COPD. *Chest* 108: 41-47, 1995.

CHAPTER 5. EFFECTS OF AIRWAY TREE ASYMMETRY ON THE EMERGENCE AND SPATIAL PERSISTENCE OF VENTILATION DEFECTS

5.1 ABSTRACT

Asymmetry and heterogeneity in the anatomical structure of the human bronchial tree is well documented but the effect of anatomical asymmetry on bronchoconstriction and ventilation distribution during asthma attacks is unclear. In a series of seminal studies, Venegas et al. have shown that bronchoconstriction may lead to self-organized patterns of patchy ventilation in a computational model that well explained the ventilation defects (VDefs) observed in positron emission tomography images during induced bronchoconstriction. This model was in a symmetric branching tree where defect locations were determined by small differences in random perturbations, and did not consider the role of structural heterogeneity in the airway branching tree structure in the development of VDefs and their distribution. Using the computational model of bronchoconstriction that Venegas and Winkler developed, we investigated the effects of anatomical asymmetry using 13 generations of an asymmetric airway tree provided by M. Tawhai (U. Auckland) in comparison to a symmetric tree, and three trees with intermediate asymmetry. Ventilation patterns, lung resistance (R_L), lung elastance (E_L), and the entropy (H) of the ventilation distribution were compared at different levels of airway smooth muscle activation (Tr). Our results show that airway trees with normal asymmetry similarly produced patchy ventilation, but which were largely stable and reached steady state sooner. Interestingly, bronchoconstriction in normal asymmetry

resulted in lower R_L (~%50) and greater E_L (~%25). We found that although VDefs were universally triggered by airway instability, the locations of the VDefs were largely persistent due to anatomically normal asymmetry in airway branching, which may explain the emergence and the persistence in location VDefs found clinically.

5.1.1 INTRODUCTION

Bronchoconstriction that occurs in asthma or during induced bronchoprovocation can lead to airway instability (Anafi and Wilson 2001) resulting in different airway behaviors as some airways narrow and some other airways paradoxically dilate. Importantly, this behavior can be reproduced using a model of airway behavior that is fully symmetric in its anatomical and functional properties, yet produces markedly heterogeneous patchy patterns of ventilation suggesting that airway instability and airway interdependence could be principle mechanism for the emergence of ventilation defects (VDefs) during bronchoconstriction(Venegas JG 2005). However, depending on small random differences in the perturbation, which affects interdependencies among airways and, thus, symmetry breaking, VDef formation was random in location. Yet in subjects with asthma the majority of VDefs are observed to be fairly persistent in their location after individual challenges even over time periods of days to months (de Lange, Altes et al. 2007; Kirby M 2010).

Ventilation heterogeneity is well known to be a common symptom of many lung diseases, and has been observed using imaging techniques in obstructive diseases such as asthma (Samee, Altes et al. 2003) and COPD (Mathew, Evans et al. 2008; Kirby M

2011), as well as restrictive diseases such as cystic fibrosis (Kirby M 2012), and was also shown to develop in healthy elderly patients (Parraga G 2008). This widespread observation of ventilation heterogeneity within so many different types of lung disease and aging suggests a possible commonality that leads to VDefs in the lung. Several computational models of airway behavior have shown that the airway narrowing associated with bronchoconstriction may lead to multiple stable airway radii at the same transpulmonary pressure, as demonstrated in single airways (Anafi and Wilson 2001; Affonce and Lutchen 2006), and in branching lung models (Venegas JG 2005; Winkler and Venegas 2007). Venegas and Winkler demonstrated that airway closure and patchy ventilation was an emergent phenomenon that arose from the functional interactions of dynamic forces acting on the airway wall during bronchoconstriction (Venegas JG 2005). The heterogeneity in airway narrowing, and thus in ventilation, emerged from the dynamic mechanical interactions among bronchoconstriction, transmural pressures, and parenchymal tethering forces for each individual airway, but also arose from redistribution of airflow that alters these tethering forces and the tidal oscillations that affect the developed force of the smooth muscle on airways throughout the airway tree (Winkler and Suki 2011). Strikingly, they showed that the heterogeneity emerged in a model with an anatomically and functionally fully symmetric airway tree that lacked the natural structural variation within an airway tree including airway radii, airway lengths and asymmetry in airway branching geometries (Venegas JG 2005; Winkler 2007; Winkler and Venegas 2007; Winkler and Venegas 2011). The locations of VDefs in a symmetric tree model have no preferred pattern, which is in contrast to the imaging evidence to date that shows that while some defects change over time with repeated

bronchoprovocation, more defects are persistent and reappear in the same locations (de Lange, Altes et al. 2007; Kirby M 2010), and the underlying mechanisms for this persistence is not understood.

We hypothesized that the asymmetric airway branching of the human lung affects airway behavior and lung function during bronchoconstriction including the emergence of VDefs and their location. We investigated the formation of VDefs during simulated bronchoconstriction with varying levels of branching tree asymmetry: from a fully symmetric lung to a typical asymmetric branching geometry as found in the human lung. We quantified the heterogeneity and persistence in VDefs as well as the relationship between lung asymmetry and lung impedance. Finally, we aimed to identify the difference between sister airways that predict differences in their behavior and, thus, the location of VDefs.

5.2 METHODS

5.2.1 CONSTRUCTION OF AIRWAY TREES

To investigate how anatomical asymmetry in terms of airway radius and length between daughter airways at branching points of the human airway tree contributes to lung function and spatial pattern of ventilation during constriction, five different airway trees were generated spanning in their degree of asymmetry from symmetric to an asymmetric tree based on human anatomy, which was provided by M. Tawhai, University of Auckland (Tawhai, Nash et al. 2009). Briefly, the structure for the asymmetric human tree was generated using x-ray multi-detector computed tomography

(MDCT) imaging (Tawhai, Nash et al. 2009) to identify airway lengths and radii up to the eight generation. Additionally, a volume-filling algorithm (Tawhai, Nash et al. 2009) was used to generate the distal airway generations maintaining daughter radius ratios and lengths consistent with published morphometric data (Horsfield and Cumming 1968). For this study, we used the airways from one half of the Tawhai tree starting at the main bronchus corresponding to generation 1 and then spanning over 12 generations. This airway tree is similar to the tree employed by Venegas et al.(Venegas JG 2005) and Winkler et al.(Winkler and Venegas 2007) that also used 13 generations, but their tree was symmetric and based on Weibel's morphometric data spanning the 4^{th} to 16^{th} generations. We compared our asymmetric tree behavior to a symmetric tree where both trees began at a larger airway, at generation 1. This was done in order to avoid a larger number of airways being included in the symmetric tree but not in the asymmetric tree, as the human airway tree has many airways that terminate between generations 13-17. The symmetric airway tree was created using airway radii and lengths of each generation equal to the mean radii and lengths of the same generation from the asymmetric tree. In order to eliminate the difference in total lung resistance between the symmetric and asymmetric trees, which were 0.6418 cmH2O/l/s and 0.8476 cmH2O/l/s respectively, the airways of the symmetric tree were scaled by $(0.6418/0.8476)^{0.25}$ so that total lung resistance was identical without any loss of symmetry.

Each airway tree model from symmetric to fully asymmetric consisted of 13 branching generations. However, the fully asymmetric tree model included pathways with different numbers of airways in generations between central and terminal airways. In order to use the same set of equations that was used for the symmetric tree of Venegas

et al.(Venegas JG 2005) and Winkler et al.(Winkler and Venegas 2007), the resistance of the model's airway elements distal to a terminal airway was set to zero so that they became connectors to the compliance elements of the model without affecting the distribution of airflows. Intermediate asymmetric airway trees were constructed by linearly scaling the difference in radii and lengths between the symmetric and the asymmetric tree, achieving trees with 0%, 25%, 50%, 75%, and 100% asymmetry for ventilation simulation. The variation in radii and lengths for the anatomically based asymmetric tree can be observed at each generation in Fig. 20. All airway trees with intermediate asymmetry had the same number of airway generations between central and terminal airways as the symmetric tree.

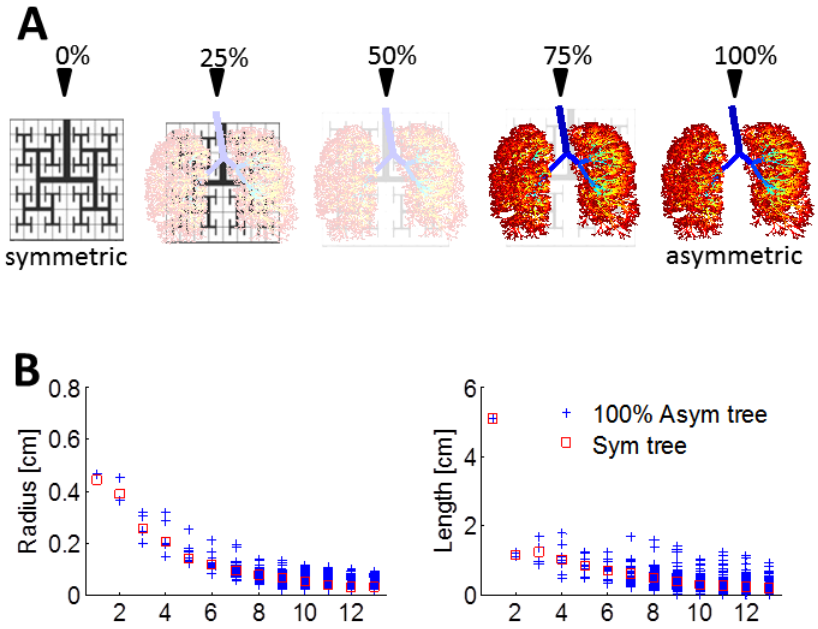

Figure 20. The symmetric tree as well as 3 intermediate airway trees with increasing degrees of asymmetry was generated by linear scaling of airway radius and length relative to the anatomically based asymmetric airway tree. Airway radius and length were distributed at each generation in the asymmetric tree (+), while they were identical in the symmetric tree (squares).

The total compliance in each airway tree was equivalent to a compliance of the respiratory system of 100 ml/cmH_2O scaled to the size of our reduced airway tree. Thus we set the compliance equal for all trees at 50 ml/cmH_2O, since this sub-tree is approximately 1/2 the volume of normal lungs, approximately one half of the normal human lung compliance. In the symmetric lung, each terminal unit has a compliance that was equal to the total tree compliance divided by the number of terminating airways. Since the asymmetric airway tree had a smaller number of terminal airways than the other trees, a weighting vector was used to properly adjust the model's compliance units such that the asymmetric lung sub-tree would have equal compliances among its terminal units, and the same total lung compliance as the symmetric lung. The adjustment resulted in a slight increase in compliance of each terminal unit of the asymmetric tree. However, we chose this method so that all airway trees with different degrees of asymmetry had equal pressure swings under the initial conditions of the models, so that the terminal units of all airway trees initially experienced the same relative tidal stretch, and thus the same airway smooth muscle stretch during a single pressure swing.

5.2.2 *MODEL OF BRONCHOCONSTRICTION*

As described above, a model of bronchoconstriction that can explain the emergence of VDefs due to multistate airway constriction was previously described by Venegas et al. (Winkler and Venegas 2011) and Winkler et al. (Winkler and Venegas 2007). Briefly, the mechanics of the airway wall and tethering forces are modeled using

the standard Lai-Fook equations relating parenchymal distortion to parenchymal tethering stress (Lai-Fook 1979). The airway mechanics, including the smooth muscle in response to dynamic stretch, were empirically included as modeled by Anafi and Wilson (Anafi and Wilson 2001) based on previous measurements of isometric force-length curves (Gunst 1983; Fredberg, Inouye et al. 1997; Shen X 1997). Thus the airway wall of a given airway is stretched by the tethering forces, which change dynamically during the breathing cycle due to tidal expansion of the parenchyma associated with the tidal changes in the gas volume. The behavior of the forces experienced by each airway and the resulting distributions of pressure, flow, and volume along the airway tree were solved numerically over a time course of 600 breaths to determine the steady state radii of airways (Venegas JG 2005; Winkler and Venegas 2007).

To explore the behaviour of the different airway trees at varying levels of smooth muscle stimulation, we introduced a relative smooth muscle activation level (*Tr*) as done previously (Winkler and Venegas 2007) which scaled the smooth muscle tension relative to the maximal tension used by Anafi and Wilson(Anafi and Wilson 2001). We conducted simulations for relative levels ranging from $Tr = 0.6$ which corresponded to baseline tone, increasing to a maximal activation of $Tr = 1.0$ in steps of 0.05 corresponding roughly to exponentially increasing methacholine concentrations. Evolution and patterns of bronchoconstriction of airways were compared across different airway trees for each degree of asymmetry. As also was done previously (Venegas JG 2005; Winkler and Venegas 2007), the initial level of airway smooth muscle contraction of $Tr=0.6$ corresponded to the predicted inner airway radius that coincided with in vivo

measurements of individual airway baseline size during quiet breathing, reported by Brown et al.(Brown and Mitzner 2001; Brown R 2011)

5.2.3 RANDOM PERTURBATION

A random perturbation is necessary in a symmetric airway tree to disturb the perfect symmetry in airflow throughout the branching network of airways, which would prevent any self-organized differentiation among different pathways. Thus, a random variation in airway wall thickness was added using 1% coefficient of variation (COV) in all airway trees for comparability. The effect of this perturbation was examined by running the simulations 10 times with different random perturbations.

5.2.4 CALCULATION OF IMPEDANCE

The impedance of the airway tree for a given realization of airway radius distribution was calculated using a lumped element approach where the impedance of the airways was summed following the branching patterns using well known series and parallel network impedance relations. Airway resistance for each branch was approximated using Pouseille's flow given by

$$R = \frac{128\eta L}{\pi d^4} \tag{31}$$

where η is the dynamic viscosity of humid air at 37 C, L is the length, and r is the radius of the airway. Each terminal unit was prescribed an elastance E_t to act functionally as the alveolar compartment accounting for parenchymal stretch, surface tension and any gas

compression (Tgavalekos, Venegas et al. 2003). This neglects any contribution from airway wall compliance or any gas compression within the airways, but this effect is much smaller than the effect of the alveolar compartment. The impedance for a terminal airway was defined as

$$Z_t = R_a + iX_t = R_a + iI_a\omega - i\frac{E}{\omega} \quad (32)$$

where X_t is the reactance of a terminal airway, I_a is the inertance calculated as

$$I_a = \frac{\rho_{air}L}{\pi r^2} \quad (33)$$

with L and r of the terminal airway and ρ_{air} the air density, and ω is the angular FOT frequency. The airway impedance for a non-terminal airway was calculated as

$$Z_a = R_a + iI_a\omega \quad (34)$$

The airway impedance of the entire airway tree could then be calculated numerically and further separated into real (resistance) and imaginary (reactance) parts. Because parallel pathways in a heterogeneous lung can lead to the product of reactances, the real part of the total impedance will have some dependence on the elastance and inertance, as was originally demonstrated in the two compartment parallel Otis lung model(Otis, McKerrow et al. 1956). We report here the resistance of the airway tree from the real part of the impedance as R_{L6}, the reactance as X_{L6} at 6 Hz and we calculated the dynamic elastance, E_L, by computing the impedance at breathing frequency (0.3Hz) and neglecting the small contribution of inertance I_L at this frequency giving

$$E_L = \omega^2 I_L - \omega X_L = \sim -2\pi * 0.3 * X_L \quad (35)$$

5.2.5 *VENTILATION MAPS AND SHANNON ENTROPY*

Ventilation maps for the lungs were produced from terminal unit ventilation organized in 2D similar to Venegas et al.(Venegas JG 2005). The final steady state flow distribution among terminal units was calculated by sending a mean normalized (a value of 1) unit of airflow at the main airway then solving for the partial flow at each individual (i^{th}) terminal airway. To determine the entropy, the probability distribution (p_i) was calculated from the relative flow of each terminal airway (using 256 bins) destined for alveoli. The Shannon entropy of flow was then calculated as a spatial heterogeneity index of flow as,

$$H = -\sum p_i \log (p_i) \tag{36}$$

At various level of muscle activation *Tr,* we compared the resultant airway tree configurations, R_{L6}, X_{L6}, the 2D mapped ventilation patterns, and H.

5.2.6 *PREDICTED AIRWAY BEHAVIOR*

We probed how initial structural and functional differences between the two sister airways at airway branching points affected the outcome in the airways constriction at the steady state. This was done by comparing several geometric and functional parameters of the airway tree to the final radii ratios of sister airways. We calculated the E value as the static value derived from a simple lumped element calculation of the parallel terminal elastances. We compared the geometric factor of the initial ratios of airway radius (r_i *ratio*), as well as the initial functional ratios R_{L6}, E, and finally the time constant (T_c=R_{L6}/E) to the final ratio of airway radii of the bifurcating sister pair at the steady

state. For the functional parameters, R_{L6}, E, and T_c, we included not only the local effect of each sister airway but also the portion of the subtending lung distal to that airway. This was done at different levels of the airway tree to examine the behavior of central (generations 2-6), mid (generations 7-9), and distal airways (generations 10-13). Initial parameter ratios were plotted against the final radius ratios forming contingency plots, where each quadrant could be considered showing a different behavior, such as a sister airway being initially smaller will also be smaller or become larger during steady state of bronchoconstriction (Fig. 26). We then calculated the fraction the ratios in the upper right and lower left quadrants of the 2x2 contingency squares, not including ratios of one, to determine the fraction of airways that exhibited initial airway asymmetry amplification, and we refer to it as the fraction of trending airways. This was similar for R_{L6}, E, and T_c ratio except that we counted the fraction when initially larger ratios (opposite quadrants) were associated with the sister airway with smaller final airway radius (lower right and upper left quadrants). The initial value of r_i, R_{L6}, E, and T_c for analysis was taken at breath 1 to allow the initialization procedure to propagate the perturbation in wall thickness into the airway tree. This was necessary since at the very start of the simulation symmetric the tree was indeed symmetric and there were no differences between sister airways. Once the symmetry was broken due to the random perturbation, the initial parameters would trend in the same manner as found in the asymmetric tree.

5.3 RESULTS

5.3.1 *RELATIVE CHANGE IN AIRWAY RADIUS*

Airway radii of the symmetric and different asymmetric airway trees with simulated bronchoconstriction of Tr = 0.9 were tracked as they narrowed in the model until steady state conditions were reached. All airways at all generations in both the symmetric and asymmetric trees initially narrowed virtually homogeneously from their respective initial radii very similarly. However after constricting to approximately 40% of their initial radii in the symmetric and 45% in the asymmetric tree, there was a bifurcation point in airway behavior as the airways began to follow different trajectories in airway radii (Fig. 21) leading to preferential flow to one of the two daughter airways. Some airways continued to narrow, while others reversed and began to dilate. This pattern, which we refer to in this work as *ventilation bifurcations* repeated in each tree was less variable at first in the symmetric tree, but then as individual airways narrowed while others dilated slightly, sometimes underwent later bifurcations, the distribution of airways radii broadened, and a larger fraction of airways were concentrated at larger radii as demonstrated in the histogram (Fig. 21). The asymmetric tree had more pronounced bifurcations at the onset and quickly reached more stable states reaching a steady state condition at approximately 200 breaths. The distribution of relative airway sizes was slightly more uniform in the asymmetric case.

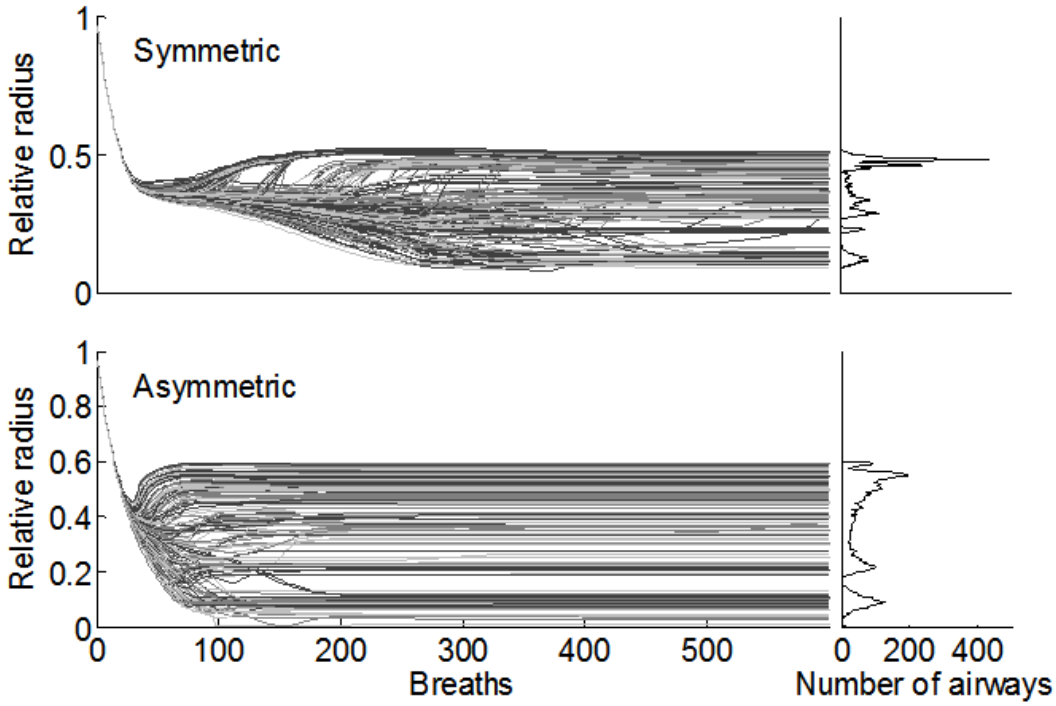

Figure 21. The relative change in airway radius of all airways for the symmetric and 100% asymmetric tree throughout the simulation at Tr = 0.9. After the first bifurcation occurs after the same number of breaths for both trees, the symmetric tree shows a greater number of bifurcation points over a greater number of breaths before equilibrium is reached.

5.3.2 *VENTILATION DISTRIBUTION*

The ventilation maps are of the mean normalized ventilation at steady state, or volume of gas exchanged over one breath, in terminal units that are connected to the terminal airways. Following bronchoconstriction, areas of reduced ventilation appear to be more spread out and less concentrated spatially in the asymmetric tree (Fig. 22A) compared to the symmetric tree (Fig. 22B), however within the defects themselves there

was less variation in ventilation. This can be seen by a more checkerboard pattern of ventilation within the area of reduced ventilation in the symmetric tree.

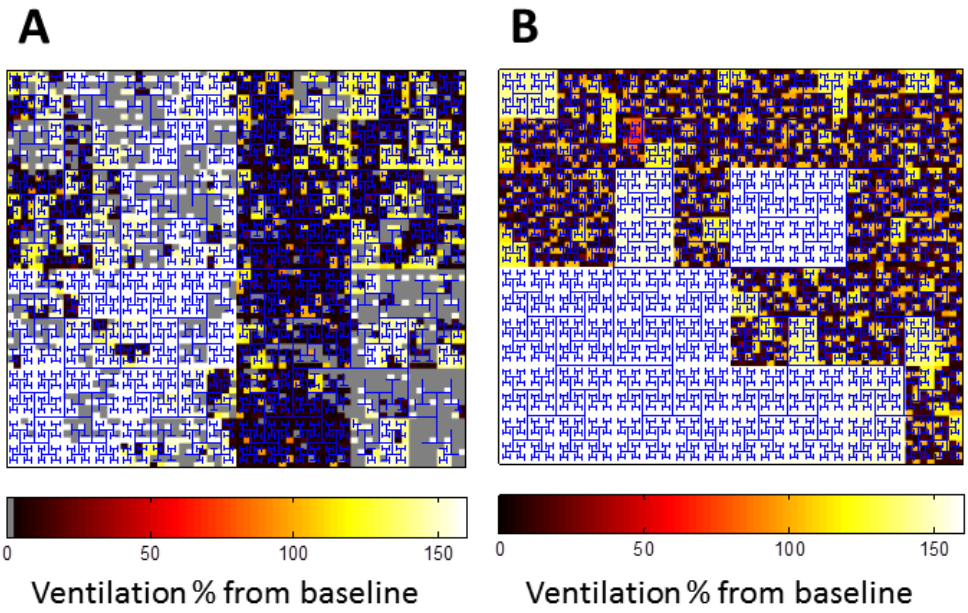

Figure 22. Relative ventilation maps of A) asymmetric and B) symmetric airway trees at steady state (breath 600) of bronchoconstriction as a result of a relative smooth muscle stimulation of Tr = 0.9 The mean normalized ventilation is indicated by color. Grey pixels in the ventilation map of the asymmetric tree indicate regions without terminal units due to some shorter pathways of the asymmetry airway tree compared to the symmetric tree so that the terminal units of the asymmetric tree do not completely fill the schematic ventilation map.

5.3.3 LUNG MECHANICS

R_{L6} and X_{L6} and E_L were calculated for each breath to track lung function as the airways evolved to a steady state where airway radius and ventilation were no longer changing from breath to breath. During the initial phase with virtually homogenous bronchoconstriction (Fig 21), R_{L6} increased (Fig 23) but started to decrease after ventilation bifurcation. Comparing different levels of branching asymmetry, the peak in R_{L6} was more pronounced, but lowered with increasing asymmetry, and the final airway

resistance was also lower with increased asymmetry. X_{L6} exhibited different behavior with different levels of asymmetry during the early phase of bronchoconstriction, however, independent of the level of constriction, the initial increase reversed at the time when the peak in R_{L6} occurred (Fig. 23). Interestingly, in the symmetric lung, X_{L6} first increased with airway narrowing but achieved a steady state value that was not that different than the lung with unconstricted airways. Increasing asymmetry resulted in decreasing steady state values of X_{L6}. We show E_L rather than reactance at low frequencies as in this report they are simply related as $E_L = -X_L\omega$ at 0.3 Hz. During the course of bronchoconstriction, E_L increased in all cases, but was slower to increase in the symmetric lung. Greater asymmetry of 25% led to earlier increases in E_L, while higher asymmetric models followed nearly the same path but with sharper and earlier increases in E_L than the symmetric tree. We observed that the increases in E_L corresponded to the early ventilation bifurcation (see supplemental video – animated VDefs emerging). At steady state, unlike R_{L6}, E_L modestly increased with asymmetry

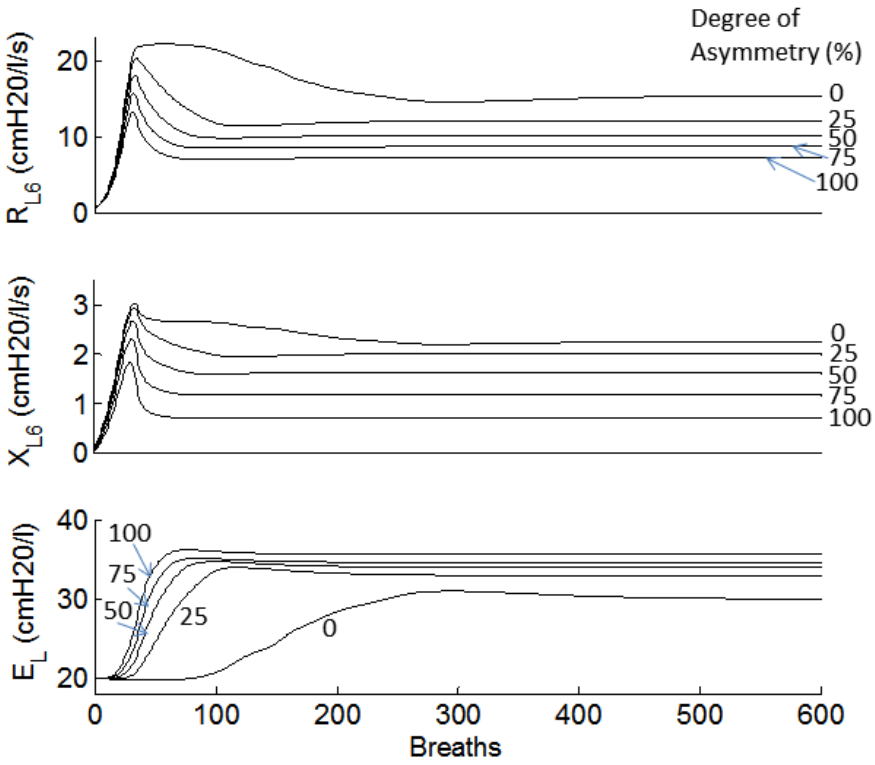

Figure 23. The evolution of R_{L6}, X_{L6} and E_L for various airway trees during the simulation of 600 breaths at $Tr = 0.9$. R_{L6} increased to a peak, at about 40 breaths, and then declines as the airway radii reached steady state where R_{L6} was lowest in the most asymmetric lungs. X_{L6} behavior was more complex containing both E_L and inertance, but also stabilized with the lowest X_{L6} for the most asymmetric lungs. E_L showed similar behavior for all degrees of asymmetry, however the symmetric lung maintained a lower E_L throughout the simulation.

We found that at all levels of smooth muscle activation the steady state of R_{L6} and X_{L6} were always lower with increasing asymmetry (Fig 24). From the ventilation maps at the steady state we computed the entropy, H, which demonstrated interesting behavior (Fig. 24). Generally, H initially increased with smooth muscle activation level to a peak followed by a descent. Low values of H occurred with low levels of constriction and in particular occurred in the more symmetric airway trees, and under these conditions ventilation bifurcations and VDefs were not observed. Increasing levels of asymmetry

caused a leftward shift of the peak in *H*, which appeared to correspond to the onset of ventilation bifurcations.

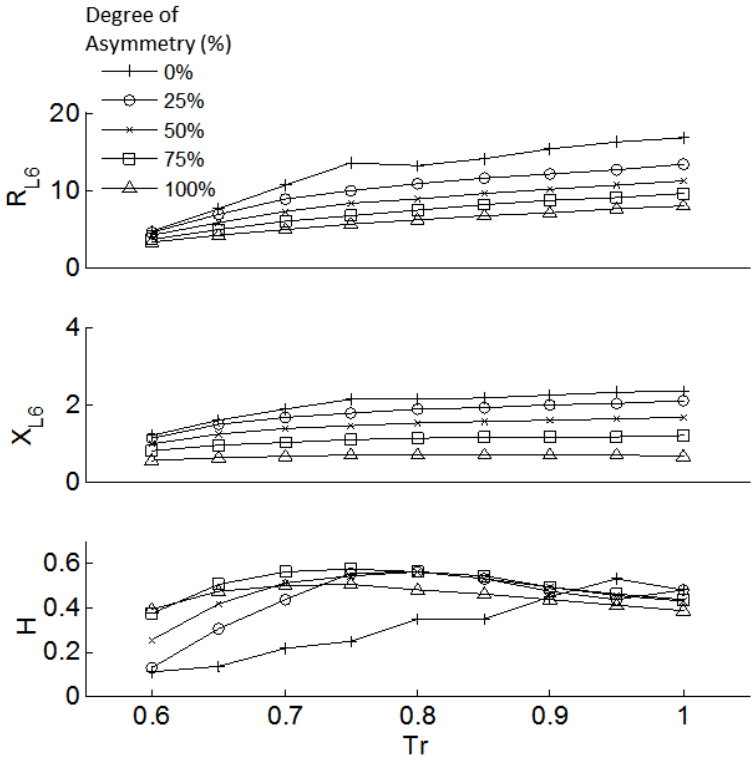

Figure 24. The R_{L6}, X_{L6} and H for all airway trees at the end of the simulation (steady state) for different levels of muscle activation Tr. In all cases of increasing Tr the resistance increased and reactance decreased. In addition, increasing asymmetry lowered resistance and reactance values for a given Tr value. The entropy (H) is the normalized entropy where the entropy is divided by the maximum possible entropy with all states occupied. H was found to reach a maximum value when a combination of Tr and asymmetry, which corresponded to the emergence of VDefs.

5.3.4 VENTILATION DEFECT PERSISTENCE

The ability for VDefs to recur in the same locations, which is the spatial persistency of ventilation heterogeneity, was examined by changing the random

perturbation in repeated simulations for each degree of asymmetry. In the symmetric tree, VDefs occurred in random locations and the ventilation pattern was completely reordered. In contrast, in the fully asymmetric tree, VDefs were very persistent in location (Fig. 25) as the maps of the standard deviation of ventilation across the repeated simulations demonstrate (bottom panels of Fig 25). The mean of the standard deviations of ventilation (taking the mean value of the standard deviation across all ventilated pixels in the lower panels of Fig 25) in the symmetric case was 65.4 (SD 10.3) % compared to 3.5 (SD 7.9) % for the asymmetric case.

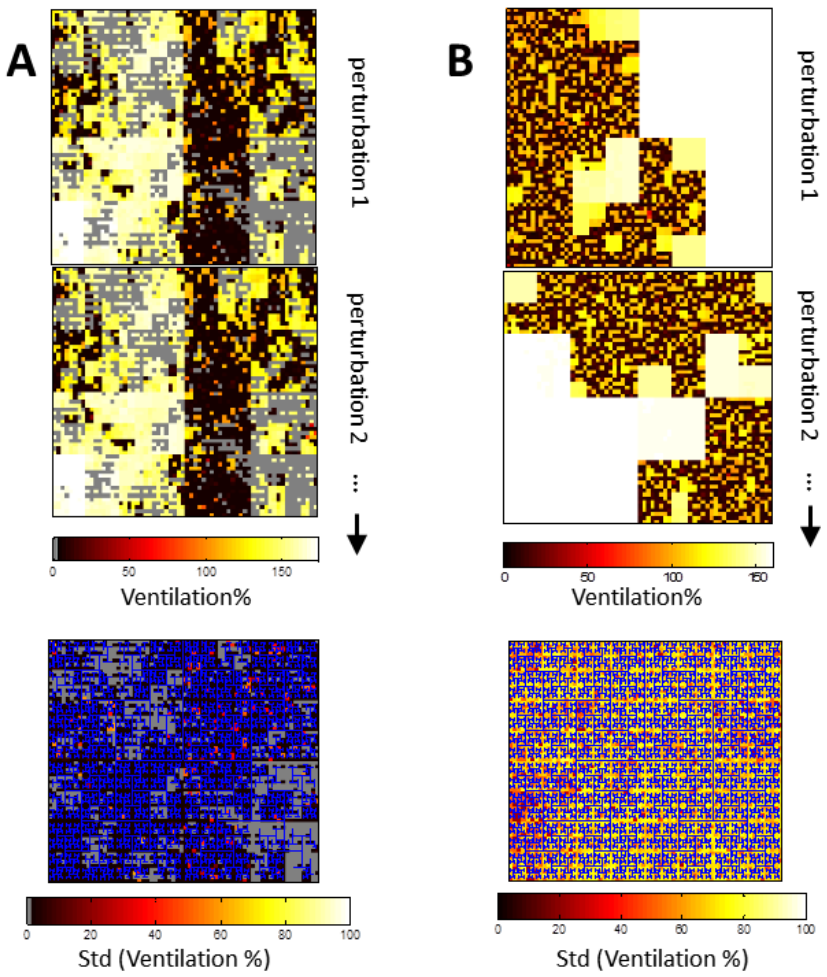

Figure 25. Representative ventilation maps of the A) asymmetric and B) symmetric tree, plotted for 2 different initial perturbations (upper plots) as well as standard deviation of the ventilation distributions of all initial perturbations. The asymmetric ventilation map has very low standard deviation amongst the 9 simulations with different initial perturbation, while the symmetric map has a very high standard deviation in ventilation pattern.

5.3.5 PREDICTED *AIRWAY BEHAVIOR*

Because the location of VDefs was largely persistent in an asymmetric tree, we investigated several parameters that may affect the feedback mechanism and the interdependence among airways during bronchoconstriction. We mostly observed that sisters with an initially smaller airway radius would have a proportionally smaller radius

during the steady state of bronchoconstriction at the end of the simulation, and sisters with larger airway radius would have the larger radius of the two sisters at the end of the simulation. This is the case when the initial airway asymmetry became amplified and these are represented as points in the top right and lower left of the contingency square in the r_i *ratio* of Figure 26A. Points in the other quadrants were initially smaller airways that dilated after the bifurcation, or initially larger airways that narrowed. For the asymmetric tree, and according to rank, we found that the most predominant association with final airway (r_f) radius ratios was r_i, along with T_c, and R_{L6} having a similar result of nearly the same magnitude. The greatest fraction of trending airways were airways in the distal generations for all associations. The central airways did have an increased association compared to mid and distal generation airways in R_{L6} and T_c relative to r_i indicated by the fraction of trending airways. The association of r_f with E was considerably less with central and mid-range near 0.5 which would suggest zero dependence as from a random distribution. For the symmetric tree, the trend of r_f, R_{L6}, and T_c to r_i was similar to that observed in the asymmetric tree, however due to the nature of the symmetric tree E was perfectly symmetric and did not populate any quadrants.

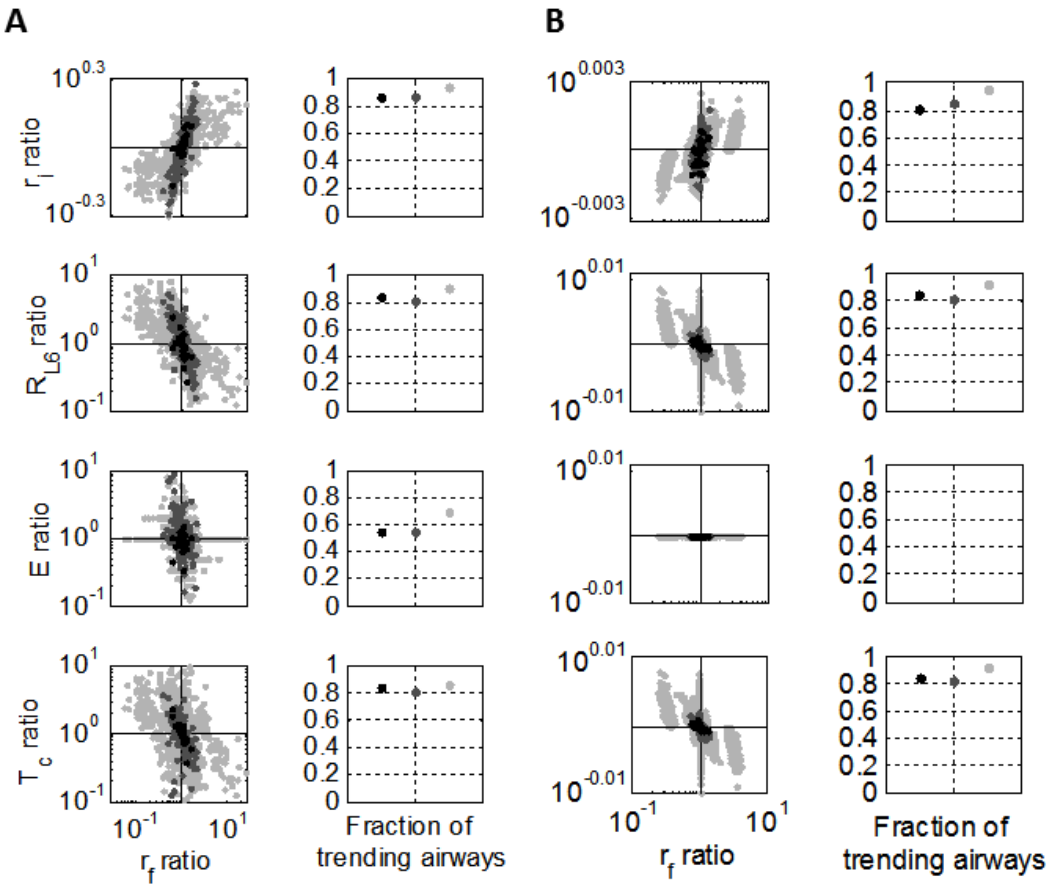

Figure 26. Sister pairs were analyzed by several anatomic and functional parameters to their final radius ratios (r_f ratio). These were to the initial ratios of initial radius size (r_i ratio, in A), airway resistance from the airway and all distal contributions (R_{L6} in A), elastance from distal contributions (E in A), and time constant (T_c in A) ratios. Initial conditions were compared in the A) asymmetric tree, and the B) symmetric tree once some asymmetric structure could develop. In all plots, the central airways from generations 2-6 are colored in black, mid generation airways 7-9 colored in dark grey, and distal airways in generations 10-13 are colored in light gray. The predominance of sister pairs that landed in quadrants due to amplifying tendencies are calculated by the number of airways in these quadrants (upper right and lower left for the radius, for example) divided by the total number of airways. These data are plotted to the right of each 2x2 quadrant plots.

5.4 DISCUSSION

We found that structural asymmetry in the airway tree of human lungs can strongly influence the emergence and location of VDefs and can lead to spatially persistent location of ventilation patterns. The formation of VDefs arose from feedback mechanics as modeled by Anafi and Wilson and the interdependence between airways as demonstrated by Venegas and Winkler, but the location of the defects was strongly determined by the structural heterogeneity of the branching airway tree. Additionally the degree of airway branching asymmetry used here strongly influenced the lung mechanics. With increased asymmetry, at a given level of smooth muscle activation, R_{L6} was lower while E_L was greater implying that asymmetry leads to airway closure with loss of the compliance of affected terminal units, but the remaining terminal units become better ventilated via airways with lower resistance. We found that the final entropy of steady state conditions was highest when lung conditions of airway smooth muscle activation and asymmetry produced ventilation patterns that were just on the verge of exhibiting ventilation bifurcation. Airway trees that produced homogeneous bronchoconstriction or high level heterogeneous ventilation patterns and more aggressive ventilation bifurcation had lower entropy (Figs 23 and 24).

Our findings are consistent with recent observations using hyperpolarized ^{3}He MRI that occurrence of VDefs and the spatial ventilation heterogeneity associated with VDefs increase with severity of asthma or increased inhaled methacholine (Samee, Altes et al. 2003). Furthermore, they are also generally consistent with observations that the locations of VDefs are largely, but not completely persistent in location even after long periods between imaging (de Lange, Altes et al. 2007; de Lange, Altes et al. 2009; Kirby

M 2010). We found most clearly that the VDefs were persistent in their locations in the asymmetric lung compared to the symmetric lung (Fig 25). This was despite the presence of similar small perturbations introduced in airway wall thickness, which are required in the symmetric tree for functional symmetry breaking (Venegas JG 2005; Winkler and Venegas 2007). These small random differences were introduced in one parameter within the lung model, but could have been introduced in other parameters to similarly break the symmetry, such as small heterogeneity in activation simulating distributed dose delivery, or differences in tone or even differences that may occur with muscle content or wall stiffness associated with airway remodeling (Brown, Zerhouni et al. 1995; Frey, Brodbeck et al. 2005; Brown, Kaczka et al. 2008). It is also possible that differences in lung volume history may add to random variation within the lung that we did not model here. Regardless of the source of introduced variation to the initial conditions, it would be expected that increasingly large imposed initial perturbations would make the locations of the VDefs in our model less spatially persistent.

In the symmetric airway tree, the mechanisms that lead to the formation and growth of defects into a patchy distribution of VDefs are the interdependence of airways tethered by the parenchyma they inflate, together with individual airway walls to stretch in a manner that is dependent on the amplitude of the tidal fluctuations they receive (Winkler and Suki 2011). We observed that the emergence of VDefs occurred after nearly (but not exactly at) the same number of breaths (Fig. 21) in both trees at which a tipping point occurred leading to some airways that narrowed while others reversed direction and began to dilate as previously shown in the second figure by Winkler et al. (31). As previously reported in vivo, during the early phase of bronchoconstriction,

airway resistance increased to a peak value (Braune, Kelly et al. 2012) reaching a tipping point that coincides in time with the onset of ventilation bifurcation. The ventilation distribution was virtually uniform up to this point suggesting that structural differences in airway geometry have no substantial influence. However, thereafter when VDefs begin to appear, the structural differences affected the feedback mechanisms on airway narrowing such that ventilation bifurcations led to preferential locations for the formation of VDefs. This is important as it suggests that the occurrence of VDefs with bronchoconstriction cannot be prevented through influencing airway geometry; only their location is affected.

When investigating the airways that dilated at a given bifurcation, due to interdependence among airways within the bronchial tree, we found that the structurally larger airways were more likely to remain open and even dilate, while original structurally narrower airways were more likely to narrow. This corresponded with the persistent location of VDefs over multiple simulations which was found to be much higher in the asymmetric lung due to its initial anatomical asymmetry. From this result, we asked what initial differences between the parameters of sister airways would predict differences in their behavior and, thus, in their final states. Interestingly, we found that both local (r_i) and more global (R_{L6} and T_c) initial tendencies influenced the fate of the proportional radius between sisters. It was interesting that E_L did not have a large influence on which sister airway ultimately narrowed, and which dilated. Nonetheless, we found similar trends in both the asymmetric and symmetric trees that differences in initial parameters between sister pairs were associated with a more dilated or more contracted state of an airway relative to its sister airway, and that these effects of asymmetry on final radii, R_{L6} and E could be profound. We found large ratios in constriction between sister

airways, which can be seen in the extreme quadrants of Fig. 26 when r_f *ratio* was greater than 3 (and less than 0.3). These are the sister pairs that led to VDefs, and in all of these cases amplified the initial parametric difference between sisters. Importantly, the end fate of the sister airway relationship did have a predominant tendency to its initial anatomic and physiological conditions that triggered VDefs. Indeed, this is reasoning for the asymmetric lung to yield location persistent VDefs found in this study. However, a fraction of airways did not follow the predominant tendency to amplify initial geometry showing a behavior different from the majority. This may be evidence for increased susceptibility to variation in VDef location, or possibly larger scale heterogeneity that is being amplified. In fact, the higher association of functional parameters (R_{L6} and T_c) compared to r_i in central airways of the symmetric tree is further evidence that severe constriction of airways is not caused solely by local conditions, but rather highly associated with distal effects through serial interdependence among airways. This finding suggests local treatments such as bronchial thermoplasty may be limited, and therefore more global or systemic treatments are likely required. However an important limitation is that our study was limited to only the effects of the normal structural heterogeneity found in a representative healthy lung. Diseases that alter the lung structure locally such as airway remodeling in asthma may alter the preferential location of VDefs, indeed our findings indicate heterogeneity and thus likely local structural alterations could lead to potential VDefs. Then it may be possible that in asthma if the degree of heterogeneity is sufficient, or site specific, that perhaps some interventions in problematic airways may decrease the sensitivity to the onset of VDef formation.

Another limitation of our study is that the size and location of VDefs could be affected by changes in tidal volume or deep inspirations that we did not study. Deep inspirations could recruit and re-ventilate some regions of the lung altering the location of VDefs. Similarly we have assumed smooth muscle tone or compliance of the alveoli to be uniform throughout the lung, however these variables are likely heterogeneous in location and time and history dependent which could affect VDef location and size (Politi, Donovan et al. 2010; Seow and Fredberg 2010). It is important to note that the asymmetric lung used in this study, although based on an actual lung, was not tested for correctness in impedance or asymmetric time constants T_c for the subject or for airway interdependence during bronchoconstriction. Some work suggests(Bates and Irvin 2002) that the real lung may be less asymmetric in function than the anatomically based asymmetric airway tree we used. That is because the T_c values are a function of both resistance of the pathway from central to terminal airways and of the elastance of the terminal unit. The distribution of elastance between sister airways could be more symmetric than we have modeled as we assumed identical terminal elastances at each terminal airway. Also, it is unclear if currently available anatomical data of asymmetric branching and different lengths of pathways from central to terminal airways include all characteristics that are relevant for feedback mechanisms within the lungs during bronchoconstriction. In fact, an airway with a smaller diameter at a bifurcation of the airway tree may have a shorter pathway to total termination than the larger airway, and may be anatomically linked to a smaller fraction of the lung. However, the time constants of the two pathways may be similar or even identical if they have similar or identical ratios of resistance over subtending elastance. This important distinction between

anatomical and functional aspects explains why the initial ratio of the time constants of two sister airways was in central airway generations a better predictor for differences in their behavior than the ratio of their radii. While more needs to be done to probe mechanisms that could alter how and where VDefs occur, here we show that intrinsic heterogeneity in the pulmonary structure strongly governs both the location and persistence of VDefs.

The differences in the degree of asymmetry in the airway trees greatly influenced lung mechanics following airway smooth muscle activation as demonstrated by the differences in R_{L6} and X_{L6} (Fig. 24). As expected, increasing smooth muscle activation led to increases in R_{L6} irrespective of airway asymmetry, as is well established with inhaled histamine or methacholine (Brown and Mitzner 1998). The fact that R_{L6} was lower in the asymmetric lung at all activation levels was interesting. Structural heterogeneity appears to have provided an advantageous effect helping to maintain relatively lower airway resistance during bronchoconstriction, however the elastance also increased as the number of ventilated terminal units decreased relative to the symmetric lung therefore the gas exchange could be affected. This trend between resistance and elastance was more pronounced with increased levels of smooth muscle activation.

However we found that the decreased R_{L6} with greater asymmetry came at the cost of dramatic decreases in the X_{L6}, after the development of VDefs. This corresponds well to the decreasing reactances (or increasing E_L) observed in asthma and with bronchoprovocation (Lutchen and Gillis 1997; Campana, Kenyon et al. 2009). Interestingly while E_L was very sensitive to the onset of airway closure given by the rise with constriction, the final E_L showed only a modest dependence on the degree of initial

lung structural heterogeneity, indicating more similarity in the number of lost terminal airways compared with the differences in airway diameters evidence by the resistance. This smaller dependence on E_L with the degree of asymmetry is in agreement with the similarity in H for activations greater than $T_r = 0.7$, possibly indicating that E_L could be a good index of VDef heterogeneity, but this would need imaging studies to examine this further.

In this study we examined the entropy H, which provided an assessment of the number of ventilation 'states' by enumerating the different flows amongst the terminal airways. For steady state conditions, the behavior of H had two regimes depending on whether or not the lung conditions would produce VDefs. For small values of *Tr* or trees with little or no asymmetry, the lung would mostly bronchoconstrict with little or no observable defects, and H increased with increased *Tr* or asymmetry as more VDefs would develop, as expected. However, something interesting occurred once lung conditions were such that VDefs would occur (a tipping point of either asymmetry or *Tr*). In this regime, high levels of *Tr* or asymmetry in the simulation would produce substantial defects, and lungs that had greater *Tr* or asymmetry would produce more VDefs and resulted in a lower H, i.e. an inverse relationship indicating a fewer number of ventilation states with increased VDefs. Entropy is often used to quantify the disorder in a system, but in this case it is more of a quantification of the range of available states of constriction within the airway tree. We found that airway trees that had little or no VDef emergence had a large variety of states of constriction, but as VDefs were more pronounced, there is less variety, and several branches share similar flow states. Taken together, the emergence of ventilation heterogeneity that occurs in lungs may work to

make the best of a poor situation by better utilizing working areas of the lung, helping to maintain relatively lower airway resistance, sharing airflow more equitably in the working regions, but at the expense of a relatively stiffer lung.

The fact that with activation, *H* increased from a region with relatively homogenous airway narrowing to a maximum value (Fig 24) meant that *H* followed the emergence of bifurcations and VDefs, and thus quantified increasingly varied and complex flow distribution in the lungs. However at higher levels of either muscle activation or asymmetry, *H* decreased since more airways were closed, and fewer are involved in ventilation reducing the variety of different flows in the terminal airspaces. Thus while *H* may be a good index of heterogeneity, heterogeneity does not always increase with muscle activation. This may be important as it has recently been of great interest to quantify peripheral airway heterogeneity as a measure of peripheral airway closures, utilizing such measures as the frequency dependence of R_{L6} and nitrogen breath washout (Lutchen, Habib et al. 1990). However we show that heterogeneity may in fact decline at high levels of airway constriction.

In summary, we found that ventilation defects emerged during bronchoconstriction in airway trees regardless of the degree of asymmetry. This demonstrates that previous results of characteristic airway behaviors governing emergence of VDefs using a symmetric airway tree (Venegas JG 2005) also apply to human airway trees with asymmetric airway branching. The simulated heterogeneous ventilation patterns generated here also agree with findings of imaging studies that show similar patterns in ventilation distribution. However, in contrast to a symmetric airway tree, our findings show that predetermined anatomical asymmetry and structural

heterogeneity of the airway tree acts to initiate the emergence of VDefs with less muscle activation, and that it results in high persistence of VDef location similar to reported persistency of the location of VDefs in vivo. Our results suggest that asymmetry in airway radii has a strong effect on airway behavior, but is closely followed by functional asymmetry in resistances and time constants of different pathways of the airway tree. Ventilation defects are largely persistent but over long times of months as much as 50% of defects change in size and location (de Lange, Altes et al. 2007). Our findings contribute to a better mechanistic understanding of bronchoconstriction, and of imaging studies showing a high degree of persistence in the location of ventilation defects but also raise the question what is occurring in the lung to alter defect location. For example is the movement of defects an indication of airway remodelling, or is it associated with worsening or improvement in disease? This work suggests the potential that altering the airway structure (either physically or pharmaceutically) to reverse the narrowing at a particular site prone to defect creation may potentially improve airflow to the periphery.

5.5 CHAPTER 5 REFERENCES

1. **Affonce DA, and Lutchen KR**. New perspectives on the mechanical basis for airway hyperreactivity and airway hypersensitivity in asthma. *J Appl Physiol* 101: 1710-1719, 2006.
2. **Anafi RC aWT**. Airway stability and heterogeneity in the constricted lung. *J Appl Physiol* 91: 1185-1192, 2001.
3. **Braune A, Kelly V, Harris R, Musch G, Venegas J, and and Winkler T**. Dynamics Of Airway Resistance During Bronchoconstriction. *American Journal of Respiratory and Critical Care Medicine* 185: A2686, 2012.

4. **Brown R HC, Zerhouni EA, and Mitzner W.** Spontaneous Airways Constrict During Breath Holding Studied by High-Resolution Computed Tomography. *Chest* 106: 920-924, 2011.
5. **Brown RaM, W.** Effects of tidal volume stretch on airway constriction in vivo. *J Appl Physiol* 91: 1995-1998, 2001.
6. **Brown RH aMW**. The myth of maximal airway responsiveness in vivo. *J Appl Physiol* 85: 2012-2017, 1998.
7. **Brown RH, Kaczka DW, Fallano K, Chen S, and Mitzner W**. Temporal variability in the responses of individual canine airways to methacholine. *Journal of Applied Physiology* 104: 1381-1386, 2008.
8. **Brown RH ZE, Mitzner W.** Variability in the size of indi-vidual airways over the course of one year. *Am J Respir Crit Care Med* 151: 119-1164, 1995.
9. **Campana L, Kenyon J, Zhalehdoust-Sani S, Tzeng YS, Sun Y, Albert M, and Lutchen KR**. Probing airway conditions governing ventilation defects in asthma via hyperpolarized MRI image functional modeling. *Journal of Applied Physiology* 106: 1293-1300, 2009.
10. **de Lange EE, Altes TA, Patrie JT, Parmar J, Brookeman JR, Mugler JP, and Platts-Mills TAE**. The variability of regional airflow obstruction within the lungs of patients with asthma: Assessment with hyperpolarized helium-3 magnetic resonance imaging. *Journal of Allergy and Clinical Immunology* 119: 1072-1078, 2007.
11. **de Lange EE AT, Patrie JT, Battiston, JJ, Juersivich, AP, Mugler JP, Platts-Mills TA**. Changes in Regional Airflow Obstruction over Time in the Lungs of Patients with Asthma:Evaluation with ^{3}He MR Imaging. *Radiology* 250: 567-575, 2009.
12. **Florens M, Sapoval B, and Filoche M**. Optimal Branching of Asymmetry of Hydrodynamic Pulsatile Trees. *Phys Rev Letters* 106: 178104, 2011.
13. **Fredberg JJ ID, Miller B, Nathan M, Jafari S, Raboude SH, Butler JP, and Shore SA.** Airway Smooth Muscle, Tidal Stretches, and Dynamically Determined Contractile States. *Am J Respir Crit Care Med* 156: 1752-1759, 1997.
14. **Frey U, Brodbeck T, Majumdar A, Robin Taylor D, Ian Town G, Silverman M, and Suki B**. Risk of severe asthma episodes predicted from fluctuation analysis of airway function. *Nature* 438: 667-670, 2005.
15. **Gunst S**. Contractile force of canine airway smooth muscle during cyclical length changes *J Appl Physiol* 55: 759-769, 1983.
16. **Horsfield K, and Cumming G**. Morphology of the bronchial tree in man. *J Appl Physiol* 24: 373-383, 1968.
17. **Kirby M HM, Svenningsen S, Wheately A, McCormack DG, Etemad-Rezai R, and Parraga G.** Hyperpolarized ^{3}He Magnetic Resonance Functional Imaging Semiautomated Segmentation. *Academic Radiology* 19: 141-152, 2012.
18. **Kirby M ML, Heydarian M, Etemad-Rezai R, McCormack DG, and Parraga G.** Chronic Obstructive Pulmonary Disease: Quantification of Bronchodilator Effects by Using Hyperpolarized ^{3}He MR Imaging. *Radiology* 261: 283-292, 2011.
19. **Kirby M ML, Wheatley A, Santyr GE, McCormack DG, and Parraga G.** Chronic Obstructive Pulmonary Disease: Longitudinal Hyperpolarized ^{3}He MR Imaging *Radiology* 256: 280-289, 2010.
20. **Lai-Fook S**. A continuum mechanics analysis of pulmonary vascular interdependence in isolated dog lobes. *J Appl Physiol* 46: 419-429, 1979.

21. **Lutchen K, and Gillis H**. Relationship between heterogeneous changes in airway morphometry and lung resistance and elastance. *J Appl Physiol* 83: 1192-1201, 1997.

22. **Lutchen KR, Habib RH, Dorkin HL, and Wall MA**. Respiratory impedance and multibreath N2 washout in healthy, asthmatic, and cystic fibrosis subjects *J Appl Physiol* 68: 2139-2149, 1990.

23. **Mathew L, Evans A, Ouriadov A, Etemad-Rezai R, Fogel R, Santyr G, McCormack DG, and Parraga G**. Hyperpolarized 3He Magnetic Resonance Imaging of Chronic Obstructive Pulmonary Disease: Reproducibility at 3.0 Tesla. *Academic Radiology* 15: 1298-1311, 2008.

24. **Otis A, McKerrow C, Bartlett R, and et al.** Mechanical factors in distribution of pulmonary ventilation. *J Appl Physiol* 8: 427-443, 1956.

25. **Parraga G ML, Etemad-Rezai R, McCormack DG, and Santyr GE.** Hyperpolarized ^{3}He Magnetic Resonance Imaging of Ventilation Defects in Healthy Elderly Volunteers: Initial Findings at 3.0 Tesla. *Academic Radiology* 15: 776-785, 2008.

26. **Politi A, Donovan G, Tawhai M, Sanderson M, Lauzon A, Bates J, and Sneyd J**. A multiscale, spatially distributed model of asthmatic airway hyper-responsiveness. *Journal of Theoretical Biology* 266: 614-624, 2010.

27. **Samee S AT, Powers P et al.** Imaging the lungs in asthmatic patients by using hyperpolarized helium-3 magnetic resonance: assessment of respose to methacholine and exercise challenge. *J Alllergy Clin Immunol* 111: 1205-1211, 2003.

28. **Seow CY, and Fredberg JJ**. Emergence of airway smooth muscle functions related to structural malleability. *Journal of Applied Physiology* 110: 1130-1135, 2010.

29. **Shen X WM, Tepper RS, and Gunst SJ.** Mechanisms for the mechanical response of airway smooth muscle to length oscillation. *J Appl Physiol* 83: 731-738, 1997.

30. **Tawhai MH, Nash MP, Lin CL, and Hoffman EA**. Supine and prone differences in regional lung density and pleural pressure gradients in the human lung with constant shape. *J Appl Physiol* 107: 912-920, 2009.

31. **Tgavalekos NT, Venegas JG, Suki B, and Lutchen KR**. Relation between structure, function, and imaging in a three-dimensional model of the lung. *Ann Biomed Eng* 31: 363-373, 2003.

32. **Venegas J, Schroeder T, Harris S, Winkler R, and Melo M**. The distribution of ventilation during bronchoconstriction is patchy and bimodal: A PET imaging study. *Respiratory Physiology & Neurobiology* 148: 57-64, 2005.

33. **Venegas JG WT, Musch G, Vidal Melo MF, Layfield D, Tgavalekos N, Fischman AJ, Callahan RJ, Bellani G, and Harris RS**. Self-organized patchiness in asthma as a prelude to catastrophic shifts. *Nature* 434: 777-782, 2005.

34. **Winkler T**. In silico modeling of airway mechanics. *Drug Discovery Today: Disease Models* 4: 125-129, 2007.

35. **Winkler T, and Suki B**. Emergent Structure–Function relations in Emphysema and Asthma. *Crit Rev Biomed Eng* 39: 263-280, 2011.

36. **Winkler T, and Venegas JG**. Complex airway behavior and paradoxical response to bronchoprovocation. *J Appl Physiol* 103: 655 - 663, 2007.

37. **Winkler T, and Venegas JG**. Self-organized patterns of airway narrowing. *J Appl Physiol* 110: 1482-1486, 2011.

CHAPTER 6. DISCUSSION

6.1 SUMMARY

6.1.1 VARIABILITY OF LUNG RESISTANCE

This thesis has studied temporal variability of the airway diameters by comparing SDR_L to mean airway resistance $\overline{R_L}$ and found that they follow a robust relationship (Que, Kenyon et al. 2001; Diba, Salome et al. 2007) that linearly scales with homogeneous bronchoconstriction, bronchodilation, or the occurrence of VDefs (Chapter 3). However, in order to reproduce the same reported slope as found in the literature from FOT measurements, it was necessary that airways exhibit some localized constriction coherency between joining airways. Although, the mathematical relationship between mother and daughter airways was likely oversimplified, the required coherency of diameter variation between joining airways suggests that variation of airway diameter is not independent between airways. Previously unknown, the SDR_L was found to increase with an increase in defect size. This is possibly due to a reduced number of available airway configurations within the airway tree, and thus increasing sensitivity of SDR_L to fluctuations amongst airway diameters. By adding patient specific ventilation defects identified by hyperpolarized ^{3}He MRI (Chapter 4), more realistic and complex VDefs were investigated than in the previous chapter. The model predictions from these airway trees also produced a robust slope between SDR_L and R_L; however when implementing only ventilation defects to the airway tree with the level of typical diameter variability as used in Chapter 3, a slightly lower slope was observed than purely homogeneous bronchoconstriction. These findings give a clearer understanding of airway variability

and how it relates to airway diameter and VDefs. This is an interesting finding since it may mean that the robust relationship between airway size and variability may exist regardless of the pathology that led to the change in mean airway calibre, which may be useful across a number of lung diseases. Moreover, subjects that deviate from this robust relationship may have an atypical response from a particular mechanism. For example, some subjects have a proportionally higher SDR_L than $\overline{R_L}$ suggesting that the diameter variability may be atypically higher in their airways. Conversely, those subjects have a proportionally lower SDR_L than $\overline{R_L}$, which may suggest that they may have an atypical increase in number of ventilation defects with a lower amount of bronchoconstriction typically observed in subjects.

6.1.2 USING VENTILATION DEFECTS TO PREDICT RESPIRATORY MECHANICS

In Chapter 4, the impedance predictions from 25 asthmatic patients correlated strongly ($R=0.90$, $p<0.001$ for R_L and $R=0.93$, $p<0.001$ for X_L) to VDP at all levels of stimulation: baseline, post-methacholine, and post-salbutamol. This suggests that impedance values from FOT devices could be more clinically useful than FEV_1 from spirometry that are currently for assessing patient VDefs, which has found modest but significant correlations in asthma (de Lange, Altes et al. 2006) and COPD (Kirby M 2011), while others did not find a correlation in asthmatics (Costella M, Kirby M et al. 2012). One possible explanation for this result may be that FEV_1 is not sensitive to the peripheral airways. We found that using the most distal airways ($>14^{th}$ generation) significantly improved the correlation for the X_L data. This suggests two things: 1) the VDefs are best described using more peripheral airways, and 2) that X_L describes the

periphery of the lung better than R_L, since X_L is more sensitive to missing alveoli and less sensitive to airway constriction.

6.1.3 EMERGENCE OF VDEFS IN A NORMAL HUMAN ASYMMETRIC BRANCHING AIRWAY TREE

In Chapter 5, I then investigated both temporal and spatial heterogeneity by using a time-dependent model that examined the emergence of VDefs during bronchoconstriction in airway trees with different degrees of asymmetry: from completely symmetric to the degree of asymmetry typical in the human lung. Here the natural anatomical asymmetry and structural heterogeneity of the airway tree acted to initiate the emergence of VDefs. This occurred with less muscle activation and resulted in high persistence of VDef location similar to reported persistency of VDefs in vivo. The fact that asymmetry plays such a strong role in the development and persistence of VDefs suggests that an alteration to the airway structure, that might occur with pathological airway remodeling, might easily lead to the emergence of a persistent defect. Because of this, and since asymmetry led to the onset of VDefs at lower activation levels, altering the airway structure (either physically or pharmaceutically) to reverse the narrowing at a particular site prone to defect creation may potentially improve airflow to the periphery.

The asymmetric (human) lung was predicted to have lower steady state R_L values (~50%) and greater E_L values (~25%) after bronchoconstriction that a symmetric branching lung, resulting in a lung that is smaller in functional size due to a reduced number of available communicating airspaces, but breathes more easily. The steady state entropy measured in all cases was the highest for lungs that initiated only modest ventilation bifurcations. Comparatively, lungs that either did not develop or had fully

developed VDefs had lowered entropy. This altered functionality of the asymmetric lung is interesting and may be an evolutionary development in the human lung where VDefs develop to improve functionality under challenged conditions, and this development may be entropy driven. The development of ventilation defects seems to be linked to both local and global functional asymmetry. This was determined by comparing ratio of sister airway radii, resistance, elastance, and time constants at the start of the simulation and compared with the ratio of final sister radii at the end of simulation. There was a strong local predisposition to the development of a VDef based on radii where one sister airway that was larger at the start of simulation would end in being much larger. This was always the case for extreme final ratios where VDefs formed. However, there was also evidence of a global predisposition as the ratio of initial resistance between sister airways had a greater association to VDefs for more central airways than for distal airways. Interestingly, elastance did not seem to be associated with the emergence of VDefs; however, as found in Chapter 4, elastance is a sensitive metric for existing VDefs.

These findings contribute to a better mechanistic understanding of bronchoconstriction in a multibranch airway tree, interpretation, and correlation of FOT data to imaging data, and the possible causality associated with location persistent ventilation defects.

6.2 SIGNIFICANCE AND IMPLICATIONS

Chapter 3

Chapter 3 studied how the relationship between airway caliber and variation in airway caliber relates to total lung resistance and variability of resistance (measured as the standard deviation of airway resistance SDR_L). This investigation was important to help understand why there exists a robust proportional relationship between the mean *Rrs* and *SDRrs* that has been seen in many FOT studies. From this work, however, there was an important realization that connecting airways must be similar in the level of bronchoconstriction, termed the coherency parameter. Interestingly, the incorporation of coherency between airways led to localized or 'patchy' ventilation as observed in imaging studies of pathologic lungs. Importantly, this study showed that the robust relationship between R_L and SDR_L as found in studies with FOT measurements, can be explained through either homogeneous bronchoconstriction of airways throughout the lung or the development of a ventilation defect.

Chapter 4

Here I developed a model based on an image-guided study to incorporate much more complicated patient specific ventilation defect patterns from ^{3}He hyperpolarized MRI. From these data, the linear relationship between R_L and SDR_L was well reproduced; however, the slope was found to be slightly lower in a more complex tree that included defects, than in an airway tree that only experienced bronchoconstriction. This is important because it suggests the hypothesis that FOT may be useful in differentiating pathology between bronchoconstriction and ventilation heterogeneity. Also from this study, I found the patient specific impedance predictions were highly correlated with *VDP,* with the strongest correlation when allowing only distal airways to close. This suggests that FOT may be a better measurement of *VDP* compared to FEV_1 metrics from

classic spirometry. This is important and clinically useful because it is possible that VDefs are more indicative of pathology within the lung, and that VDefs could be tracked with more sensitivity using FOT rather than spirometry. Finally, this study predicted that reactance was more representative of *VDP* than resistance, and that distal airways are mostly responsible for the ventilation defect patterns observed.

Chapter 5

Here I developed several airway trees with increasing degrees of asymmetry ranging from symmetric to the degree of asymmetry found in the human lung. Each airway tree was 'challenged' with various degrees of smooth muscle activation to simulate an asthmatic episode, and then evolved over time developing ventilation defects. From these simulations and design of the experiment, I could separate two mechanisms: 1) the asymmetric structural influence and 2) airway instability that leads to ventilation defect formation and influences mechanical impedance. This work suggested that a challenged asymmetric lung breathes more easily over a smaller part of the lung than a challenged symmetric lung. When I calculated the entropy of all the airways trees under each condition simulated in steady state conditions, I found the highest entropy occurred in lungs that were only partially developing ventilation defects. This suggests that ventilation defect formation lowers the disorder within the lung according to the calculated entropy. Importantly, this study points to the structural asymmetry as a mechanism for persistence of the location of ventilation defects. This is a result that was previously observed in imaging studies, but a mechanism for the persistance was unknown. To determine what initial conditions could lead to ventilation defects, I studied association of initial radius, resistance, elastance and time constants of all sister

airway pairs to steady state radius of sister pairs. I found that both local (r_i) and global (R_L and T_c) functional asymmetry were found to be closely associated with the development of ventilation defects, but the elastance (E) had little influence. This is particularly interesting, since E (via X_L) was found in this thesis to be a very sensitive measure of existing defect formation, however E seems to have little influence on the emergence of VDefs.

6.3 ORIGINAL CONTRIBUTIONS MADE

(1) I developed a 65000 branch computer model based on an atomically correct airway branching tree with variable airway diameters, capable of predicting lung impedance distributions.

(2) With this model I showed that the robust relationship between variation in airway resistance (SDR_L) and R_L could arise from 3 mechanisms (airway diameter variability, coherent diameter variability, and defect formation). This was important since although this relationship had been observed, it was not understood.

(3) With this model I found that coherence variation amongst parent and daughter airways was very important in order to describe the dependence between SDR_L , and R_L, since airway variability alone could not describe these measurements found in the literature.

(4) I found that adding a defect into a multibranch model would not only increase the mean resistance, but it would also increase the proportional standard deviation of resistance. This novel finding may be useful clinically in interpreting FOT measurements.

(5) I developed a method and modified the model to determine patient specific airway impedance by closing specific airways of the 3D airway tree model that were inside of ventilation defect volumes as determined from their MRI scans.

(6) I found that patient specific lung impedance (particularly reactance) predictions correlated very well with MRI VDP. This would be a very useful finding clinically as FOT measurements are far less expensive to perform, and therefore could be useful for early diagnosis of lung disease and VDefs.

(7) I have predicted two slopes between SDR_L, and R_L when either varying the degree of bronchoconstriction, or increasing the VDP. I have also shown that most patients fall along a single (average) slope suggesting their condition is a combination of the two. However, noting that these two mechanisms drive the slope differently is potentially also very useful clinically for patient measurements that deviate from the averaged slope.

(8) I have developed a model to determine the effects of asymmetric branching as found in the human lung that led to a mechanism and explanation of the persistent location of ventilation defects found in imaging studies.

(9) I found that entropy, defined by the number of available states of ventilation, is lower with the development of ventilation defects.

(10) From the same simulations, I have found that the normal asymmetric branching as found in the human lung leads to a reduced lung resistance by about 50% and an increase in lung elastance by about 25% compared to a symmetric lung during bronchoconstriction (or asthmatic) events.

6.4 SUGGESTIONS FOR FUTURE WORK

The work of chapter 4 points to the need for a follow-up study where patients had FOT measurements sequentially with hyperpolarized gas MRI. In this future study, the modeling predictions from imaged based data would be compared to the measured FOT data. This would provide independent measurements to the impedance predictions done here that suggest the strong correlation between lung impedance and *VDP*. This would be important to help understand the functional role of Vdefs, but it would also improve understanding of FOT measurements, particularly *Xrs*. In addition, the modeling results of the SDR_L vs R_L have demonstrated a robust linear relationship when either homogeneous bronchoconstriction or defects are incorporated. However, there are subjects from FOT data that are outliers away from the linear relationship. Some patients have either a larger relative R_L or SDR_L response. Having both FOT and hyperpolarized gas MRI would answer the hypothesis that FOT measurements are sensitive to VDefs (possibly more sensitive that spirometry measurements) and would be clinically useful to assess lung condition.

The modeling that was done to predict lung impedance for patient specific ventilation patterns correlated well to *VDP*. Further improvements to the methods would have been improved registration of the lung model to the patient lung. This would become more important to further understanding of which airway generations are responsible for defect formations. Another improvement to the patient specific lung modeling would have graded constriction or dilation on each airway based on the HP MRI intensity. This would likely provide more precise lung impedance predictions.

Future study could describe how much dynamic variability is necessary to override the geometric structure that drives the location of VDefs when the lung is challenged. This study allowed for 1% airway wall variability as was done previously, and this led to very persistent locations of ventilation defect. Allowing airway remodeling to introduce some temporal variability during the simulation would be interesting. This study would test to see how much variability or remodeling is necessary to overcome the branching asymmetry that led to the persistent defects. A suggestion would be to start with the plausible temporal variability determined in Chapter 3, for example.

Another useful study would be to understand what pathological conditions can lead to VDefs and if they can be predicted, and what physical and mechanical conditions thought to occur in asthma or COPD could lead to VDef emergence and possibly airway hyperresponsiveness. That is the emergence of VDefs at low concentrations of an inhaled bronchoconstrictor. This would be an extension of the association study in Chapter 5 to try to determine sensitive parameters (or combinations of parameters) that would lead to the formation of VDefs. This could be done by engineering an airway tree with symmetric elastance, but asymmetric resistance for example to test associations related to VDef formation due to functional asymmetry one parameter at a time. This study could also include imposing a VDef (by reducing a single airway to 10% of its initial diameter) within the airway tree, and comparing what degree of muscle activation is required to develop VDef emergence to the muscle activation levels without an initial VDef. The question is: do VDefs lead to more VDefs? Understanding these relationships would be useful towards preventative or curative medicine where physical alteration of lung

structure through the use of a physical stent or a local pharmaceutical agent that could lead to improved lung function.

REFERENCES

Affonce, D. A. and K. R. Lutchen (2006). "New perspectives on the mechanical basis for airway hyperreactivity and airway hypersensitivity in asthma." J Appl Physiol **101**: 1710-1719.

Albert, M. S., C. G. D., Driehuys B., Happer W., Saam B., Springer C. S. Jr., Wishnia A. (1994). "Biological magnetic resonance imaging using laser-polarized 129Xe." Nature **370**: 199-201.

Altes, T. A., E. M., and Puderbach M, (2007). "Magnetic resonance imaging of the lung in cystic fibrosis." Proc Am Thorac Soc **4**(4): 312-327.

Altes, T. A., J. Mata, et al. (2006). "Assessment of lung devel-opment using hyperpolarized helium-3 diffu-sion MR imaging." J Magn Reson Imaging **24**: 1277-1283.

Altes, T. A., P. P., Knight-Scott J et al. (2001). "Hyperpolarized 3He MR lung ventilation imaging in asthmatics: preliminary findings." J Magn Reson Imaging **13**(3): 378-384.

American Thoracic Society (2000). Guidelines for Methacholine and Exercise Challenge Testing-1999, Am J Respir Crit Care Med. **161:** 309-329.

Anafi, R. C. and T. A. Wilson (2001). "Airway stability and heterogeneity in the constricted lung." J Appl Physiol **91**: 1185-1192.

Bates, J. (2009). Lung Mechanics. An Inverse Modeling Approach. Cambridge, UK, Cambridge University Press.

Bates, J., C. G. Irvin, et al. (2011). "Oscillation Mechanics of the Respiratory System." Comprehensive Physiology **1**: 1233-1272.

Bates, J. H. T. (1998). "A micromechanical model of lung tissue rheology." Ann Biomed Eng **26**: 679-687.

Bates, J. H. T. (2007). "A Recruitment Model of Quasi-Linear Power-Law Stress Adaptation in Lung Tissue." Ann Biomed Eng **35**(7): 1165-1174.

Bates, J. H. T., M. Decramer, et al. (1986). "Respiratory resistance with histamine challenge by single-breath and forced oscillation methods." J Appl Physiol **61**(3): 873-880.

Bates, J. H. T. and C. G. Irvin (2002). "Time dependence of recruitment and derecruitment in the lung: a theoretical model." J Appl Physiol **93**: 705-713.

Bates, J. H. T., F. R. Shardonofsky, et al. (1989). "The low frequency dependence of respiratory system resistance and elastance in normal dogs." Respir Physiol **78**: 369-382.

Black, L. D., R. Dellaca, et al. (2003). "Tracking variations in airway caliber by using total respiratory vs. airway resistance in healthy and asthmatic subjects." J Appl Physiol **95**(2): 511-518.

Braune, A., V. Kelly, et al. (2012). "Dynamics Of Airway Resistance During Bronchoconstriction." American Journal of Respiratory and Critical Care Medicine **185**: A2686.

Brown R, H. C., Zerhouni EA, and Mitzner W. (2011). "Spontaneous Airways Constrict During Breath Holding Studied by High-Resolution Computed Tomography." Chest **106**: 920-924.

Brown, R. and W. Mitzner (2001). "Effects of tidal volume stretch on airway constriction in vivo." J Appl Physiol **91**: 1995-1998.

Brown, R. H., D. W. Kaczka, et al. (2008). "Temporal variability in the responses of individual canine airways to methacholine." J Appl Physiol **104**(5): 1381-1386.

Brown, R. H. and W. Mitzner (1998). "The myth of maximal airway responsiveness in vivo." J Appl Physiol **85**: 2012-2017.

Brown, R. H., E. A. Zerhouni, et al. (1995). "Variability in the size of individual airways over the course of one year." Am J Respir Crit Care Med **151**: 119-1164.

Campana, L., J. Kenyon, et al. (2009). "Probing airway conditions governing ventilation defects in asthma via hyperpolarized MRI image functional modeling." J.Appl.Physiol **106**(4): 1293-1300.

Campana, L. M., R. L. Owens, et al. (2013). "Variability of respiratory mechanics during sleep in overweight and obese subjects with and without asthma." Respir Physiol Neurobiol.: [Epub ahead of print].

Campana, L. M., R. L. Owens, et al. (2011). "Measuring Upper and Lower Airway Resistance During Sleep with the Forced Oscillation Technique." Ann Biomed Eng **40**(4): 925-933.

Costella M, Kirby M, et al. (2012). "Regional pulmonary response to a methacholine challenge using hyperpolarized ^{3}He magnetic resonance imaging." Respirology **17**: 1238-1246.

de Lange, E. E., T. A. Altes, et al. (2006). "Evaluation of asthma with hyperpolarized helium-3 MRI: correlation with clinical serverity and spirometry." Chest **130**(4): 1055-1062.

de Lange, E. E., T. A. Altes, et al. (2007). "The variability of regional airflow obstruction within the lungs of patients with asthma: assessment with hyperpolarized helium-3 magnetic resonance imaging." J Alllergy Clin Immunol **119**(5): 1072-1078.

de Lange, E. E., T. A. Altes, et al. (2009). "Changes in regional airflow obstruction over time in the lungs of patients with asthma: evaluation with 3He MR imaging." Radiology **250**(2): 567-575.

de Lange, E. E., T. A. Altes, et al. (2006). "Evaluation of Asthma With Hyperpolarized Helium-3 MRI: Correlation With Clinical Severity and Spirometry." Chest **130**(4): 1055-1062.

de Lange, E. E., J. P. Mugler, 3rd, et al. (1999). "Lung air spaces: MR imaging evaluation with hyperpolarized 3He gas." Radiology **210**(3): 851-857.

Delacourt, C., H. Lorino, et al. (2000). "Use of the forced oscillation technique to assess airway obstruction and reversibility in children." Am.J.Respir.Crit Care Med. **161**(3 Pt 1): 730-736.

Dellaca, R. L., M. A. Olerud, et al. (2009). "Lung recruitment assessed by total respiratory system input reactance." Intensive Care Med **35**: 2164-2172.

Desager, K., W. Buhr, et al. (1991). "Measurement of total respiratory impedance in infants by the forced oscillation technique." J Appl Physiol **71**: 770-776.

Diba, C., C. M. Salome, et al. (2007). "Short-term variability of airway calibre - a marker of asthma?" J.Appl.Physiol.

Donnelly, L. F., J. R. MacFall, et al. (1999). "Cystic fibrosis: combined hyperpolarized 3He-enhanced and conventional proton MR imaging in the lung-preliminary observations." Radiology **212**(3): 885-889.

Downie, S. R., C. M. Salome, et al. (2007). "Ventilation heterogeneity is a major determinant of airway hyperresponsiveness in asthma, independent of airway inflammation." Thorax **62**(8): 684-689.

Dubois, A. B., A. W. Brody, et al. (1956). "Oscillation mechanics of lungs and chest in man." J Appl Physiol **8**: 587-594.

Ducharme, F. M., G. M. Davis, et al. "Pediatric reference values for respiratory resistance measured by forced oscillation." Chest **113**: 1322-1328.

Ebert M., G. T., Heil W et al. (1996). "Nuclear magnetic resonance imaging with hyperpolarised helium-3." Lancet **9011**: 1297-1299.

Fain, S., M. L. Schiebler, et al. (2010). "Imaging of Lung Function using Hyperpolarized Helium-3 Magnetic Resonance Imaging: Review of Current and Emerging Translational Methods and Applications." J Magn Reson Imaging **32**(6): 1398-1408.

Farre, R., R. Peslin, et al. (1999). "Forced oscillation total respiratory resistance and spontaneous breathing lung resistance in COPD patients." Eur Respir J **14**: 172-178.

Farre, R., J. Rigau, et al. (2001). "Evaluation of a simplified oscillation technique for assessing airway obstruction in sleep apnoea." Eur Respir J **17**: 456-461.

Fredberg, J. J., D. Inouye, et al. (1997). "Airway Smooth Muscle, Tidal Stretches, and Dynamically Determined Contractile States." Am J Respir Crit Care Med **156**: 1752-1759.

Frey, U., T. Brodbeck, et al. (2005). "Risk of severe asthma episodes predicted from fluctuation analysis of airway function." Nature **438**(7068): 667-670.

Frey, U., G. N. Maksym, et al. (2011). "Temporal Complexity in Clinical Manifestations of Lung Disease." J Appl Physiol **110**(6): 1723-1731.

Gast KK, P. M., Rodriguez I et al. (2003). "Distribution of ventilation in lung transplant recipients: evaluation by dynamic 3He-MRI with lung motion correction." Invest. Radiol **38**(6): 341-348.

Gimeno, F., L. T. van der Weele, et al. (1993). "Variability of forced oscillation (siemens siregnost fd 5) measurements of total respiratory resistance in patients and healthy subjects. ." Ann Allergy **71**: 56-60.

Goldman, M. D., H. J. Smith, et al. (2005). "Whole-body plethysmography." Eur. respir. Mon **31**: 15-43.

Gunst, S. (1983). "Contractile force of canine airway smooth muscle during cyclical length changes " J Appl Physiol **55**(3): 759-769.

Hantos, Z., S. B., et al. (1987). "Constant-phase modelling of pulmonary tissue impedance." Bull. Eur. Physiopathol. Respir.23, Suppl. 326s.

Hantos, Z., B. Daroczy, et al. (1987). "Low-frequency respiratory mechanical impedance in the rat." J Appl Physiol **63**(1): 36-43.

Happer, W., E. Miron, et al. (1984). "Polarization of the nuclear spins of noble-gas atoms by spin exchange with optically pumped alkali-metal atoms." Phys Rev. A **29**(6): 3092-3110.

Harris, R., H. Fujii-Rios, et al. (2012). "Ventilation Defect Formation in Healthy and Asthma Subjects Is Determined by Lung Inflation." PLOS ONE **7**(12): 1-9.

Harris, R. S. (2006). "Regional Pulmonary Perfusion, Inflation, and Ventilation Defects in Bronchoconstricted Patients with Asthma." American Journal of Respiratory and Critical Care Medicine **174**(3): 245-253.

Hayden, M. J., F. Petak, et al. (1998). "Using low-frequency oscillation to detect bronchodilator responsiveness in infants." Am. J. Respir. Crit. Care Med. **157**: 574-579.

Hellinckx, J., K. De Boeck, et al. (1998). "No paradoxical bronchodilator response with forced oscillation in children with cystic fibrosis." Chest **113**: 55-59.

Horsfield, K. and G. Cumming (1968). "Morphology of the bronchial tree in man." J Appl Physiol **24**(3): 373-383.

Jackson, A. C. and K. R. Lutchen (1984). "Modeling of respiratory system impedances in dogs." J Appl Physiol **62**(2): 414-420.

Jackson, S. (1985). Anatomy & Physiology for Nurses. London, Bailliere Tindall.

Jensen, A., H. Atileh, et al. (2001). "Selected contribution: airway caliber in healthy and asthmatic subjects: effects of bronchial challenge and deep inspirations." J.Appl.Physiol **91**(1): 506-515.

Kaczka, D. W., R. H. Brown, et al. (2009). "Assessment of heterogeneous airway constriction in dogs: a structure-function analysis." J Appl Physiol **106**(2): 520-530.

Kaczka, D. W., E. P. Ingenito, et al. (1999). "Airway and lung tissue mechanics in asthma. Effects of albuterol." Am J Respir Crit Care Med **159**(1): 169-178.

Kaczka, D. W., E. P. Ingenito, et al. (1997). "Partitioning airway and lung tissue resistances in humans: effects of bronchoconstriction." J Appl Physiol **82**(5): 1531-1541.

Kauzor, H. U., R. Surkau, et al. (1998). "MRI using hyperpolarized noble gases." Eur Respir J **8**: 820-827.

Kirby M, H. M., Svenningsen S, Wheately A, McCormack DG, Etemad-Rezai R, Etemad-Rezai R, and Parraga G. (2012). "Hyperpolarized ^{3}He Magnetic Resonance Functional Imaging Semiautomated Segmentation." Academic Radiology **19**(2): 141-152.

Kirby M, M. L., Heydarian M, Etemad-Rezai R, McCormack DG, and Parraga G. (2011). "Chronic Obstructive Pulmonary Disease: Quantification of Bronchodilator Effects by Using Hyperpolarized ^{3}He MR Imaging." Radiology **261**(1): 283-292.

Kirby M, M. L., Wheatley A, Santyr GE, McCormack DG, and Parraga G. (2010). "Chronic Obstructive Pulmonary Disease: Longitudinal Hyperpolarized ^{3}He MR Imaging " Radiology **256**: 280-289.

Kitaoka, H. and B. Suki (1997). "Branching design of the bronchial tree based on a diameter-flow relationship." Journal of Applied Physiology **82**(3): 968-976.

Kitaoka, H., R. Takaki, et al. (1999). "A three-dimensional model of the human airway tree." J Appl Physiol **87**(6): 2207-2217.

Koumellis, P., E. J. van Beek, et al. (2005). "Quantitive analysis of regional airways obstruction using dynamic hyperpolarized 3He MRI-preliminary results in children with cystic fibrosis." J Magn Reson Imaging **22**(3): 420-426.

Lai-Fook, S. (1979). "A continuum mechanics analysis of pulmonary vascular interdependence in isolated dog lobes." J Appl Physiol **46**(3): 419-429.

Lai-Fook SJ, Wilson TA, et al. (1976). "Elastic constants of inflated lobes of dog lungs." J Appl Physiol **40**: 508-513.

Lall, C. A., N. Cheng, et al. (2007). "Airway resistance variability and response to bronchodilator in children with asthma." Eur.Respir.J.

Leary, D., S. A. Bhatawadekar, et al. (2011). "Modeling stochastic and spatial heterogeneity in a human airway tree to determine variation in variation system resistance." J Appl Physiol **112**(1): 167-175.

Louis, B. and D. Isabey (1993). "Interaction of oscillatory and steady turbulent flows in airway tubes during impedance measurement." Journal of Applied Physiology **74**(1): 116-125.

Lutchen, K. R. and H. Gillis (1997). "Relationship between heterogeneous changes in airway morphometry and lung resistance and elastance." J Appl Physiol **83**: 1192-1201.

Lutchen, K. R., R. H. Habib, et al. (1990). "Respiratory impedance and multibreath N2 washout in healthy, asthmatic, and cystic fibrosis subjects " J. Appl. Physiol. **68**: 2139-2149.

Maksym, G. N. and J. H. T. Bates (1997). "A distributed nonlinear model of lung tissue elasticity." J Appl Physiol **82**: 32-41.

Mathew, L., A. Evans, et al. (2008). "Hyperpolarized 3He Magnetic Resonance Imaging of Chronic Obstructive Pulmonary Disease: Reproducibility at 3.0 Tesla." Academic Radiology **15**(10): 1298-1311.

Mathew, L., M. Kirby, et al. (2011). "Hyperpolarized ^{3}He magnetic resonance imaging: Preliminary evaluation of phenotyping potential in chronic obstructive pulmonary disease." Eur Respir J **79**(1): 140-146.

McAdams HP, P. S., Donnelly LF et al. (1999). "Hyperpolarized 3He-enhanced MR imaging of lung transplant recipients: preliminary results." AJR Am J Roentgenol **173**(4): 955-959.

McMahon CJ, D. J., Hill C et al. (2006). "Hyperpolarized 3helium magnetic resonance ventilation imaging of the lung in cysitc fibrosis: comparison with high resolution CT and spirometry." Eur. Radiol. **2006**(11): 2483-2490.

Mead, J. (1979). Problems in interpreting common tests of pulmonary mechanical function. The Lung in Transition between Health and Disease. P. Macklem and S. Permutt. New York, Mercel Dekker**:** 43-52.

Mentore, K., D. K. Froh, et al. (2005). "Hyperpolarized HHe 3 MRI of the lung in cystic fibrosis: assessment at baseline and after bronchodilator and airway clearance treatment." Acad. Radiol. **12**(1423-1429).

Miller, M. R., R. Crapo, et al. (2005). "General considerations for lung function testing." European Respiratory Journal **26**: 153-161.

Miller, M. R., J. Hankinson, et al. (2005). "Standardisation of spirometry." European Respiratory Journal **26**: 319-338.

Mochizuki, H., K. Hirai, et al. (2012). "Forced Oscillation Technique and Childhood Asthma." Allerg Int **61**: 373-383.

Musch, G. (2005). "Positron Emission Tomography Imaging of Regional Pulmonary Perfusion and Ventilation." Proceedings of the American Thoracic Society **2**(6): 522-527.

Muskulus, M., A. M. Stats, et al. (2010). "Fluctuations and determinism of respiratory impedance in asthma and chronic obstructive pulmonary disease." J Appl Physiol **109**: 1582-1591.

Oostveen, E., D. MacLeod, et al. (2003). "The forced oscillation technique in clinical practice: methodology, recommendations and future developments." European Respiratory Journal **22**(6): 1026-1041.

Otis, A., C. McKerrow, et al. (1956). "Mechanical factors in distribution of pulmonary ventilation." J Appl Physiol **8**: 427-443.

Parraga, G., L. Mathew, et al. (2008). "Hyperpolarized 3He magnetic resonance imaging of ventilation defects in healthy elderly volunteers: initial findings at 3.0 Tesla." Acad Radiol **15**(6): 776-785.

Parraga, G., A. Ouriadov, et al. (2007). "Hyperpolarized 3He ventilation defects and apparent diffusion coefficients in chronic obstructive pulmonary disease: preliminary results at 3.0 Tesla." Invest Radiol **42**(6): 384-391.

Pellegrino, R., G. Viegi, et al. (2005). "Interpretative strategies for lung function tests." European Respiratory Journal **26**: 948-968.

Peslin, R., S. J. da Felicio, et al. (1993). "Respiratory mechanics studied by forced oscillations during artificial ventilation." European Respiratory Journal **6**: 772-784.

Politi, A., G. Donovan, et al. (2010). "A multiscale, spatially distributed model of asthmatic airway hyper-responsiveness." Journal of Theoretical Biology **266**: 614-624.

Que, C. L., C. M. Kenyon, et al. (2001). "Homeokinesis and short-term variability of human airway caliber." J.Appl.Physiol **91**(3): 1131-1141.

Salazar, E. and J. H. Knowles (1964). "An analysis of pressure-volume characteristics of the lung." J Appl Physiol **19**: 97-104.

Salerno, M., T. A. Altes, et al. (2001). "Hyperpolarized noble gas MR imaging of the lung: potential clinical applications." Eur J Radiol **40**(1): 33-44.

Samee, S., T. Altes, et al. (2003). "Imaging the lungs in asthmatic patients by using hyperpolarized helium-3 magnetic resonance: assessment of response to methacholine and exercise challenge." J.Allergy Clin.Immunol. **111**(6): 1205-1211.

Seow, C. Y. and J. J. Fredberg (2010). "Emergence of airway smooth muscle functions related to structural malleability." Journal of Applied Physiology **110**(4): 1130-1135.

Shen X, W. M., Tepper RS, and Gunst SJ. (1997). "Mechanisms for the mechanical response of airway smooth muscle to length oscillation." J Appl Physiol **83**: 731-738.

Srikasibhandha, S. (1983). "Measurement of respiratory resistance in newborn infants with the oscillation method." Anaesthesist **32**: 214-218.

Suki, B. (1993). "Nonlinear phenomena in respiratory mechanical measurements." J Appl Physiol **74**(5): 2574-2584.

Suki, B., A. Barabasi, et al. (1994). "Lung tissue viscoelasticity: a mathematical framework and its molecular basis " J Appl Physiol **76**(6): 2749-2759.

Suki, B. and J. H. T. Bates (2011). "Lung tissue mechanics as an emergent phenomenon." J Appl Physiol **110**: 1111-1118.

Suki, B. and U. Frey (2003). "Temporal dynamics of recurrent airway symptoms and cellular random walk." J Appl Physiol **95**(5): 2122-2127.

Suki, B., Q. Zhang, et al. (1995). "Relationship between frequency and amplitude dependance in the lung: a nonlinear block-structured modeling approach." J Appl Physiol **79**(2): 660-671.

Tawhai, M., A. J. Pullan, et al. (2000). "Generation of an Anatomically Based Three-Dimensional Model of the Conducting Airways." Ann Biomed Eng **28**: 793-802.

Tawhai, M. H., P. Hunter, et al. (2004). "CT-based geometry analysis and finite element models of the human and ovine bronchial tree." J Appl Physiol **97**(6): 2310-2321.

Tawhai, M. H., M. P. Nash, et al. (2009). "Supine and prone differences in regional lung density and pleural pressure gradients in the human lung with constant shape." J Appl Physiol **107**(3): 912-920.

Tgavalekos, N. T., G. Musch, et al. (2007). "Relationship between airway narrowing, patchy ventilation and lung mechanics in asthmatics." Eur.Respir.J. **29**(6): 1174-1181.

Tgavalekos, N. T., M. Tawhai, et al. (2005). "Identifying airways responsible for heterogeneous ventilation and mechanical dysfunction in asthma: an image functional modeling approach." J Appl Physiol **99**: 2388-2397.

Tgavalekos, N. T., J. G. Venegas, et al. (2003). "Relation between structure, function, and imaging in a three-dimensional model of the lung." Ann. Biomed. Eng **31**(4): 363-373.

Trubel, H. and W. K. R. Banikol (2005). "Variability analysis of oscillatory airway resistance in children." EUR. J. Appl. Phyisol **94**: 364-370.

Tzeng, Y., E. Hoffman, et al. (2008). "Investigation of Hyperpolarized 3He Magnetic Resonance Imaging Utility in Examining Human Airway Diameter Behavior in Asthma Through Comparison with High-Resolution Computed Tomography1." Academic Radiology **15**(6): 799-808.

Tzeng, Y. S., K. Lutchen, et al. (2009). "The difference in ventilation heterogeneity between asthmatic and healthy subjects quantified using hyperpolarized 3He MRI." J.Appl.Physiol **106**(3): 813-822.

van Beek EJ, H. C., Woodhouse N et al. (2007). "Assessment of lung disease in children with cystic fibrosis using hyperpolarized 3-Helium MRI: comparison with Shwachman score, Chrispin-Norman score and spirometry." Eur. Radiol. **17**(4): 1018-1024.

Van de Woestijne, K. P. (1993). "The forced oscillation technique in intubated, mechanically ventilated patients." European Respiratory Journal **6**: 767-769.

Van Noord, J. A., J. Clement, et al. (1991). "Total respiratory resistance and reactance in patients with asthma, chronic bronchitis and emphysema." Am. Rev. Respir. Dis. **143**: 922-927.

Venegas, J., T. Schroeder, et al. (2005). "The distribution of ventilation during bronchoconstriction is patchy and bimodal: A PET imaging study." Respiratory Physiology & Neurobiology **148**(1-2): 57-64.

Venegas, J. G., T. Winkler, et al. (2005). "Self-organized patchiness in asthma as a prelude to catastrophic shifts." Nature **434**(7034): 777-782.

Wang C, A. T., Mugler JP III et al. (2008). "Assessment of the lung microstructure in patients with asthma using hyperpolarized 3He diffusion MRI at two time scales:

comparison with healthy subjects and patients with COPD." J Appl Physiol **28**(1): 80-88.

Weibel, E. R. (1963). Geometric and dimensional airway models of conductive, transitory, and respiratory zones of the human lung. West Berlin, Germany, Springer-Verlang KG.

West, J. B. (1990). Respiratory Physiology. Baltimore, MD, Williams & Wilkins.

Winkler, T. (2007). "In silico modeling of airway mechanics." Drug Discovery Today: Disease Models **4**(3): 125-129.

Winkler, T. and B. Suki (2011). "Emergent Structure–Function relations in Emphysema and Asthma." Crit Rev Biomed Eng. **39**(4): 263-280.

Winkler, T. and J. G. Venegas (2007). "Complex airway behavior and paradoxical response to bronchoprovocation." J. Appl. Physiol. **103**: 655 - 663.

Winkler, T. and J. G. Venegas (2011). "Self-organized patterns of airway narrowing." J Appl Physiol **110**(5): 1482-1486.

Woodhouse N, W. J., van Beek EJR et al. (2009). "Assessment of hyperpolarized 3He lung MRI for regional evaluation of interventional therapy: A pilot study in pediatric cystic fibrosis." J Magn Reson Imaging **30**(5): 981-988.

Woods, J. C., C. K. Choong, et al. (2006). "Hyperpolarized ^{3}He diffusion MRI and histology in pulmonary emphysema." Magn. Reson. Med. **56**(6): 1293-1300.

Zaporozhan J, L. S., Gast KK et al. (2004). "Functional analysis in single-lung transplant recipients: a comparative study of high-resolution CT, 3He-MRI, and pulmonary function tests." Chest **248**(2): 655-661.

Zerah, F., A. M. Lorino, et al. (1995). "Forced oscillation technique vs. spirometry to assess bronchodilation in patients with asthma and COPD." Chest **108**: 41-47.

APPENDIX - A: COPYRIGHT PERMISSIONS

August 19, 2013

Journal of Applied Physiology

I am preparing my PhD thesis for submission to the Faculty of Graduate Studies at Dalhousie University, Halifax, Nova Scotia, Canada. I am seeking your permission to include a manuscript version of the following paper(s) as a chapter in the thesis:

Leary et al., Modeling stochastic and spatial heterogeneity in a human airway tree to determine variation in respiratory system resistance, J Appl Physiol, 112: 167-175, 2012.

Canadian graduate theses are reproduced by the Library and Archives of Canada (formerly National Library of Canada) through a non-exclusive, world-wide license to reproduce, loan, distribute, or sell theses. I am also seeking your permission for the material described above to be reproduced and distributed by the LAC(NLC). Further details about the LAC(NLC) thesis program are available on the LAC(NLC) website (www.nlc-bnc.ca).

Full publication details and a copy of this permission letter will be included in the thesis.

Yours sincerely,

Del Leary

Permission is granted for:

a) the inclusion of the material described above in your thesis.

b) for the material described above to be included in the copy of your thesis that is sent to the Library and Archives of Canada (formerly National Library of Canada) for reproduction and distribution.

Name: Mark L. Goodwin Title: Editorial Manager

Signature: [redacted] Date: 8/20/2013